

Stony Brook University



OFFICIAL COPY

The official electronic file of this thesis or dissertation is maintained by the University Libraries on behalf of The Graduate School at Stony Brook University.

© All Rights Reserved by Author.

**Using geochemical tracers and mathematical models to
estimate sinking particle interaction rate constants**

A Dissertation Presented

by

Weilei Wang

to

The Graduate School

in Partial Fulfillment of the

Requirements

for the Degree of

Doctor of Philosophy

in

Marine and Atmospheric Sciences

Stony Brook University

May 2015

Stony Brook University

The Graduate School

Weilei Wang

We, the dissertation committee for the above candidate for the
Doctor of Philosophy degree, hereby recommend
acceptance of this dissertation.

Robert A. Armstrong – Dissertation Advisor
Associate Professor Emeritus, School of Marine and Atmospheric Sciences
Stony Brook University

Cindy Lee - Chairperson of Defense
Distinguished Professor, School of Marine and Atmospheric Sciences
Stony Brook University

J. Kirk Cochran
Professor, School of Marine and Atmospheric Sciences
Stony Brook University

Kamazima Lwiza
Professor, School of Marine and Atmospheric Sciences
Stony Brook University

Gillian Stewart
Associate Professor, School of Earth and Environment Sciences
Queens College, CUNY

This dissertation is accepted by the Graduate School

Charles Taber
Dean of the Graduate School

Abstract of the Dissertation

**Using geochemical tracers and mathematical models to
estimate sinking particle interaction rate constants**

by

Weilei Wang

Doctor of Philosophy

in

Marine and Atmospheric Sciences

Stony Brook University

2015

Abstract of Dissertation

This dissertation has three parts; all concern the behavior of sinking particles in the ocean; all data come from the MedFlux program.

Sinking particles play an important role in the oceanic biogeochemical cycle, because they are in the core position of the “biological pump” that is responsible for transporting photosynthesized organic matter and energy into the deep ocean. On the one hand, this transportation fuels benthic organisms; on the other hand, it reduces carbon dioxide partial pressure in the surface water and promotes absorption of elevated atmospheric carbon dioxide. Particle sinking velocity, which controls particle

residence time in the water column as well as the efficiency of the biological pump. Particle aggregation and disaggregation can influence particle sinking velocity, because large particles sink faster than small particles according to Stokes' law.

Thorium data collected using Indented Rotating Sphere-Settling Velocity (IRS-SV) sediment traps during the MedFlux program were analyzed using two contrasting models. In both cases, the 11 settling velocity categories collected by these traps were optimally divided into two settling velocity classes ("slow" versus "fast") using maximum likelihood estimation. In the first analysis, particle aggregation, disaggregation, remineralization, thorium adsorption, and desorption rate constants were estimated using likelihood methods; these methods do not require any prior estimates of parameter values. Estimated adsorption and desorption rate constants of both slow- and fast-sinking particles were found to increase with depth, while aggregation and disaggregation rate constants were found to decrease with depth. Process contribution results showed that radioactive decay loss of slow-sinking particulate ^{234}Th was compensated by continuous adsorption of dissolved thorium, resulting in that measured flux densities at different depths were approximately the same. Continuous supply from adsorption and aggregation, and negligible radioactive decay loss, explained why ^{234}Th flux densities of fast-sinking particles at deeper depths were higher than those at shallower depths.

In contrast, a widely used mathematical method, the total inverse method, which requires specifying prior estimates of parameter values, was examined by seeding it with different priors to examine the extent to which its results depend on prior information. The results indicate that adsorption, remineralization, and slow-sinking

particle desorption rate constants can be relatively well constrained by the total inverse method, but that disaggregation rate constants are highly dependent on prior parameter estimates, suggesting that the latter method should be replaced by the simpler likelihood method.

A conceptual model describing pigment cycling was built. The settling velocity (5 m/d) dividing slow from fast settling particles was much slower than that estimated (98 m/d) using thorium data. Compared with rate constants estimated using thorium, aggregation rate constants estimated using pigment data were lower, and disaggregation rate constants were higher.

Dedication

To my parents, my wife, and my son

Table of Contents

LIST OF FIGURES	X
LIST OF TABLES	XIII
LIST OF ABBREVIATIONS	XIV
ACKNOWLEDGMENTS	XV
CHAPTER 1 : INTRODUCTION AND BACKGROUND	1
1. INTRODUCTION	1
2. BACKGROUND	3
2.1. <i>The ocean's response to increased CO₂</i>	3
2.2. <i>The MedFlux project</i>	5
2.3. <i>Geochemical tracers</i>	6
2.4. <i>Mathematical Models</i>	9
3. RESEARCH QUESTIONS	11
4. THESIS ORGANIZATION	11
REFERENCES	12
CHAPTER 2 : USING MAXIMUM LIKELIHOOD ESTIMATION TO ANALYZE DATA FROM MEDFLUX SETTLING VELOCITY SEDIMENT TRAPS TO INVESTIGATE PARTICLE CYCLING IN THE OCEAN	23
ABSTRACT	23
1. INTRODUCTION	24
2. METHODS	26
2.1. <i>The data</i>	26
2.1.1. Dissolved ²³⁸ U, ²³⁴ U, ²³⁴ Th, and ²³⁰ Th	26
2.1.2. Sediment trap data	27
2.2. <i>The box model</i>	28
2.3. <i>Mathematical description</i>	29
2.4. <i>Theory and algorithm of the likelihood method</i>	32
3. RESULTS	33
3.1. <i>Division of fast and slow-sinking classes</i>	34
3.2. <i>Parameter estimates</i>	34
3.2.1. Model parameters	34
3.2.2. Processes that influence the balance of ²³⁴ Th	35
3.2.3. Processes that dominate the balance of ²³⁰ Th	35
4. DISCUSSION	36
4.1. <i>Uniqueness of the current study</i>	36

4.2. Adsorption rate constants.....	38
4.3. Desorption rate constants	39
4.4. Remineralizaion	41
4.5. Aggregation and disaggregation.....	41
4.6. Explanations for the depth distributions of ²³⁴ Th flux density	42
CONCLUSIONS	43
REFERENCE.....	44
CHAPTER 3 : SYSTEMATIC INVESTIGATION OF THE SENSITIVITY OF THE TOTAL INVERSE METHOD TO PRIOR PARAMETER VALUES	60
ABSTRACT.....	60
1. INTRODUCTION:.....	61
2. METHODS	64
2.1. Data acquisition and analysis.....	64
2.2. Box models	65
2.3. Total inverse method.....	66
2.3.1. Theory and algorithm	66
2.3.2. Prior information and covariance matrix determinations.....	69
2.4. Posterior results and covariance	70
2.5. Sensitivity tests	71
3. RESULTS	72
3.1. Total inverse method parameter estimations.....	72
3.2. Parameter sensitivities to varied priors.....	73
3.3. Posterior estimates of data.....	74
4. DISCUSSION.....	75
4.1. Uniqueness of posterior estimates	75
4.2. Sensitivity tests	76
4.3. Posterior estimates of data and model error.....	78
CONCLUSIONS	79
REFERENCE:	80
CHAPTER 4 : USING MAXIMUM LIKELIHOOD METHOD AND MEDFLUX PIGMENT DATA TO CONSTRAIN PARTICLE EXCHANGE AND ORGANIC MATTER REMINERALIZATION RATE CONSTANTS	90
ABSTRACT.....	90
1. INTRODUCTION	91
2. METHODS	93
2.1. Sampling location and sampling methods	93
2.2. The box model	95
2.3. Mathematical description of the box model	96
3. RESULTS	99
3.1. Division SV.....	99
3.2. Rate constants	99
4. DISCUSSION.....	100
4.1. Division SV.....	101

4.2. Aggregation and disaggregation rate constants	101
4.3. Chl a and OM degradation rate constants	103
4.4. Parameter value sensitivity tests	104
4.5. Process contributions	106
5. CONCLUSIONS	106
REFERENCES	107
CHAPTER 5 : CONCLUSIONS	121
CONCLUSIONS:	121
REFERENCES	125
BIBLIOGRAPHY	126

LIST OF FIGURES

Figure 1.1. Time series of atmospheric CO₂ at Mauna Loa (in parts per million volume, ppmv) (red), surface ocean pH (cyan), and pCO₂ (µatm) (tan) at Ocean Station ALOHA in the subtropical North Pacific Ocean; (Reproduced from Doney et al., 2009)..... 18

Figure 1.2. A cartoon illustrating biological and physical pumps of carbon dioxide (Reproduced from Ducklow et al., 2001). 19

Figure 1.3. Schematic of the IRS sediment trap. (Reproduced from Peterson et al., 2009)..... 20

Figure 1.4. Particle size versus average sinking velocity (Reproduced from McDonnell and Buesseler, 2012). The pictures show that particle size and sinking velocity are not linearly correlated. ESD is an abbreviation of Equivalent Spherical Diameter, which is a measurement of particle size. 21

Figure 1.5. ²³⁴Th time-integrated flux density at different depths for 2005 MedFlux. For details of the flux density calculations, please consult Armstrong et al. (2009). (Reproduced from Szlosek et al., 2009). 22

Figure 2.1. Location of the DYFAMED time-series site (Reproduced from Bourguet et al., 2009). 55

Figure 2.2. A box model describes thorium cycling. Dissolved thorium interacts with particulate thorium via adsorption, desorption, and remineralization of slow-sinking particles. In addition, dissolved thorium has a source from uranium radioactive decay and is lost via radioactive decay. Thorium on different sinking classes is exchanged via particle aggregation and disaggregation. Particulate thorium is lost through radioactive decay, vertical export, and desorption; and is gained from adsorption. 56

Figure 2.3. A box model describes particle cycling. Slow-sinking particles can turn into fast-sinking particles by aggregation; and fast-sinking particles can disaggregate to form slow-sinking particle. Slow-sinking particles are also lost by remineralization, which process is ignored for fast-sinking particles. 57

Figure 2.4. Maximum likelihood versus division settling velocity (SV), at which sinking particles were separated into fast- and slow-sinking classes as shown in the box model. The division SV means particles with sinking velocity equal to or great than the division SV are grouped in the fast-sinking class; the rest are grouped into the slow-sinking class..... 58

Figure 2.5. Time-integrated ^{234}Th flux density versus settling velocity with depth: SV2 at 313 m, average of SV1 and SV2 at 524 m and 1918 m. The red line separate different distribution patterns: on its left ^{234}Th flux densities were the same at different depths; on its right ^{234}Th flux density generally increased with depth. (Reproduced from Szlosek et al., 2009). 59

Figure 3.1. Likelihood sensitivity tests. These tests were done by systematically changing a parameter at the same time fixing data and other parameters. A maximum likelihood was calculated for each change, and then was plotted with the changing parameter. 88

Figure 3.2. Posterior parameter ratios at 313 m, 524 m, and 1918 m. The red dots are the ratios of posterior parameter results calculated based likelihood results versus themselves. The green square represent the ratios of posterior parameter values based on half the likelihood results as versus corresponding posterior parameter values based on likelihood results. The blue triangles represent the ratios of posterior parameter values based on twice the likelihood results versus corresponding posterior parameter values based on likelihood results. 89

Figure 4.1. A conceptual model describing particulate pigment cycling. Slow- and fast-sinking particle sinking rates were measured using IRS Settling Velocity (SV) sediment traps. Since the shallowest trap depth was 313 m, primary production is neglected. Aggregation and disaggregation describe particle exchange between the two groups: slow-sinking particles aggregate to form faster sinking particles, and fast-sinking particles disaggregate into slower sinking particles. Chl-a degradation products (pheophorbide, pheophytin, and pyropheophorbide) in slow-sinking particles have two sources: in-situ degradation of Chl a and disaggregation of fast-sinking particles containing the pheopigments. Chl a in fast-sinking particles can increase due to aggregation of slow-sinking particles, and can be lost by disaggregation (degradation is neglected since much of the pheopigment production occurs during grazing process in the euphotic zone). d_1 is defined as the rate constant of Chl-a degradation into pheophorbide, pheophytin, and pyropheophorbide, and we assume this is the only way that Chl a is lost. To account for Chl a lost in other reactions, we make the assumption that the rate of loss is similar to that of total organic matter; this gives us a minimum loss rate, as we might expect pigment loss to be somewhat faster than total OM. Therefore, d_2 is defined as the degradation rate constant of organic matter including all the chloropigments. Degradation loss of both Chl a and organic matter in fast-sinking particles is assumed to be slow enough to be neglected. Chl a and organic matter degradation, aggregation, and disaggregation are assumed to have first-order reaction kinetics. 115

Figure 4.2. Maximum likelihood versus division SV. The division SV means that particles with SVs equal to or greater than the division SV will be grouped into the fast-sinking class, and particles with lower SV than the division SV will be grouped into slow-sinking class in the box model. We tentatively divided the 11 SV categories separated by the IRS SV traps into two classes at every possible SV, and maximum likelihoods were calculated at each division SV, then were plotted versus division SV. 116

Figure 4.3. Parameter sensitivity tests. The sensitivity tests were done by progressively changing the tested parameter, which were set the same for all the three depths, while keeping other parameters at their optimized values and data constant. 118

Figure 4.4. Chl-a concentration ($\mu\text{g}/\text{m}^3$) plotted versus particle sinking velocity (m/d). Chl-a concentrations were calculated by applying Eq. 2. The calculated concentrations actually represent the concentrations outside the sediment trap (Armstrong et al., 2009). 119

Figure 4.5. Cartoon explanation of sinking flux. According to Eq. 1, sinking flux is the difference between flux-in and flux-out. If flux-in is greater than flux-out, the sinking flux is positive and server as a source, and vice versa 120

LIST OF TABLES

Table 2.1. Original and newly added data. Mass flux was measured using IRS. Data that are in bold are newly added data. $^{230}\text{Th}_{\text{xs}}$ means excess ^{230}Th , which is calibrated using ^{232}Th to correct for terrestrial influence ($^{230}\text{Th}_{\text{xs}} = ^{230}\text{Th} - 0.57 \times ^{232}\text{Th}$)*.	49
Table 2.2. Summary of rate constants estimated by thorium isotopes.	51
Table 2.3. The source and sink terms for ^{234}Th (upper) and ^{230}Th (lower). A negative sign before a number indicates a sink; a positive number indicates a source. (Units: dpm/m ³ /y).....	52
Table 2.4. Particle compositions for fast- and slow-sinking classes (Reproduced from Lee et al., 2009).	54
Table 3.1. Posterior result comparisons at the depth of 313 m. Two sets of prior information were used in the total inverse method: one set was from the likelihood results; the other was from Nozaki et al. (1987), the results of which was frequently cited as prior information in similar studies. All units are y ⁻¹	83
Table 3.2. Result of the total inverse method at three trap depths with prior parameter information from the likelihood method. The units of adsorption, desorption, remineralization, aggregation, and disaggregation rate constants are y ⁻¹ . Thorium activities, both ^{234}Th and ^{230}Th , have the same unit of dpm/m ³ with uranium (^{238}U and ^{234}U); particle concentration has mg/m ³ ; thorium vertical export has dpm/m ³ /y; and particle vertical export has a unit of mg/m ³ /y.	84
Table 4.1. Settling velocity fluxes (ug/m ² /d) for 2005 of composite pigments and organic matter. In 2005 deployment, there were two SV traps at each depth. Data in two SV traps are combined via the following equation: $f_{\text{composite}} = \text{SV1}_{\text{mass}} / (\text{SV1}_{\text{mass}} + \text{SV2}_{\text{mass}}) * \text{SV1}(f) + \text{SV2}_{\text{mass}} / (\text{SV1}_{\text{mass}} + \text{SV2}_{\text{mass}}) * \text{SV2}(f)$	111
Table 4.2. Parameters estimated by the pigment data and the maximum likelihood method at a division settling velocity of 5 m/d. (unit: y ⁻¹).....	112
Table 4.3. Rate constants (y ⁻¹) calculated with thorium data at division SVs of 5 m/d and 98 m/d. Values at division SV of 98 m/d are those cited from Chapter II, in which total particle mass rather than organic matter was used (see text for further explanations).	113
Table 4.4. Contribution of each process. Negative values indicate sinks. Positive values are sources (units: mg/m ³ /y for OM, μg/m ³ /y for chloropigments).	114

LIST OF ABBREVIATIONS

Chl a—chlorophyll *a*

CO₂—carbon dioxide

L—likelihood

MLE—Maximum Likelihood Estimate

POC—Particulate Organic Matter

ppmv—Parts Per Million by Volume

Pr—probability

IRS—Indented Rotating Sphere

SV—Settling Velocity

Th—Thorium

TOC—Total Organic Matter

TS—Time Series

U—Uranium

ACKNOWLEDGEMENTS

I would like to express my most sincere and heartfelt appreciation to my advisor, Dr. Robert A. Armstrong, for his continuous guidance and support throughout the past years. Without his encouragement, I cannot imagine how I could finish my thesis. Rob is a friend rather than an advisor. Whenever I need help, he always shows up in **my** office weekdays or weekends. It was him who brought me into the world of statistical model, and patiently illustrated how a mathematical model works. I still remember he inspected my slides one by one before my teaching practicum, before every committee meeting, gave out his opinions and instructions. Instead of telling me how to do something, he always encourages me to find out the right way by myself, and to find out why this way is right but not that way.

Great appreciation to my other dissertation committee, Drs. Cindy Lee, J. Kirk Cochran, Kamazima Lwiza, and Gillian Stewart for their brilliant comments and suggestions to this dissertation. I give special thanks to Cindy and Kirk, with whom I attended several research cruises. As senior scientists, they stayed up for sediment or pump deployment and recovery, and for sample processing. Their enthusiasm and dedication set an excellent example for me. Thanks Kirk for allowing me the access to his lab for analyses of radioisotope samples, and gave me much advice on thorium-particle model, which is presented in Chapter II. It was Cindy who gave me inspiration on the use of pigment tracers to estimate particle exchange rate constants, and gave me lots of advice on pigment conceptual model (Chapter IV).

I thank many faculty and staff members in MSRC. I first thank Dr. John Mak, who brought me to Stony Brook, and was as my first year counselor and MS advisor. Christina Heilbrun taught me experiments on chromatography, electronic plating, and alpha spectrometry. Carol Dovi is always there whenever help is needed; she is so patient to answer every question I may have. Special thanks go to Bruce and Anne's family for their invitations to attend Thanksgiving party every year with them. Except for the always delicious foods, my wife, my son, and I had a chance to learn American culture. Many thanks go to my course instructors: Robert Aller, Malcolm Bowman, Jackie Collier, Roger Flood, Glenn Lopez, Mary Scranton, Robert Wilson, and Qingzhi Zhu.

I thank the MedFlux project colleagues for collecting, analyzing, and sharing such beautiful data, which were the basis of my thesis. I thank crewmembers of R/V Endeavor and R/V Atlantic. Many thanks to the technician, Lynne Butler, on R/V Endeavor, who taught me many sea-going skills, such as skills on CTD deployment and recovery. I thank temporary lab mates, Carolina Cisternas Novoa, Abel Guihou, Patrick Fitzgerald, and Teresa King, who made the time on the sea a pleasure time.

I thank all my friends –Luping Su, Tracer Evan, Ling Liu, Dongming Yang, Zhenhai Zhang, Jindong Wang, Xi Chen, Zhihui Wang and his family, Key Hong Park and his family, and many others - for their support, and friendship.

Last but not the least, I express my love and great gratitude to my family. Without their understanding and support, the journey of pursuing my degree abroad would not be possible. Every phone call with them always ends with “concentrate on your study,

do not worry about us”. Many thanks go to my parents-in-law for all of the sacrifices that they have made on behalf of my little family. I thank my son, Zicheng (Chris), who has been giving me tremendous fun since he was born. His contagious laugh is the best remedy for my tiredness and frustrations. At the end I would send my appreciation to my beloved wife, whose unconditional love, support, and encouragement give me strength and push me forward. I am lucky to have you in my life.

This work was financially supported by the NSF Chemical Oceanography Program’s BarFlux project.

Chapter 1 : Introduction and background

1. Introduction

Biogeochemical cycles of carbon are among the most intensively studied areas in oceanographic research, mainly due to the importance of carbon dioxide (CO₂). The atmospheric CO₂ concentration has been increasing since the Industrial Revolution due to the combustion of fossil fuels (Siegenthaler & Sarmiento, 1993); it has resulted in global warming due to the greenhouse effect of CO₂ (Barnett et al., 2005) and in ocean acidification (Doney et al., 2009) due to adsorption of CO₂ by seawater. In the ocean, CO₂ is used to produce organic matter by phytoplankton; it is also used by many planktonic species for the production of carbonate shells. Because carbonate and many components of organic matter are denser than seawater, these shells and associated organic matter will sink after the death of these organisms (e.g., Armstrong et al., 2002).

Sinking particles connect the surface ocean to the deep sea, and transport energy and organic matter produced in the euphotic zone to the deep ocean and sediments. However, due to the high efficiency of heterotrophic remineralization, greater than 90% of particulate organic carbon formed in the surface water is returned to inorganic form in the euphotic zone or the upper ocean; only about 1% of organic matter

survives transit from the surface ocean to the sediments (e.g., Wakeham and Lee, 1993; Feely et al., 2001).

Particle aggregation and disaggregation have a great impact on particle sinking velocity, which determines how much particle remineralization occurs in the water column, and consequently the efficiency of the “biological pump”. This is because, according to Stokes’ law, large particles sink faster than smaller particles of the same density (Mann and Lazier, 1991; Waite et al., 1997); and faster sinking particles have shorter residence times in the water column. Particle remineralization is also an important control on nutrient cycling (Murnane et al., 1996).

For these reasons, particle aggregation, disaggregation, and remineralization have been intensively studied (e.g., Nozaki et al., 1987; Cochran et al., 1993, 2000; Murnane, 1994; Murnane et al., 1990, 1994, 1996; Kriest and Evans, 2000; Karakas et al., 2009; Abramson et al., 2010). Because direct study of particle exchange is difficult, most of the above-cited authors studied particle exchange using geochemical tracers, among which the thorium isotopes are one of the most useful because it is a particle reactive element and has multiple isotopes in the ocean (^{228}Th , ^{230}Th , ^{232}Th , and ^{234}Th); these isotopes have the same chemical character, but different sources and decay half-lives. By using a combination of thorium isotopes, we can obtain more information for evaluating models than with a single tracer.

In addition to thorium isotopes, pigments are an important geochemical tracer. Chlorophyll *a*, an important absorber of light during photosynthesis, is produced in the euphotic zone, and degraded by either bacteria or zooplankton in the euphotic zone or

deeper in the water column. Chlorophyll *a* is used to represent biomass of phytoplankton, which are small in size and sink slowly. However, chlorophyll *a* degradation products- pheophorbide, pheophytin, and pyropheophorbide (pheopigments for short), are present in zooplankton fecal pellets and aggregates, which are larger in size and sink faster. The distinct origin of chlorophyll *a* and pheopigments and their known degradation pathways make these compounds useful geochemical tracers of surface source and particle remineralization (Lee et al., 2000).

This thesis focuses on estimating particle-thorium adsorption and desorption rate constants, particle-particle aggregation and disaggregation rate constants, and particle remineralization rate constants, by using the likelihood method (Edwards, 1992; Armstrong et al., 2002, 2009) on both thorium tracers and on pigment tracers. Additionally, the widely used “total inverse” method (e.g., Murnane, 1994; Murnane et al., 1990, 1994, 1996; Marchal and Lam, 2012) used to estimate particle-thorium rate constants was evaluated against the likelihood-based results. In the following, I summarize pertinent background information and bring up questions to be addressed in this thesis.

2. Background

2.1. The ocean’s response to increased CO₂

Since the Industrial Revolution, atmospheric CO₂ has increased sharply from approximately 280 ppmv (parts per million volume) to 384 ppmv in 2007 (**Fig. 1.1**) (Solomon et al., 2007) due to fossil fuel combustion and deforestation (Doney and Schimel, 2007). The elevated CO₂ concentration both induces climate change since CO₂ is a greenhouse gas, and also decreases pH in the ocean, causing ocean acidification.

The ocean covers approximately 70% of the Earth's surface, and is the major sink of anthropogenic CO₂. According to Sabine and Feely (2007), about one third of the anthropogenic CO₂ input is absorbed by the ocean; without oceanic uptake atmospheric CO₂ concentration would be even higher.

One mechanism by which the ocean takes up CO₂ is the “biological pump” (**Fig. 1.2**). In the euphotic zone, which is defined as the depth at which light level equals to 0.1% of the surface light level, phytoplankton synthesize organic matter from CO₂ during photosynthesis. Because organic matter is denser than seawater, phytoplankton as well as other organisms and their waste sink after death. Some phytoplankton are consumed by zooplankton, and are repackaged into zooplankton fecal pellets. Most synthesized organic matter returns to inorganic form by degradation. Only about 10% of OM sinks out of the euphotic zone (Eppley and Peterson, 1979; Bacon et al., 1996); and only about 1% sinks to the sediment (e.g., Wakeham and Lee, 1993).

Particles are thought to exchange extensively with each other while they are sinking (Clegg and Whitfield, 1990, 1991; Cochran et al., 1993; Jackson and Burd, 1998); small particles can aggregate to form larger particles, and large particles can disaggregate into smaller particles.

2.2. The MedFlux project

Due to the vast area of the ocean, it is impossible to sample at every location. Oceanographers conduct *in-situ* observations at typical study areas, and then use models to extrapolate their results to the whole ocean. The MedFlux project is one example, and was conducted between 2003 and 2005 to study particle fluxes and exchanges in the “twilight zone” (Lee et al., 2009), which is defined as the depth between euphotic zone and 1000 meters (Buesseler et al., 2007). Particle samples were collected using IRS sediment traps (see below) and *in-situ* large volume pumps at the French Joint Global Ocean Flux Studies DYFAMED time-series site (43.25 °N, 7.52 °E) in the Mediterranean Sea.

The DYFAMED site has many characteristics that make it ideal for oceanographic study. Geographically, it is only ~53 km off the coast of Nice in the Ligurian Sea, yet has many open-ocean characters because surface terrestrial influence has largely been cut off by the cross-coastal Ligurian current (Marty, 2002). This location receives periodical dust input, which is well characterized (Buat-Menard et al., 1989; Migon, 1993; Lee et al., 2009). Geochemically, as a site located in the northern hemisphere mid-latitudes, it experiences a phytoplankton spring bloom from March to April followed by stratification and low primary production in summer. The decrease of stratification in autumn promotes another, smaller phytoplankton bloom, which is terminated by decreased temperature and intensified mixing in winter (Abramson et al., 2012).

One technique used in the MedFlux project was the Indented Rotating Sphere (IRS) sediment trap, which was originally designed to exclude “swimmers” (zooplankters that swim into a trap) (Peterson et al., 1993 (**Fig. 1.3**)). The trap has three parts: a mass interceptor, an indented rotating ball, and a mass collector. Particles are first caught by the mass interceptor and deposited on the indented ball, which rotates on a programmed time schedule. Due to the rotation of the sphere, particles fall into the mass collector. An innovative use of the IRS trap, as used in MedFlux, is to program the sampling carousel to sort particles based on settling velocity (SV) (Peterson et al., 2005).

2.3. Geochemical tracers

Particle aggregation, disaggregation, and remineralization impact biogeochemical cycles of carbon, nutrients, and trace elements. Some trace elements, such as thorium isotopes, in turn have been used as proxies to study how particles transform when they sink (e.g., Nozaki et al., 1981; Cochran et al., 1993, 2000; Bacon and Anderson, 1982; Honeyman and Santschi, 1989; Murnane et al., 1996; Bourne et al., 2012). This is due to the fact that thorium is a particle-reactive element, which is easily scavenged onto particle surfaces. When particles aggregate and disaggregate, thorium can follow these changes.

There are several thorium isotopes commonly used in oceanographic studies: for example, ^{234}Th , ^{230}Th , and ^{228}Th with half-lives of 24.1 days, 75,380 years, and 5.75

years, respectively. Since isotopes have the same chemistry, different decay half-lives and activities offer modelers more degrees of freedom to evaluate models. In oceanography, thorium isotopes have been used to evaluate sediment trap efficiency (e.g., Fleisher and Anderson, 2003; Roy-Barman et al., 2009) and to calculate POC flux out of the photic zone (e.g., Santschi et al., 1979; Coale and Bruland, 1985; Tsunogai et al., 1986; Buesseler, 1998); they also have been used to estimate particle aggregation, disaggregation, adsorption, and desorption (e.g., Murnane, 1994; Murnane et al., 1994, 1996).

In previous box models describing thorium cycling (Murnane, 1994; Murnane et al., 1994, 1996), particles were separated based on particle size; sinking velocity of large particles was arbitrarily assigned; and small particles were assumed to be “non-sinking” particles, which, according to McDonnell and Buesseler (2010), might be wrong. McDonnell and Buesseler (2010) studied the relationship between particle size and average sinking velocity for particles with sizes ranging from 70 μm to 6 mm; their results (shown in **Fig. 1.4**) suggest that particle size and sinking velocity are not linearly correlated. Instead of separating particles based on their size and assuming small particles were “non-sinking”, we built a box model that separated particles based on sinking velocities that were measured using IRS SV traps in the 2005 MedFlux program.

Szlosek et al. (2009) showed that between the depths of 1918 m and 313 m, the time-integrated ^{234}Th flux densities of slow-settling particles were almost equal (e.g., see $\text{SV} < 49$ m/d from their data reproduced as **Fig. 1.5**), whereas ^{234}Th flux densities of fast-settling particles were higher at deeper depths than at shallower depths.

Considering the decay half-life of ^{234}Th (24.1 days), particles with slower settling

velocities will take at least one and a half decay half-lives to finish the transit from 313 m to 1918 m, by which time more than 65% of ^{234}Th will have decayed away. However, the measured fluxes of slow-settling particles at these two depths were essentially the same. For fast-settling particles (e.g., $\text{SV} \geq 100$ m/d), it takes less than 16 days to reach the deeper depth; during this period of time the radioactive decay loss would be less than 40%. Therefore, we would expect that ^{234}Th flux densities are similar at the two depths. However, the measurements presented in **Fig. 1.5** suggest that during the sinking journey particles gain ^{234}Th either from dissolved forms by scavenging or from exchange with other particles.

Szlosek et al. (2009) considered a conceptual model to describe the processes that could influence thorium activities in each phase. Conceptually, fast-settling particles can disaggregate to form slow-settling particles; and slow-settling particles also can aggregate into fast-settling particles. Particles and dissolved phases interact via biotic and abiotic processes such as adsorption, remineralization, and dissolution. Thorium isotopes with different decay half-lives but the same chemistry can provide valuable information on particle interactions (Marchal and Lam, 2012). Because particles were sorted by settling velocities in MedFlux studies, we are able to determine thorium distributions on particles with different settling velocities. When we put the activities and settling velocities into a likelihood model, the particle interaction rate constants can be calculated. These rate constants are extremely important for understanding particle dynamics in the ocean.

Chlorophyll *a*, which is produced in the euphotic zone, degrades during the sinking of particles from the surface water to the deep sea. Degradation can be caused

by either photolysis into colorless compounds, or biologically by zooplankton to pheopigments (pheophorbide, pheophytin, and pyropheophorbide) (Szymczak-Zyla et al., 2008), which have similar ring structures as Chl *a* (Sun et al., 1993). Chl *a* is used as a proxy to represent biomass of algae, which are small in size and sink slowly. However, since pheopigments are the products of herbivore grazing, they are inside the zooplankton or their fecal pellets, which are assumed to sink faster in the water column (Welschmeyer and Lorenzen, 1985). During the sinking transit, it is thought that particles continuously exchange material through aggregation and disaggregation (Hill, 1998). Chl *a* and pheopigments can be used as proxies to record particle exchange due to their distinct sources and known degradation pathways. Abramson et al. (2010) applied these ideas to Medflux data to obtain a qualitative view of particle exchange.

2.4. Mathematical Models

The total inverse method, which was developed by geophysicists to deal with largely underdetermined problems, was adopted by marine scientists as a routine method to quantify particle-thorium interactions rate constants (e.g., Murnane, 1994; Murnane et al., 1994, 1996; Marchel and Lam, 2010). Instead of using single quantities (for example, means or medians), the total inverse method describes data and parameters with probability densities. Theoretical relationships connecting data and parameters are also described with probability densities for incorporation of theoretical errors, which come from incomplete theoretical knowledge or inappropriate assumptions. In this method, the posterior estimates are assumed to have normal

distributions when both the prior information and the theoretical equations are assumed to have normal distributions (Tarantola and Valette, 1982a, 1982b).

The total inverse method is designed to deal with linear or weakly non-linear problems and can deal with both over-determined and under-determined problems (Tarantola and Valette, 1982a, 1982b). The prior estimates come either from direct measurements or from the literature. For non-linear problems, results are found by iteration. In the inverse process, prior estimates adjust themselves based on a least-square criterion in ranges defined by their variances.

The likelihood method, another optimization method, is similar to the least-square method when data have normal distributions (Hilborn and Mangel, 1997). A useful feature of the likelihood method is that it is multipliable, therefore log-likelihoods are additive, which makes it feasible to combine different types of data into one likelihood model. This feature is very important when dealing with thorium data, because thorium isotopes have up to 3-orders of magnitude differences in activity and decay half-life. If we put them directly into one likelihood model, the one with higher activity will dominate the results, which will give biased results.

In this thesis, we estimated particle-thorium adsorption and desorption rate constants, and particle-particle aggregation and disaggregation rate constants by the likelihood method with both thorium and pigment tracers, and made comparison on the results estimated with the two tracers. Multiplications of calculated rate constants with corresponding concentrations gave estimations about process contributions, about which we discussed their biogeochemical meanings. We also evaluated the total

inverse method by seeding with different prior estimates to check if this method could make a constant prediction.

3. Research Questions

Generally, I tried to address the following main research questions in my thesis.

- Can we understand the depth distribution of thorium-234 measured by the IRS SV sediment traps at three different depths by applying the likelihood method to thorium tracers?
- Is the “total inverse method,” reliable enough to make useful predictions of particle interaction rate constants when applied to thorium data?
- Can we obtain “better” estimates of particle exchange rate constants by using pigment tracers? Or will these estimates always be different because thorium and pigments trace different properties of particles?

4. Thesis organization

In this thesis, I discuss two mathematical methods, the total inverse method and the likelihood method, and two geochemical tracers, radioactive elements (thorium) and chloropigments. Chapter I summarizes background information and poses research questions. Chapter II builds two box models describing geochemical cycles of thorium

isotopes and sinking particles, respectively, and applies the likelihood method to estimate thorium-particle adsorption and desorption rate constants, and particle-particle aggregation and disaggregation rate constants, and answers the question posed by Szlosek et al. (2009). Chapter III investigates the total inverse method that has been widely used by the community to estimate particle-thorium interaction rate constants. Chapter IV uses pigment tracers and the likelihood method to estimate particle exchange rate constants and makes comparisons to rate constants estimated using thorium tracers. Chapter V summarizes major findings of the thesis.

References

- Abramson, L., Lee, C., Liu, Z., Wakeham, S.G., Szlosek, J., 2010. Exchange between suspended and sinking particles in the northwest Mediterranean as inferred from the organic composition of in situ pump and sediment trap samples. *Limnol. Oceanogr.*, 55(2), 725-739.
- Alonso-Gonzalez, I.J., Aristegui, J., Lee, C., Sanchez-Vidal, A., Calafat, A., Fabres, J., Sangra, P., Pere, M., Hernandez-Guerra, A., & Beritez-Barrios, V., 2010. Role of slowly settling particles in the ocean carbon cycle. *Geophysical Research Letters*, L13608, doi:10.1029/2010GL043827.
- Armstrong, R.A., Lee, C., Hedges, J.I., Honjo, S., Wakeham, S., 2002. A new, mechanistic model for organic carbon fluxes in the ocean based on the quantitative association of POC with ballast material. *Deep-Sea Res. II* 49, 219–236.
- Armstrong, R., Lee, C., Peterson, M., Cochran, J., & Wakeham, S., 2009. Sinking velocity spectra and the ballast ratio hypothesis. *Deep-Sea Research II*, 1470-1478.
- Bacon, M. and Anderson, R., 1982. Distribution of Thorium isotopes between dissolved and particulate forms in the Deep Sea. *Journal of Geophysical Research*, 87(C3), 2045-2056.
- Bacon, M.P., Huh, C.A., Moore, R.M., 1989. Vertical profiles of some natural radionuclides over the Alpha Ridge, Arctic Ocean, *Earth Planet. Sc. Lett.*, 95, 15–22.

- Bacon, M. P., Cochran, J. K., Hirschberg, D., Hammar, T. R., and Fler, A. P., 1996. Export flux of carbon at the equator during the EqPac time-series cruises estimated from Th-234 measurements. *Deep-Sea Research II* 43, 1133-1153.
- Barnett, T.P., Adam, J.C., Lettenmaier, D.P., 2005. Potential impacts of a warming climate on water availability in snow-dominated regions. *Nature*, 438, 303-309.
- Bourne, M. D., Thomas, A. L., Niocaill, C. M., & Henderson, G. M., 2012. Improved determination of marine sedimentation rates using ^{230}Th s. *Geochemistry Geophysics Geosystems*, 13(1). doi:10.1029/2012GC004295.
- Buat-Menard, P., J. Davis, E. Remoudaki, J.C. Miquel, G. Bergametti, G. Lambert, C.E. Ezat, C. Quétel J., La Rosa and S.W. Fowler., 1989. Non-steady-state biological removal of atmospheric particles from Mediterranean surface waters. *Nature*, 340: 131-134.
- Buesseler, K.O., 1998. The decoupling of production and particulate export in the surface ocean. *Global Biogeochemical Cycles*, 12(2), 297-310.
- Buesseler, K.O., Lamborg, C.H., Boyd, P.W., Lam, P.J., Trull, T.W., Bidigare, R.R., Bishop, J.K.B., Casciotti, K.L., Dehairs, F., Elskens, M., Honda, M., Karl, D.K., Siegel, D.A., Silver, M.W., Steinberg, D.K., Valdes, J., Mooy, B. V., Wilson, S., 2007. Revisiting carbon flux through the ocean's twilight zone. *Science*, 316, 567-570.
- Clegg, S.L. and Whitfield, M., 1990. A generalized model for the scavenging of trace metals in the open ocean, I, Particle cycling, *Deep Sea Res.*, 37, 809-832.
- Clegg, S.L. and Whitfield, M., 1991. A generalized model for the scavenging of trace metals in the open ocean, II, thorium scavenging, *Deep Sea Research, Part A*, 38, 91-120.
- Clegg, S.L., Bacon, M.P., Whitfield, M., 1991. Application of a generalized scavenging model to thorium isotope and particle data at Equatorial and high-latitude sites in the Pacific Ocean, *J. Geophys. Res.*, 96, 20655-20670.
- Coale, K. and Bruland, K., 1985. ^{234}Th and ^{238}U disequilibria within the California Current. *Limnology and Oceanography*, 32(2), 189-200.
- Cochran, J.K., Buesseler, K.O., Bacon, M.P., Livingston, H., 1993. Thorium isotopes as indicators of particle dynamics in the upper ocean: results from the JGOFS North Atlantic Bloom Experiment. *Deep-Sea Research I* 40, 1569-1595.
- Cochran, J.K., Buesseler, K.O., Bacon, M.P., Wang, H.W., Hirschberg, D.J., Ball, L., Andrews, J., Crossin, G., Fler, A., 2000. Short-lived thorium isotopes (^{234}Th , ^{228}Th) as indicators of POC export and particle cycling in the Ross Sea, Southern Ocean. *Deep-Sea Research II*, 47, 3451-3490.
- Doney, S.C. and Schimel, D.S., 2007. Carbon and climate system coupling on timescales from the precambrian to the anthropocene. *Annual Review of Environment and Resources*, 32, 31-66.

- Doney, S.C., Fabry, V.J., Feely, R.A., Kleypas, J.A., 2009. Ocean Acidification: the other CO₂ problem. *Annual Review of Marine Sciences*, 1, 169-192.
- Ducklow, H.W., Steinberg, D.K., Buesseler, K.O., 2011. Upper Ocean Carbon Export and the Biological Pump. *Oceanography*, 14(4), 50-58.
- Edwards, A.W.F., 1992. *Likelihood*. Johns Hopkins University Press, Baltimore, MD.
- Eppley, R. W. and Peterson, B. J., 1979. Particulate organic matter flux and planktonic new production in the deep ocean. *Nature* 282, 677-680.
- Feely, R., Sabine, C., Takahashi, T., Wanninkhof, R., 2001. Uptake and storage of carbon dioxide in the oceans: the global CO₂ survey. *Oceanography*, 14(4), 18–32.
- Fleisher, M. and Anderson, R., 2003. Assessing the collection efficiency of Ross Sea sediment traps using ²³⁰Th and ²³¹Pa. *Deep-Sea Research II*, 50, 693-712.
- Hilborn, R. and Mangel, M., 1997. *The ecological detective: confronting models with data*. Princeton University Press, Princeton, New Jersey, pp.133.
- Hill, P.S., 1998. Controls on floc size in the sea. *Oceanography* 11: 13-18.
- Honeyman, B. and Santschi, P., 1989. A Brownian-pumping model for oceanic trace metal scavenging: Evidence from Th isotopes. *Journal of Marine Research*, 47, 951-992.
- Jackson, G.A. and Burd A.B., 1998. Aggregation in the marine environment. *Environ Sea Technol* 32:2805–2814.
- Karakas, G., Nowald, N., Schäfer-Neth, C., Iversen, M.,H., Barkmann, W; Fischer, G. Marchesiello, P, Schlitzer, R., 2009. Particle camera and settling chamber measurements at site PC (GeoB11834-3) and SC (GeoB12914-4) off Cape Blanc/Mauritania. doi:10.1594/PANGAEA.755951.
- Kriest, I. and Evans, G., 2000. A vertically resolved model for phytoplankton aggregation, *Proc. Indian Acad. Sci. (Earth Planet. Sci.)*, 109, 453–469.
- Lee, C., Wakeham, S.G., Hedges, J.I., 2000. Composition and flux of particulate amino acids and chloropigments in equatorial Pacific seawater and sediments. *Deep-Sea Res. I* 47: 1535-1568.
- Lee, C., Armstrong, R.A., Cochran, J.K., Engel, A., Fowler, S.W., Goutx, M., Masqué, P., Miquel, J.C., Peterson, M., Tamburini, C., Wakeham, S., 2009. MedFlux: Investigations of particle flux in the Twilight Zone. *Deep-Sea Res. II* ; 56: 1363–1368.
- Mann, K. H. and Lazier, J. R. N., 1991. *Dynamics of marine ecosystems : biological/physical interactions in the oceans*. Blackwell Scientific Publications, Boston.
- Marchel, O. and Lam, P.J., 2012. What can paired measurements of Th isotope activity and particle concentration tell us about particle cycling in the ocean? *Geochimica et Cosmochimica Acta*. 90, 126-148.

- Marty, J.C., 2002. The DYFAMED time-series program (French JGOFS). *Deep-Sea Research II*, 49, 1963-1964.
- McDonnell, A.M.P., and Buesseler, K.O., 2010. Variability in the average sinking velocity of marine particles. *Limnol. Oceanogr.*, 55(5), 2085-2096.
- Migon, C., 1993. Riverine and atmospheric inputs of heavy metals in the Ligurian Sea. *Science of the Total Environment*, 138, 289-299.
- Murnane, R.J., 1994. Determination of thorium and particulate matter cycling parameters at station P: A reanalysis and comparison of least square techniques. *Journal of Geophysical Research*, 99(C2), 3393-3405.
- Murnane, R.J., Sarmiento, J.L., Bacon M.P., 1990. Thorium isotopes, particle cycling models, and inverse calculations of model rate constants. *Journal of Geophysical Research*, 95(C9), 16195-16206.
- Murnane, R.J., Cochran, J.K., Sarmiento, J., 1994. Estimates of particle- and thorium-cycling rates in the northwest Atlantic Ocean. *Journal of Geophysical Research*, 99(C2), 3373-3392.
- Murnane, R.J., Cochran, J.K., Buesseler, K.O., Bacon, M., 1996. Least-squares estimates of thorium, particle, and nutrient cycling rate constants from the JGOFS North Atlantic Bloom Experiment. *Deep-Sea Research I*, 43(2), 239-258.
- Nozaki, Y., Horibe, Y., Tsubota, H., 1981. The water column distributions of thorium isotopes in the western North Pacific. *Earth and Planetary Science Letters*, 54, 203-216.
- Nozaki, Y., Yang, J.S., Yamada, M., 1987. Scavenging of thorium in the ocean, *J. Geophys. Res.*, 92, 772-778.
- Peterson, M.L., Thoreson, D.S., Hedges, J.I., Lee, C., Wakeham, S.G., 1993. Field evaluation of a valved sediment trap. *Limnology and Oceanography* 38, 1741–1761.
- Peterson, M. L., Wakeham, S. G., Lee, C., Askea, M. A., & Miquel, J. C., 2005. Novel techniques for collections of sinking particles in the ocean and determining their settling rates. *Limnology and Oceanography: Methods*, 3, 520-532.
- Peterson, M.L., Fabres, J., Wakeham, S.G., Lee, C., Alonso, I.J., & Miquel, J.C., 2009. Sampling the vertical particle flux in the upper water column using a large diameter free-drifting NetTrap adapted to an Indented Rotating Sphere sediment trap. *Deep-Sea Research II*, 1547-1557.
- Roy-Barman, M., Lemaitre, C., Ayrault, S., Jeandel, C., Souhaut, M., & Miquel, J.-C., 2009. The influence of particle composition on Thorium scavenging in the Mediterranean Sea. *Earth and Planetary Science Letters*, 286, 526-534.
- Sabine, C.L. and Feely, R.A., 2007. The oceanic sink for carbon dioxide. In *Greenhouse Gas Sinks*, ed. D. Reay, N. Hewitt, J. Grace, K., Smith, pp. 31-49. Oxfordshire:CABI Publishing.

- Santschi, P., Li, Y., Bell, J., 1979. Natural radionuclides in the water of Narragansett Bay. *Earth and Planetary Sciences Letters*, 45, 201-213.
- Siegenthaler, U. and Sarmiento, J., 1993. Atmospheric carbon dioxide and the ocean. *Nature*, 365, 119-125.
- Solomon, S., D. Qin, M. Manning, R.B. Alley, T. Berntsen, N.L. Bindoff, Z. Chen, A. Chidthaisong, J.M. Gregory, G.C. Hegerl, M. Heimann, B. Hewitson, B.J. Hoskins, F. Joos, J. Jouzel, V. Kattsov, U. Lohmann, T. Matsuno, M. Molina, N. Nicholls, J. Overpeck, G. Raga, V. Ramaswamy, J. Ren, M. Rusticucci, R. Somerville, T.F. Stocker, P. Whetton, R.A. Wood and D. Wratt, 2007: Technical Summary. In: *Climate Change 2007: The Physical Science Basis. Contribution of Working Group I to the Fourth Assessment Report of the Intergovernmental Panel on Climate Change* [Solomon, S., D. Qin, M. Manning, Z. Chen, M. Marquis, K.B. Averyt, M. Tignor and H.L. Miller (eds.)]. Cambridge University Press, Cambridge, United Kingdom and New York, NY, USA.
- Sun, M.-Y., Lee, C., Aller, R.C., 1993. Laboratory studies of oxic and anoxic degradation of chlorophyll-a in Long Island Sound sediments. *Geochim. Cosmochim. Acta*. 57, 147-157.
- Szlosek, J., Cochran, J.K., Miquel, J.C., Masque, P., Armstrong, R.A., Fowler, S.W., Gasser, B., Hirschberg, D.J., 2009. Particulate organic carbon-²³⁴Th relationships in particles separated by settling velocity in the northwest Mediterranean Sea. *Deep-Sea Research II*, 56, 1519-1532.
- Szymczak-Zyla, M., Kowalewska, G., Louda, J.W., 2008. The influence of microorganisms on chlorophyll a degradation in the marine environment. *Limnol. Oceanogr.*, 53(2), 85-862.
- Tarantola, A. and Valette, B., 1982a. Inverse problem=Quest for information. *Journal of Geophysics*. 50, 159-170.
- Tarantola, A. and Valette, B., 1982b. Generalized nonlinear inverse problems solved using the least square criterion. *Reviews of Geophysics and Space Physics* 20(2), 219-232.
- Trull, T.W., Bray, S.G., Buesseler, K.O., Lamborg, C.H., Manganini, S., Moy, C., Valdes, J., 2008. In situ measurements of mesopelagic particle sinking rates and the control of carbon transfer to the ocean interior during the Vertical Flux in the Global Ocean (VERTIGO) voyages in the North Pacific. *Deep-Sea Res. II* 55: 1684–1695.
- Tsunogai, S., Taguchi, K., Harada, K., 1986. Seasonal variation in the difference between observed and calculated particulate fluxes of ²³⁴Th in Funaka Bay, *Journal of the Oceanographical Society of Japan*., 42, 91-98.
- Waite, A., Fisher, A., Thompson, P. A., and Harrison, P. J., 1997. Sinking rate versus cell volume relationships illuminate sinking rate control mechanisms in marine diatoms. *Marine Ecology-Progress Series* 157, 97-108.

- Wakeham, S. G. and Lee, C., 1993. Production, transport, and alteration of particulate organic matter in the marine water column. In: M.H. Engel and S. A. Macko (eds) *Organic Geochemistry*, pp. 145-169. Plenum Press.
- Welschmeyer, N.A. and Lorenzen, C.J., 1985. Chlorophyll budgets: zooplankton grazing and phytoplankton growth in a temperate fjord and the Central Pacific Gyres. *Limnol. Oceanogr.*, 30(1), 1-21.

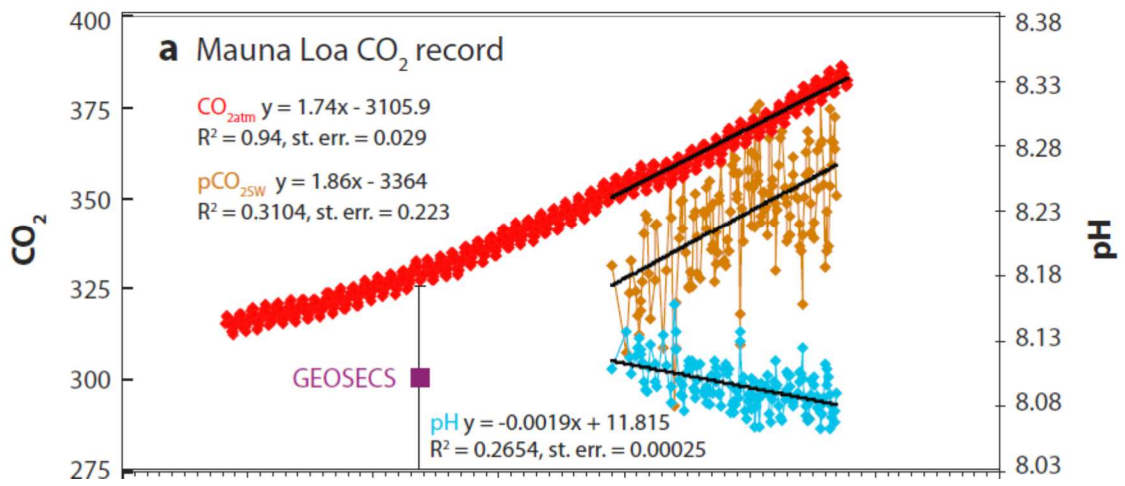


Figure 1.1. Time series of atmospheric CO₂ at Mauna Loa (in parts per million volume, ppmv) (red), surface ocean pH (cyan), and pCO₂ (μatm) (tan) at Ocean Station ALOHA in the subtropical North Pacific Ocean; (Reproduced from Doney et al., 2009)

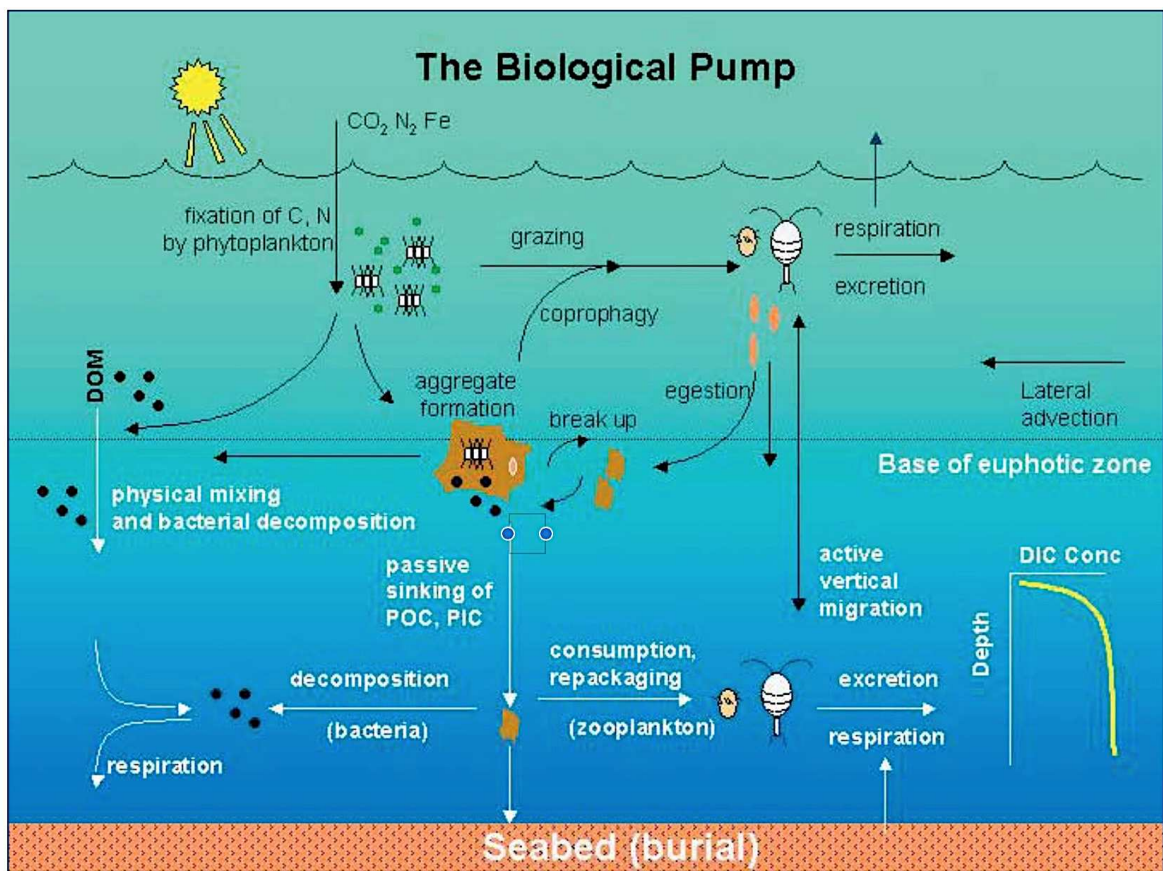


Figure 1.2. A cartoon illustrating biological and physical pumps of carbon dioxide (Reproduced from Ducklow et al., 2001).

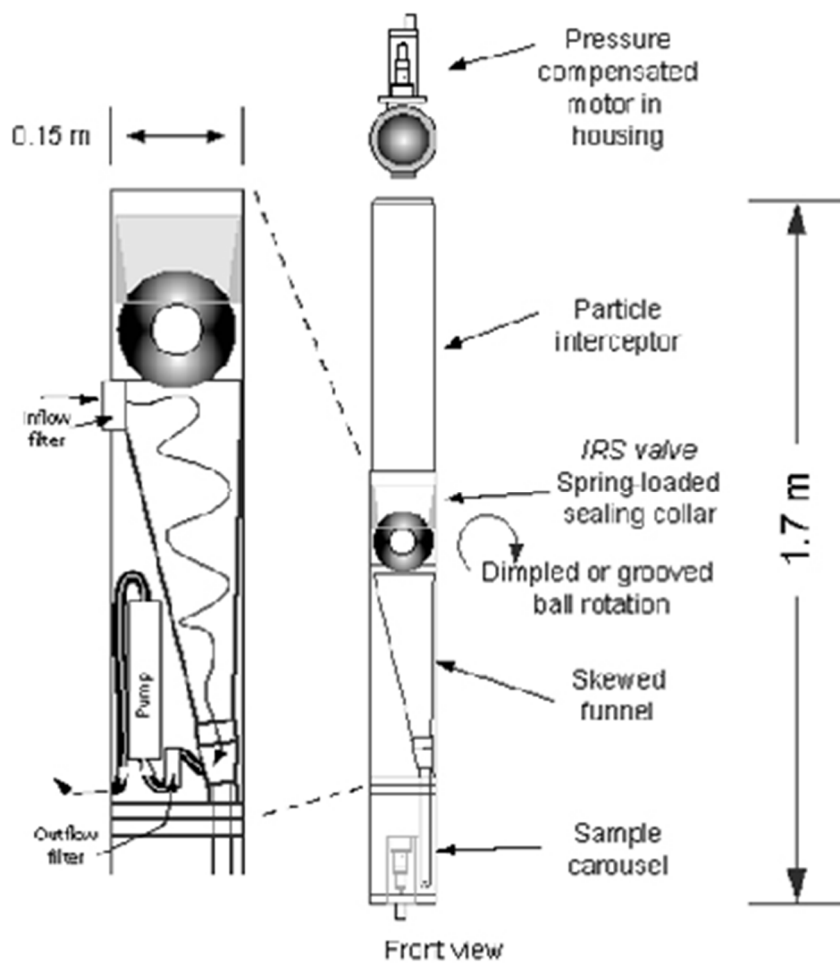


Figure 1.3. Schematic of the IRS sediment trap. (Reproduced from Peterson et al., 2009)

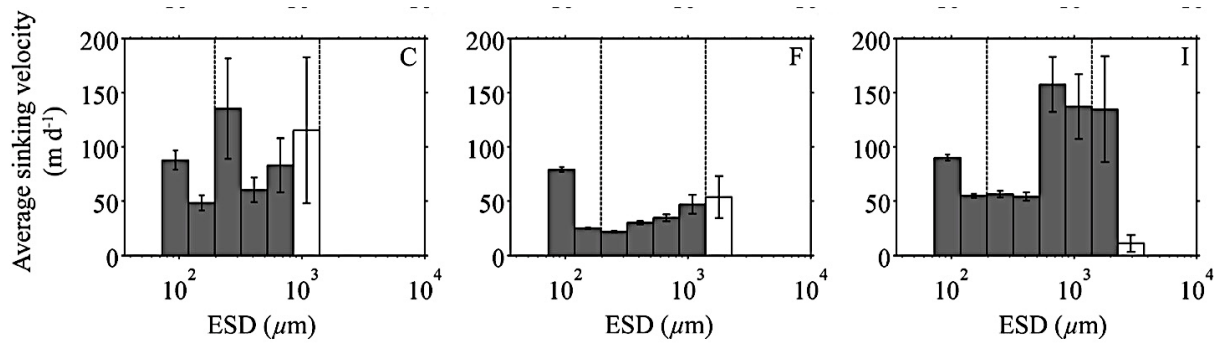


Figure 1.4. Particle size versus average sinking velocity (Reproduced from McDonnell and Buesseler, 2012). The pictures show that particle size and sinking velocity are not linearly correlated. ESD is an abbreviation of Equivalent Spherical Diameter, which is a measurement of particle size.

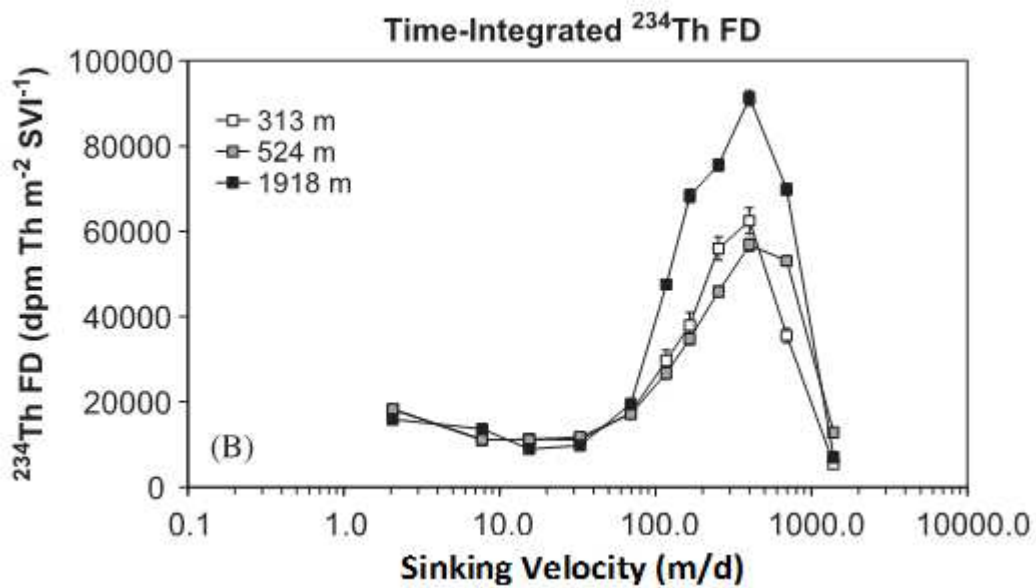


Figure 1.5. ^{234}Th time-integrated flux density at different depths for 2005 MedFlux. For details of the flux density calculations, please consult Armstrong et al. (2009). (Reproduced from Szlosek et al., 2009).

Chapter 2 : Using maximum likelihood estimation to analyze data from MedFlux settling velocity sediment traps to investigate particle cycling in the ocean

Abstract

We applied maximum likelihood estimation to MedFlux settling velocity (SV) sediment trap data; that data include particle settling velocity, particle mass fluxes, and thorium isotope (^{234}Th and ^{230}Th) fluxes in each settling velocity category. A box model that describes thorium-particle interactions was formulated by assuming steady state and first-order reaction kinetics for thorium adsorption and desorption, and for particle aggregation, disaggregation, and remineralization. The maximum likelihood method indicates that particles with settling velocities equal to or greater than 98 m/d should be treated as the fast-sinking class in the box model, and the remaining SV categories as the slow-sinking class. Adsorption rate constants for both slow- and fast-sinking particles increase slightly with depth. Desorption rate constants increase with depth from 0.04 to 15.43 y^{-1} for slow-settling particles, and from 0.30 to 52.03 y^{-1} for fast-settling particles. Aggregation and disaggregation rate constants decrease with depth from 2.11 to 0.09 y^{-1} , and from 2.42 to 1.16 y^{-1} , respectively. Production from ^{238}U radioactive decay is the main source of dissolved ^{234}Th ; radioactive decay and adsorption by particles are the main sinks for dissolved ^{234}Th . For rapid-sinking particles, adsorption is the main source; sinking is the main sink. For slow-sinking

particles, adsorption is the main source; radioactive decay and desorption are the main sink. For particulate ^{230}Th , the contributions from aggregation become more important compared to the role they play in the ^{234}Th budget.

1. Introduction

Oceanic carbon cycles have been intensively studied for many decades, due mainly to the importance of CO_2 . The atmospheric concentration of CO_2 has been increasing since the Industrial Revolution due to the combustion of fossil fuels (Siegenthaler & Sarmiento, 1993). The elevated atmospheric CO_2 concentration has induced climate changes because of the greenhouse effect (Barnett et al., 2005), and has resulted in ocean acidification because of absorption of CO_2 by seawater (Doney et al., 2009). In the euphotic zone, phytoplankton use CO_2 to synthesize organic matter; some planktonic species also utilize CO_2 to produce their carbonate shells, which along with organic matter sink after the death of organisms due to their density excess over seawater.

Sinking particles play an important role in the “biological pump”, which transports energy and organic matter from the surface water to the deep ocean and sediments. However, due to the high efficiency of heterotrophic remineralization, greater than 90% of particulate organic carbon formed in the surface water is returned to inorganic form in the euphotic zone or the upper ocean; only about 1% of organic matter survives transit from the surface ocean to depth (Wakeham and Lee, 1993; Feely et al., 2001).

Particle production, transportation, and remineralization have profound impacts on biogeochemical cycles of carbon and trace elements. Paradoxically, a few elements, such as thorium, which are not biogenic, provide an avenue by which one can study how particles change during their downward transport, including the rates at which they aggregate and disaggregate (e.g., Nozaki et al., 1981; Honeyman and Santschi, 1989; Murnane et al., 1994, 1996) and the velocity at which they are sinking (e.g., Nozaki et al., 1981; Bacon and Anderson, 1982; Bourne et al., 2012). This is because thorium isotopes are particle-reactive, and are easily scavenged onto particle surfaces: when a particle experiences a transformation such as remineralization, aggregation, or disaggregation, thorium can be used to follow these changes.

When thorium isotopes (^{234}Th and ^{230}Th , with half-lives of 24.1 days and 75,380 years, respectively) are used together, they become significantly more valuable. The application of thorium isotopes, in oceanography history, evolved from a “single isotope application” to evaluate sediment trap efficiency (e.g., Fleisher and Anderson, 2003; Roy-Barman et al., 2009), and to calculate POC flux from the surface water (e.g., Santschi et al., 1979; Coale and Bruland, 1985; Buesseler, 1998), to a “multiple isotope application” to estimate particle aggregation, disaggregation, adsorption, desorption, and sinking rates (e.g., Cochran et al., 1993, 2000; Murnane, 1994; Murnane et al., 1994, 1996;). The “multiple isotope application” has been implemented by creating box models that include dissolved thorium, plus large “sinking” and small “non-sinking” particulate thorium. In early publications (Clegg et al., 1991; Murnane et al., 1990, 1994, 1996; Cochran et al., 1993, 2000; Murnane, 1994; Marchal and Lam, 2012), the sinking rate of large “sinking” particles was arbitrarily assigned. By contrast, in the MedFlux

program, *in-situ* particle settling velocities were measured using an Indented Rotating Sphere (IRS) sediment trap in Settling Velocity (SV) mode (Peterson et al., 1993, 2009; Armstrong et al., 2009). With measured particle settling velocities, we can avoid the assumption that sinking velocity is determined only by particle size, which was a critical assumption in previous models.

The objective is to try to explain the depth distribution of ^{234}Th flux that was observed in the MedFlux program, as reported in Szlosek et al. (2009), in which slow-sinking (SV less than ≤ 49 m/d) particulate ^{234}Th flux densities were approximately the same in shallow as in deep traps, whereas fast-sinking particulate ^{234}Th flux densities in deep traps were higher than in shallow traps. Our goal here is to assess which process(es) is (are) responsible for compensating for loss by radioactive decay on slow-sinking particles and which process(es) is (are) responsible for adding ^{234}Th to fast-sinking particles when they are sinking.

2. Methods

2.1. The data

2.1.1. Dissolved ^{238}U , ^{234}U , ^{234}Th , and ^{230}Th

The distribution of ^{238}U is essentially uniform in the studied depths (313-1918 m); a constant value of 2700 dpm/m³ was therefore used at all the three trap depths. This value was measured at the DYFAMED site, and was reported in Cochran et al. (2009); this value is also consistent with the relationship between salinity and ^{238}U (Owens et al.,

2011) at a salinity of 38. The activity of ^{234}U was calculated based on the relationship $^{234}\text{U} = 1.14 \times ^{238}\text{U} = 1.14 \times 2700 = 3078 \text{ dpm/m}^3$ (Marchal and Lam, 2012).

In contrast, thorium (^{234}Th and ^{230}Th) activities vary with depth. The activities of dissolved ^{234}Th activities were from Cochran et al. (2009), in which dissolved ^{234}Th were calculated by taking differences between total thorium ^{234}Th and particulate ^{234}Th ; these quantities were sampled using Niskin bottles and Challenger Oceanic battery-operate *in-situ* pumps, respectively. However, there were no dissolved ^{234}Th data at the exact trap depths of 313 m, 524 m and 1918 m. At 313 m, dissolved ^{234}Th concentration was linearly interpolated using the data sampled at 200 m and 400 m on March 13, 2005; at 524 m, ^{234}Th concentration was linearly interpolated using the data sampled at 400 m and 600 m on March 9, 2005; at 1918 m, dissolved ^{234}Th was taken as the data sampled at 1800 m on March 9, 2005, because no deeper data were available. Based on this method, the concentration of dissolved ^{234}Th is 2518 dpm/m³ at 313 m, 2469 dpm/m³ at 524 m, and 2520 dpm/m³ at 1918 m. The activities of dissolved ^{230}Th were taken from Roy-Barman et al. (2002), who sampled at the DYFAMED site. After the unit transformation from fg/kg (used in Roy-Barman et al., 2002) to dpm/m³, the activity of dissolved ^{230}Th is 0.13 dpm/m³ at 313 m, 0.16 dpm/m³ at 524 m, and 0.17 dpm/m³ at 1918 m.

2.1.2. Sediment trap data

The data used here are from the MedFlux program, specifically from data sampled using IRS SV traps deployed in 2005 at the DYFAMED site (**Fig. 2.1**) in the Mediterranean Sea. A full description of how an IRS SV sediment trap works can be

found in Peterson et al. (1993, 2005, 2009). Generally, a chain of IRS sediment traps are bottom-tethered for a fixed interval; in the 2005 MedFlux program, the deployment time was 55 days, with actual sampling depths at 313 m, 524 m, and 1918 m. As shown in **Fig. 1.3**, sinking particles are first captured by a column-shaped particle interceptor, and fall onto an indented ball that rotates on a programmed time schedule. The rotation of sphere transfers the particles into a skewed funnel that leads to a sampling carousel, in which there are 12 sampling tubes. The carousel is programmed to rotate, and particles with different settling velocities will fall into different tubes. The full data set is available online at: <http://www.msrb.sunysb.edu/MedFlux/>. The data related to the current research are presented in **Table 2.1**.

2.2. The box model

The box model used to describe thorium cycling here (**Fig. 2.2**) differs slightly from models used in other studies (e.g., Murnane, 1994; Murnane et al., 1994, 1996; Marchal and Lam, 2012). Instead of dividing particles based on their sizes into large and small classes, we divided particles based on their sinking velocities into fast- and slow-sinking classes. Even though particles were sorted into 11 SV categories, we combined them into two classes to limit the number of parameters that are needed to be estimated. In our model we allow thorium exchange between the dissolved phase and fast-sinking class via adsorption and desorption, and ignore remineralization of fast-sinking particles. For particle cycling, the box model we used (**Fig. 2.3**) is almost

identical to that used by Murnane (1994), Murnane et al. (1994, 1996), and Marchal and Lam (2012), except that we divided particles into sinking velocity classes.

Dissolved thorium isotopes, have a source from the radioactive decay of uranium and a loss from radioactive decay. Dissolved thorium is also lost by adsorption onto sinking particles, and is added by desorption from particles and from remineralization from the slow-sinking class. For the slow-sinking class, thorium is lost by radioactive decay, desorption, particle remineralization, particle aggregation, and sinking, and is added by adsorption and fast-sinking particle disaggregation. For the fast-sinking class, thorium is lost by radioactive decay, desorption, and disaggregation, and added by adsorption and the aggregation of slow-sinking particles. All interactions are assumed to have first-order reaction kinetics.

2.3. Mathematical description

The steady state of the box model can be described by the following equation,

$$0 = flux_{in} - flux_{out} + [internal\ processes] \times \Delta z \quad (1)$$

where $flux_{in}$ term is measured by the sediment trap; however, the $flux_{out}$ term is unknown. We approximate the flux terms by assuming that they can be estimated by a flux gradient term F_i multiplied by the depth, Δz , of the box. Here comes the following equation,

$$0 = F_i \times \Delta z + [internal\ processes] \times \Delta z \quad (2)$$

Finally, we assume that F_i can be estimated using the input fluxes to two successive traps,

$$F_i = \frac{f_{i,d} - f_{i,s}}{z_d - z_s} \quad (3)$$

where i represents a specific settling velocity category; z_d and z_s mean depths of deep and shallow sediment traps, respectively; $f_{i,d}$ and $f_{i,s}$ are fluxes measured by deep and shallow sediment traps, respectively. In practice, vertical export at 313 m was calculated using data sampled at 313 m and 524 m, and at 1918 m using data sampled at 524 m and 1918 m. Vertical export at 524 m was the average of vertical exports calculated for 313 m and 1918 m.

Thorium and particle concentrations in units of dpm/m³ or mg/m³ are calculated via the following equation, which is similar to Eq. 12 in Armstrong et al. (2009):

$$[Th \text{ or } Mass] = \frac{f_i}{\omega_i} \quad (4)$$

where ω_i is a mid-point SV for category i . According to the mechanism of the SV sediment trap, SV calculated for each SV category is the minimum SV that particles have in this category. A mid-point SV is calculated by taking the mathematical average of two adjacent minimum sinking velocities.

If there are n settling categories associated with “slow-sinking” particles, the total vertical export flux by slow-sinking particles should be:

$$F_s = \frac{\sum_{i=1}^n f_i}{\Delta Z} \quad (5)$$

For thorium on slow-settling particles, the equation is:

$$F_{Th,s} = [Th_f] \times \beta_{-1} + [Th_d] \times k_s - [Th_s] \times (\lambda + k_{-1,s} + r + \beta) + Ts \quad (6)$$

For thorium on fast-settling particles, the equation is:

$$F_{Th,f} = [Th_s] \times \beta + [Th_d] \times k_f - [Th_f] \times (\lambda + k_{-1,f} + \beta_{-1}) + Tf \quad (7)$$

where $F_{Th,s}$, $F_{Th,f}$ are vertical exports of slow- and fast-sinking particulate thorium, respectively. $[Th_d]$, $[Th_s]$, and $[Th_f]$ are concentrations of dissolved thorium, slow-sinking particulate thorium, and fast-sinking particulate thorium, respectively; β_{-1} is disaggregation rate constant; k_s and k_f are adsorption rate constants of slow- and fast-sinking particles, respectively; λ is the thorium decay constant; $k_{-1,s}$ and $k_{-1,f}$ are desorption rate constants of slow- and fast-sinking particles, respectively; β and r are aggregation and remineralization rate constants; Ts and Tf are sum of advection and diffusion for slow- and fast-sinking particles, respectively. In following calculations Ts and Tf are neglected.

The following two equations describe particle cycling,

$$F_{p,s} = [P_f] \times \beta_{-1} - [P_s] \times (r + \beta) \quad (8)$$

$$F_{p,f} = [P_s] \times \beta - [P_f] \times \beta_{-1} \quad (9)$$

$F_{p,s}$ and $F_{p,f}$ are vertical export of slow- and fast-sinking particles, respectively; $[P_s]$ and $[P_f]$ are particle concentrations of slow- and fast-sinking particles, respectively.

For dissolved thorium, the equation we used is

$$Pro = [Th_d] \times (\lambda + k_s + k_f) - ([Th_s] \times k_{-1,s} + [Th_f] \times k_{-1,f}) \quad (10)$$

where Pro is the production from uranium decay. These relationships are depicted in

Fig. 2.2

2.4. Theory and algorithm of the likelihood method

Technically, if the error between a data point (y_i) and the model prediction (\hat{y}_i) of that value are normally distributed with variance σ^2 , then for that data point the best choice of parameters will be those that maximize

$$\mathcal{L}(y_i) = \frac{1}{\sqrt{(2\pi\sigma^2)}} \times \exp\left(-\frac{(y_i - \hat{y}_i)^2}{2\sigma^2}\right) \quad (11)$$

If we have n data points and assume constant variance (σ^2), the quantity to be maximized will be

$$\mathcal{L}(y_1 \cdots y_n) = \prod_{i=1}^n \left[\frac{1}{\sqrt{(2\pi\sigma^2)}} \times \exp\left(-\frac{(y_i - \hat{y}_i)^2}{2\sigma^2}\right) \right] \quad (12)$$

The natural logarithm of Eq. 10 is

$$\log \mathcal{L}(y_1 \cdots y_n) = -\frac{n}{2} \times \log[2\pi\sigma^2] - \sum \frac{(y_i - \hat{y}_i)^2}{2\sigma^2} \quad (13)$$

Finally, a standard procedure allows us to eliminate the “nuisance parameter” σ^2 (Edwards, 1992), leading to

$$\log \mathcal{L} = -\left(\frac{n}{2}\right) \times \log\left(\frac{\sum_{i=1}^n (y(i) - \widehat{y(i)})^2}{n}\right) \quad (14)$$

By maximizing likelihood, we are trying to find a set of parameters that has the highest probability of having produced the data in a sense that minimizes the difference between model predictions and measurements, thus highest likelihood. That set of

parameters is called the maximum likelihood estimate (MLE) (Hilborn and Mangel, 1997).

In this particular case, the huge differences in half-lives and concentrations between ^{234}Th and ^{230}Th lead to great differences in their variances; for example, the variance of ^{234}Th in the study area is about 9.4×10^4 ; the variance of particle mass is about 2.8×10^3 , whereas the variance of ^{230}Th is about 6.1×10^{-3} . The largely different variances apparently violate the assumption that the variance are constant. However, since likelihoods are derived from probabilities, likelihoods are multipliable:

$$\mathcal{L}\{H|data1, data2, data3, \dots\} = \mathcal{L}\{H|data1\} \times \mathcal{L}\{H|data2\} \times \mathcal{L}\{H|data3\} \times \dots, \quad (15)$$

and logarithms of likelihoods are additive:

$$\begin{aligned} \log \mathcal{L}\{H|data1, data2, data3, \dots\} \\ = \log \mathcal{L}\{H|data1\} + \log \mathcal{L}\{H|data2\} + \log \mathcal{L}\{H|data3\} + \dots \end{aligned} \quad (16)$$

This feature of likelihood enables us to include different types of data into a single framework (Hilborn and Mangel, 1997). We calculated log-likelihood separately for ^{234}Th , ^{230}Th , and particles, allowing each to have its own variance, then adding them together to get a total log-likelihood, which was maximized using a simulated annealing algorithm (Metropolis et al., 1953; Press et al., 1986; Armstrong et al., 2002). A half-million iterations were used to find the best parameter values for the model.

3. Results

3.1. Division of fast and slow-sinking classes

The division SV is defined as the SV at which the 11 SV categories were separated into two classes: categories with minimum SVs equal to or greater than the division SV are grouped into the fast-sinking class, otherwise to the slow-sinking class. Maximum likelihood versus division SV is shown in **Fig. 2.4**, which shows a distribution a little flatter than parabola with the peak at 98 m/d and a maximum log-likelihood of -52.5, which means if particles with settling velocities equal to or greater than 98 m/d are grouped as fast-sinking class and the rest as slow-sinking class, the data fit the model best.

3.2. Parameter estimates

3.2.1. Model parameters

Estimated parameter values together with reference reported values are shown in **Table 2.2**. Adsorption rate constants of slow-sinking particles increased slightly with depth from 0.61 y^{-1} to 1.04 y^{-1} . Adsorption rate constants of the fast-sinking particles are 4-7 times lower than that of slow-sinking particles, and also increase slightly with depth (0.09 to 0.25 y^{-1}). Thorium desorption rate constants increase dramatically with depth; particles. Remineralization rate constants increase from 0.01 y^{-1} at 313 m, to 0.54 y^{-1} at 1918 m. Aggregation rate constants decrease from 2.11 y^{-1} at 313 m, to 1.13 y^{-1} at 524 m to 0.09 y^{-1} at 1918 m. Disaggregation rate constants decrease from 2.42 y^{-1} at 313 m, to 1.39 y^{-1} at 524 m, and to 1.16 y^{-1} at 1918 m.

3.2.2. Processes that influence the balance of ^{234}Th

Source and sink terms for ^{234}Th are displayed in **Table 2.3 (A)**. The main source of dissolved ^{234}Th is radioactive decay of ^{238}U ; its main sink is radioactive decay. Contributions of these two processes are much higher than particle adsorption and desorption contributions, both of which increase with depth; but their differences remain relatively constant, which probably indicates that the rate particulate-dissolved thorium exchange increases with depth. For fast-sinking particulate ^{234}Th , loss through radioactive decay is relatively small, which coincides with our expectation because a large sinking speed leaves little time for radioactive decay. The major loss by vertical export is compensated by adsorption. For slow-sinking particulate ^{234}Th , due to its low sinking speed and long transition time it is mainly lost through radioactive decay, which is mainly compensated by adsorption. The loss by remineralization increases with depth, but overall its contribution is small. Aggregation of slow-sinking particles to fast-sinking particles is significant at 313 m, and decrease with depth.

3.2.3. Processes that dominate the balance of ^{230}Th

The source and sink terms for ^{230}Th are displayed in **Table 2.3 (B)**. For all three phases, the loss from radioactive decay is negligible due to its long decay half-life and low concentrations. For dissolved ^{230}Th , the source is primarily ^{234}U radioactive decay;

the major sink is adsorption by particles. For fast-sinking particulate ^{230}Th , at two shallow depths (313 m and 524 m) aggregation and adsorption together compensate the loss by vertical transport; at 1918 m, the contribution of aggregation becomes small enough to be neglected. For slow-sinking particulate ^{230}Th , adsorption is constantly a major source at all three depths; and aggregation and desorption are major sinks at 313 m and 524 m. As the aggregation contribution becomes small at 1918 m, desorption becomes the only major sink. The ^{230}Th data also indicate dissolved and particulate thorium exchange rates increase with depth. At all three depths, losses via remineralization are small enough to be ignored.

4. Discussion

4.1. Uniqueness of the current study

In previous studies, the box models were either based on data sampled by large volume pumps that sort particles based on their size (Nozaki et al., 1987), or based on a combination of pump and sediment trap data (Murnane et al., 1990, 1994, 1996). The model based solely on pump data had three phases: a dissolved phase, small particles, and large particles. Models based on those data assumed that large particles did not interact with the dissolved phase directly, but rather through small particles that were assumed to be “non-sinking”. The model based on both pump and sediment trap data

has nearly the same structure, but in this model, the “large” or “sinking” particles were sampled by sediment traps.

The previous models have three disadvantages. First, the assumption that small particles do not sink may be wrong. As reported in McDonnell and Buesseler (2010), the figures of sinking velocity versus particle size (e.g., **Fig. 1.4**) may sometimes have saddle shaped distributions; particle sinking velocity sometimes does not depend on particle size. Therefore, the assumption that small particles are “non-sinking” may be inappropriate. Second, particles caught by a large-volume pump might be a combination of “non-sinking” particles and “sinking” particles, whereas particles retained on the small pore size filter are deemed “non-sinking” particles. The last disadvantage is that the sinking velocity that these authors assigned to large particles (100 m/d in Nozaki et al., 1987, and 150 m/d in other references (Murnane et al., 1990, 1994, 1996; Marchal and Lam, 2012) might be lower than the actual particle sinking speed. For example, Armstrong et al. (2009) reported an average sinking velocity of 353 ± 76 m/d for fast-sinking fraction by modeling the data measured by settling velocity sediment traps. Xue and Armstrong (2009) gave added support and reported that particles at the DYFAMED site sank at an average velocity of 220 m/d.

The samples used in the current study were collected using IRS SV sediment traps deployed at 313 m, 524 m, and 1918 m. The advantage of the data set is that particle sinking velocities were measured directly by the SV traps, avoiding the need to arbitrarily assign a sinking speed for “large” particles. Additionally, since particles were separated by sinking speed instead of particle size, we have a direct measure of sinking velocity for “slow-sinking” particles, and do not need to rely on the indirect assumption

that “small” particles are “slow”, and that “slow” means “non-sinking”. Finally, the division between “slow” and “fast” was determined using maximum likelihood estimation, and was therefore not arbitrary.

4.2. Adsorption rate constants

To our knowledge, this is the first study using a model that separates particles into fast- and slow-sinking classes instead of large and small classes. It is also the first study that allows direct interactions between dissolved thorium and fast-sinking particles. Therefore, there is no reference available for us to make a side-by-side comparison. However, estimates of adsorption and desorption rate constants do exist, although different methods were used to obtain them. For example, Murnane et al. (1990) reported adsorption rate constants of 0.47 y^{-1} at Station P and $0.19 - 0.44 \text{ y}^{-1}$ in the western Pacific. Bacon et al. (1989) reported adsorption rate constants ranging from $0.16 - 0.47 \text{ y}^{-1}$ at the Arctic Ocean. Bacon and Anderson (1982) reported estimates of $0.2 - 1.3 \text{ y}^{-1}$ at the Panama Basin. Adsorption rate constants for slow-sinking particles in this paper range from $0.61 - 1.04 \text{ y}^{-1}$, which is in good agreement with these references. For fast-sinking particles, adsorption rate constants range from $0.09 - 0.25 \text{ y}^{-1}$, which are at the lowest end of reported values.

Our estimates of adsorption rate constants for fast-sinking particles are an order of magnitude lower than those for slow-sinking particles. We offer two explanations. First, particle composition could have an impact on thorium adsorption rate. The

composition of particles collected in the MedFlux project in the slow- and fast-sinking classes are listed in **Table 2.4**, which shows that slow-sinking particles have consistently higher organic matter content than fast-sinking particles at all three depths. Other components do not show a consistent pattern. Organic matter can enhance thorium adsorption onto particles (Chuang et al., 2014), so that it is possible that the lower organic matter content of fast-sinking particles results in lower adsorption rate constants. Another explanation is that large sinking speeds do not allow enough time for adsorption to occur. This might also explain why the adsorption rate constants for both slow- and fast-sinking particles increase with depth, even though the organic matter composition decreases with depth.

4.3. Desorption rate constants

Desorption rate constants ranged from $0.04 - 15.43 \text{ y}^{-1}$ for slow-sinking particles, and from $0.30 - 52.03 \text{ y}^{-1}$ for fast-sinking particles. For comparison, Nozaki et al. (1987) reported desorption rate constants ranging from $0.88 \pm 1.2 - 1.89 \pm 5.1 \text{ y}^{-1}$ in the western Pacific; Bacon et al. (1989) presented results that ranged from $2.6 - 9.8 \text{ y}^{-1}$ for the Arctic Ocean; and Bacon and Anderson (1982) reported a range of $1.3 - 6.3 \text{ y}^{-1}$ at the Panama Basin. Murnane et al. (1994) estimated desorption rate constants of $3.1 \pm 1.5 \text{ y}^{-1}$ at the northwestern Atlantic Ocean. Our desorption rate constant range is broader than their previously reported ranges, probably due to the use of different model structures. In addition, our prediction of a high desorption rate constant of 52.03

y^{-1} for fast-sinking particles at 1918 m indicates that ignoring the interaction between fast-sinking (“large” in the reference models) particles with the dissolved phase, as has been done in previous models, might not be appropriate. The higher desorption rate constants for fast-sinking particles than for slow-sinking particles might also be attributed to differences in organic matter content, as noted above.

An important feature of desorption rate constants is their depth distribution: the desorption rate constants for both slow- and fast-sinking particles increase with depth. The average organic carbon composition of sinking particles in SV traps decreased from 17 % at 313 m, to 12 % at 524 m, and then to 8.2 % at 1918 m; meanwhile, the opal composition decreased from 28 % at 313 m, to 18 % at 524 m, and then to 14 % at 1918 m (Lee et al., 2009). Increased desorption rate constants with depth could possibly be due to the remineralization of organic matter, or opal, or both, since the laboratory results of Chuang et al. (2014) showed that the presence of organic matter on particles could enhance the adsorption rate of radionuclides by 1 to 2 orders of magnitude.

The role that might be played by opal is still in debate. Geibert and Usbeck (2004) argued that opal is one of scavengers of the dissolved thorium. However, Chase et al. (2002) concluded that particle affinity for thorium decreases with increasing opal content. In addition, a recent study by Chuang et al. (2014) showed that silica is not responsible for enhanced sorption of radionuclide on particles. The relationship between decreasing opal content and increasing desorption rate constants is still unclear.

4.4. Remineralizaion

Remineralization rate constants in this study are lower than those reported in Clegg et al. (1991), who presented a value of 1.64 y^{-1} below 200 m and a decreasing trend with depth. Rather than showing a decreasing trend with depth, our estimates are 0.1 y^{-1} at 313 m, 0.2 y^{-1} at 524 m, and 0.54 y^{-1} at 1918 m. From Fig. 6 in Clegg et al. (1991), it can be seen that their conclusion that remineralization rate constants decrease with depth applies only to the upper 200 m, below which rate constants either increase slightly or keep constant, in good agreement with results from our two shallower depths. Unfortunately, Clegg et al. (1991) did not include a deep depth in their study. The reason for the high remineralization rate constant estimated at 1918 m in this study is not clear.

4.5. Aggregation and disaggregation

In agreement with the results reported in Clegg et al. (1991), aggregation and disaggregation rate constants in this publication decrease slightly with depth. They are lower than the average values estimated at the northwest Atlantic by Murnane et al. (1994), but are comparable with Murnane et al. (1990), in which the rate constants were modeled with data sampled at the North Pacific. Comparisons with other studies (Nozaki et al., 1987; Murnane, 1994) shows that the aggregation rate constants are comparable; disaggregation rate constants, however, are 2-3 orders of magnitude lower

than that those in the above citations. The discrepancy between our results and previous studies may be due to geographical differences, or due to the different methods used to estimate the parameters (see Chapter III). Aggregation and disaggregation fluxes are calculated by multiplying aggregation and disaggregation rate constants with slow- and fast-sinking particle concentrations, respectively. As shown in **Table 2.3**, particles do exchange via aggregation and disaggregation, which is in agreement with Abramson et al. (2010), in which the aggregation and disaggregation were studied by comparing particles' pigment and amino acid compositions sampled by large volume pumps and sediment traps in the 2005 MedFlux program.

4.6. Explanations for the depth distributions of ^{234}Th flux density

One inspiration for the current study was to seek an explanation for the flux density distributions of ^{234}Th as reported in Szlosek et al., (2009) and displayed in **Fig. 2.3**. For particles that sink very slowly (e.g., 10 m/d), the time for completing the journey from 313 m to 1918 m (depths of the shallowest and the deepest traps) is more than 5 half-lives of ^{234}Th (24.1 days), which means more than 97% ^{234}Th at 313 m will have been lost by radioactive decay when they reach 1918 m. However, **Fig. 2.3** shows that the ^{234}Th flux densities are almost the same at different depths. For fast-sinking particles, the transit time is short compared with ^{234}Th decay half-life; we therefore expect that loss by radioactive decay should be negligible, and flux density variations with depth should be small. But **Fig. 2.3** shows that deeper traps exhibit higher ^{234}Th flux densities. It is concluded that there are processes adding thorium onto sinking

particles. Our objective here was to find out which process or processes is (are) responsible for that.

For sinking particles, there are 7 processes that exert influence on the ^{234}Th budget as shown in **Fig. 2.1**: adsorption, desorption, remineralization, aggregation, disaggregation, vertical export, and radioactive decay. Their contributions to the budget are shown in **Table 2.3**. For slow-sinking particulate ^{234}Th , loss by radioactive decay is mainly compensated by adsorption of dissolved ^{234}Th . Slow-sinking particulate ^{234}Th also is lost by sinking and aggregation, but two processes together contribute about 15 - 30 % of the amount radioactive decay contributes. We conclude for slow-sinking particulate ^{234}Th , adsorption is responsible for compensating the loss by radioactive decay. For fast-sinking particulate ^{234}Th , the loss by radioactive decay is relatively small. Vertical export contributes about 80-90 % of the sink. The loss from disaggregation is negligible. Adsorption accounts for 80 – 90%, and aggregation the remaining 10 - 15% of ^{234}Th gain on fast-sinking particles. We conclude that combination of adsorption and aggregation are responsible for adding ^{234}Th to fast-sinking particles.

Conclusions

Slow-sinking particles have higher adsorption rate constants but lower desorption rate constants than fast-sinking particles. Both adsorption and desorption increase with depth. For the distribution of ^{234}Th flux density observed in the MedFlux project, our explanation is that in the transition from the surface ocean to the deep sea, the loss of

^{234}Th by radioactive decay on slow-settling particles is compensated by adsorption, and therefore that the ^{234}Th flux in slow-settling particles captured by the deep trap are approximately the same as those in the shallower traps. In contrast, fast-sinking particles also absorb thorium during sinking, but the loss from radioactive decay is low, which explains why the deep trap has higher ^{234}Th fluxes on rapidly settling particles. Interactions among slow- and fast-settling particle classes through aggregation and disaggregation are low.

Reference

- Abramson, L., Lee, C., Liu, Z., Wakeham, S.G., Szlosek, J., 2010. Exchange between suspended and sinking particles in the northwest Mediterranean as inferred from the organic composition of in situ pump and sediment trap samples. *Limnol. Oceanogr.*, 55(2), 725-739.
- Armstrong, R.A., Lee, C., Hedges, J.I., Honjo, S., Wakeham, S., 2002. A new, mechanistic model for organic carbon fluxes in the ocean based on the quantitative association of POC with ballast material. *Deep-Sea Res. II* 49, 219–236.
- Armstrong, R.A., Peterson, M.L., Lee, C., Wakeham, S.G., 2009. Settling velocity spectra and the ballast ratio hypothesis. *Deep Sea Research II*, 56, 1470-1478.
- Bacon, M.P. and Anderson, R.F., 1982. Distribution of thorium isotopes between dissolved and particulate forms in the deep sea. *Journal of Geophysical Research*, 87, 2045-2056.
- Bacon, M.P., 1984. Glacial to interglacial changes in carbonate and clay sedimentation in the Atlantic ocean estimated from ^{230}Th measurements. *Isotope Geoscience*, 2, 97-111.
- Bacon, M.P., Huh, C.A., Moore, R.M., 1989. Vertical profiles of some natural radionuclides over the Alpha Ridge, Arctic Ocean, *Earth Planet. Sc. Lett.*, 95, 15–22.

- Barnett, T.P., Adam, J.C., Lettenmaier, D.P., 2005. Potential impacts of a warming climate on water availability in snow-dominated regions. *Nature*, 438, 303-309.
- Bourguet, N., Goutx, M., Ghiglione, J.F., Mireille, P.P., Mevel, G., Momzikoff, A., Mousseau, L., Guigue, C., Garcia, N., Raimbault, P., Pete, R., Oriol, L., Lefevre, D., 2009. Lipid biomarkers and bacterial lipase activities as indicators of organic matter and bacterial dynamics in contrasted regimes at the DYFAMED site, NW Mediterranean. *Deep Sea Research II*, 56, 1454-1469.
- Bourne, M.D., Thomas, A.L., Niocail, C.M., Henderson, G.M., 2012. Improved determination of marine sedimentation rates using ^{230}Th s. *Geochemistry Geophysics Geosystems*, 13(1). doi:10.1029/2012GC004295.
- Buesseler, K.O., 1998. The decoupling of production and particulate export in the surface ocean. *Global Biogeochemical Cycles*, 12(2), 297-310.
- Chase, Z., Anderson, R.F., Fleisher, M.Q., Kubik, P.W., 2002. The influence of particle composition and particle flux on scavenging of Th, Pa and Be in the ocean. *Earth and Planetary Science Letters*, 204(1-2), 215-229.
- Chuang, C.Y., Santschi, P.H., Wen L.S., Guo, L., Xu, C., Zhang, S., Jiang, Y., Ho, Y.F., Schwehr, K.A., Quigg, A., Hung, C.C., 2014. Binding of Th, Pa, Pb, Po, and Be radionuclides to marine colloidal macromolecular organic matter. *Marine Chemistry*. doi: 10.1016/j.marchem.2014.10.014.
- Clegg, S.L., and Whitfield, M., 1991. A generalized model for the scavenging of trace metals in the open ocean, II, thorium scavenging, *Deep Sea Research, Part A*, 38, 91-120.
- Clegg, S.L., Bacon, M.P., Whitfield, M., 1991. Application of a generalized scavenging model to thorium isotope and particle data at equatorial and high-latitude sites in the Pacific Ocean. *Journal of Geophysical Research*, 96(C11), 20655-20670.
- Coale, K. and Bruland, K., 1985. ^{234}Th and ^{238}U disequilibria within the California Current. *Limnology and Oceanography*, 32(2), 189-200.
- Cochran, J.K., Buesseler, K.O., Bacon, M.P., Livingston, H., 1993. Thorium isotopes as indicators of particle dynamics in the upper ocean: results from the JGOFS North Atlantic Bloom Experiment. *Deep-Sea Research I* 40, 1569-1595.
- Cochran, J.K., Buesseler, K.O., Bacon, M.P., Wang, H.W., Hirschberg, D.J., Ball, L., Andrews, J., Crossin, G., Fleer, A., 2000. Short-lived thorium isotopes (^{234}Th , ^{228}Th) as indicators of POC export and particle cycling in the Ross Sea, Southern Ocean. *Deep-Sea Research II*, 47, 3451-3490.
- Cochran, J.K., Miquel, J.C., Armstrong, R.A., Fowler, S.W., Masque, P., Gasser, B., Hirschberg, D., Szlosek, J., Rodriguez Baena, A.M., Verdeny, E., Stewart, G.M., 2009. Time-series measurement of ^{234}Th in water column and sediment trap samples from the Northwest Mediterranean Sea. *Deep Sea Research II*, 56(18), 1487-1501.
- Doney, S.C., Fabry, V.J., Feely, R.A., Kleypas, J.A., 2009. Ocean Acidification: the other CO_2 problem. *Annual Review of Marine Sciences*, 1, 169-192.

- Edwards, A.W.F., 1992. Likelihood. Johns Hopkins University Press, Baltimore, MD.
- Feely, R., Sabine, C., Takahashi, T., & Wanninkhof, R., 2001. Uptake and storage of carbon dioxide in the oceans: the global CO₂ survey. *Oceanography*, 14(4), 18–32.
- Fleisher, M. and Anderson, R., 2003. Assessing the collection efficiency of Ross Sea sediment traps using 230Th and 231Pa. *Deep-Sea Research II*, 50, 693-712.
- Geibert, W. and Usbeck, R., 2004. Adsorption of thorium and protactinium onto different particle types: Experimental findings. *Geochimica et Cosmochimica Acta*, 68(7): 1489-1501
- Hilborn, R. and Mangel, M., 1997. The ecological detective: confronting models with data. Princeton University Press, Princeton, New Jersey, pp.133.
- Honeyman, B. and Santschi, P., 1989. A Brownian-pumping model for oceanic trace metal scavenging: Evidence from Th isotopes. *Journal of Marine Research*, 47, 951-992.
- Lavelle, J. W., Cokolet, E.D., Cannon, G.A., 1991: A model study of density intrusions into and circulation within a deep, silled estuary: Puget Sound. *J. Geophys. Res.*, 96, 16 779-16 800.
- Lee, C., Peterson, M.L., Wakeham, S.G., Armstrong, R.A., Cochran, J.K., Miquel, J.C., Fowler, S.W., Hirschberg, D., Beck, A., Xue, J., 2009. Particulate organic matter and ballast fluxes measured using time-series and settling velocity sediment traps in the northwestern Mediterranean Sea. *Deep-Sea Research II*, 56, 1420-1436.
- Marchal, O. and Lam, P., 2012. What can paired measurements of Th isotope activity and particle concentration tell us about particle cycling in the ocean? *Geochimica et Cosmochimica Acta* 90, 126-148.
- McDonnell, A.M.P. and Buesseler, K.O., 2010. Variability in the average sinking velocity of marine particles. *Limnol. Oceanogr.*, 55(5), 2085-2096.
- Metropolis, N., Rosenbluth, A.W., Rosenbluth, M.N., Teller, A.H., Teller, E., 1953. Equation of state calculations by fast computing machines. *Journal of Chemical Physics* 21, 1087–1092.
- Murnane, R.J., Sarmiento, J.L., Bacon M.P., 1990. Thorium isotopes, particle cycling models, and inverse calculations of model rate constants. *Journal of Geophysical Research*, 95(C9), 16195-16206.
- Murnane, R. J., 1994. Determination of thorium and particle matter cycling parameters at station P: A reanalysis and comparison of least squares techniques. *Journal of Geophysical Research*, 99 (C2), 3393-3405.
- Murnane, R.J., Cochran, J.K., Sarmiento, J.L., 1994. Estimates of particle- and thorium-rates in the northwest Atlantic Ocean. *Journal of Geophysical Research*, 99 (C2), 3373-3392.

- Murnane, R.J., Cochran, J.K., Buesseler, K.O., Bacon, M.P., 1996. Least-squares estimates of thorium, particle, and nutrient cycling rate constants from the JGOFS North Atlantic Bloom Experiment. *Deep-Sea Research I*, 43(2), 239-258.
- Nozaki, Y., Horibe, Y., Tsubota, H., 1981. The water column distribution of thorium isotopes in the western North Pacific, *Earth Planet Science Letter*, 54, 203-216.
- Nozaki, Y., Yang, J.S., Yamada, M., 1987. Scavenging of thorium in the ocean, *J. Geophys. Res.*, 92, 772-778.
- Owens, S.A., Buesseler, K.O., Sims, K.W.W., 2011. Re-evaluating the ^{238}U -salinity relationship in seawater: Implications for the ^{238}U - ^{234}Th disequilibrium method. *Marine Chemistry*, 127(1-4), 31-39.
- Peterson, M.L., Thoreson, D.S., Hedges, J.I., Lee, C., Wakeham, S.G., 1993. Field evaluation of a valved sediment trap. *Limnology and Oceanography*, 38, 1741-1761.
- Peterson, M.L., Wakeham, S.G., Lee, C., Askea, M., Miquel, J.C., 2005. Novel techniques for collection of sinking particles in the ocean and determining their settling rates. *Limnology and Oceanography methods*, 3, 520-532.
- Peterson, M.L., Fabres, J., Wakeham, S.G., Lee, C., Alonso, I.J., Miquel, J.C., 2009. Sampling the Vertical Particle flux in the upper water column using a large diameter free-drifting NetTrap adapted to an Indented Rotating Sphere Sediment trap. *Deep Sea Research II*, 56, 1547-1557.
- Press, W.H., Flannery, B.P., Teukolsky, S.A., Vetterling, W.T., 1986. *Numerical Recipes*. Cambridge University Press, Cambridge, England.
- Roy-Barman, M., Coppola, L., Souhaut, M., 2002. Thorium isotopes in the western Mediterranean Sea: an insight into the marine particle dynamics. *Earth and Planetary Science Letters*, 196, 161-174.
- Roy-Barman, M., Lemaitre, C., Ayrault, S., Jeandel, C., Souhaut, M., Miquel, J.C., 2009. The influence of particle composition on thorium scavenging in the Mediterranean Sea. *Earth and Planetary Science Letters*, 286, 526-534.
- Santschi, P., Li, Y., Bell, J., 1979. Natural radionuclides in the water of Narragansett Bay. *Earth and Planetary Sciences Letters*, 45, 201-213.
- Siegenthaler, U., and Sarmiento, J., 1993. Atmospheric carbon dioxide and the ocean. *Nature*, 365, 119-125.
- Szlosek, J., Cochran, J.K., Miquel, J.C., Masque, P., Armstrong, R.A., Fowler, S.W., Gasser, B., Hirschberg, D.J., 2009. Particulate organic carbon- ^{234}Th relationships in particles separated by settling velocity in the northwest Mediterranean Sea. *Deep Sea Research II*, 56, 1519-1532.
- Wakeham, S. G. and Lee, C., 1993. Production, transport, and alteration of particulate organic matter in the marine water column. In: M.H. Engel and S. A. Macko (eds) *Organic Geochemistry*, pp. 145-169. Plenum Press.

Xue, J. and Armstrong, R.A., 2009. An improved “benchmark” method for estimating particle settling velocities from time-series sediment trap fluxes. *Deep Sea Research II*, 56(18), 1479-1486.

Table 2.1. Original and newly added data. Mass flux was measured using IRS. Data that are in bold are newly added data. $^{230}\text{Thxs}$ means excess ^{230}Th , which is calibrated using ^{232}Th to correct for terrestrial influence ($^{230}\text{Thxs} = ^{230}\text{Th} - 0.57 \times ^{232}\text{Th}$)*.

Depth		Mass Flux (g/m ² /d)	Minimum SV (m/d)	Midpoint SV (m/d)	²³⁴ Th (dpm/g)	²³⁴ Th Flux (dpm/m ² /d)	²³⁰ Th (dpm/g)	²³² Th (dpm/g)	²³⁰ Thxs (dpm/g)	²³⁰ Thxs Flux (dpm/m ² /d)
313 m	SV2 02A	5.96	980	1200	4494±576	26.8	2.99±0.51	0.99±0.26	2.42	0.014
	SV2 03A	62.22	490	734.4	2803±146	174.4	3.50±0.32	3.32±0.32	1.61	0.100
	SV2 04A	75.38	326	408.0	2375±130	179.0	1.11±0.14	0.92±0.13	0.59	0.044
	SV2 05A	80.49	196	261.1	2511±138	202.1	2.09±0.19	2.27±0.20	0.80	0.064
	SV2 06A	39.30	140	167.9	2301±199	90.4	1.99±0.25	2.87±0.32	0.36	0.014
	SV2 07A	29.75	98	118.9	2517±231	74.9	2.39±0.27	2.10±0.27	1.20	0.036
	SV2 08A	26.71	49	73.5	3200±252	85.5	4.44±0.32	2.16±0.22	3.21	0.086
	SV2 09A	23.22	22	35.4	2763±273	64.2	2.05±0.22	2.04±0.23	0.88	0.021
	SV2 10A	21.83	11	16.4	2517±283	55.0	2.28±0.23	1.60±0.20	1.36	0.030
	SV2 11A	20.91	5	8.2	2594±313	54.2	3.51±0.51	0.25±0.10	3.36	0.070
	SV2 12A	88.74	0.68	3.1	3028±111	268.7	1.95±0.19	0.74±0.12	1.52	0.135
524 m	SV1 02A	33.79	980	1200	2389±86	80.7	2.23±0.18	2.43±0.20	0.85	0.029
	SV1 03B	127.75	490	734.4	2279±41	291.2	2.28±0.19	2.05±0.18	1.11	0.142
	SV1 04B	51.63	326	408.0	2804±77	144.8	3.13±0.37	2.50±0.34	1.70	0.088
	SV1 05A	55.22	196	261.1	2703±76	149.2	1.58±0.14	2.15±0.17	0.36	0.020
	SV1 06A	22.38	140	167.9	2710±122	60.6	3.88±0.32	2.76±0.27	2.31	0.052
	SV1 07A	17.74	98	118.9	2872±153	51.0	1.91±0.26	1.70±0.26	0.94	0.017
	SV1 08B	18.50	49	73.5	3072±149	56.8	4.76±0.41	1.98±0.26	3.63	0.067
	SV1 09B	16.05	22	35.4	3098±170	49.7	2.68±0.29	2.36±0.28	1.33	0.021
	SV1 10B	16.98	11	16.4	2835±161	48.1	1.83±0.23	2.81±0.32	0.23	0.004
	SV1 11B	22.28	5	8.2	3290±163	73.3	14.60±1.09	8.71±0.85	9.63	0.215
	SV1 12B	88.76	0.68	3.1	2996±78	265.9	0.98±0.14	0.61±0.11	0.63	0.056

	SV2 02B	13.68	980	1200	3308±227	45.3	4.77±0.95	5.73±1.00	1.50	0.021
	SV2 03B	100.3	490	734.4	2297±65	230.4	2.08±0.12	2.06±0.16	0.91	0.0909
	SV2 04B	71.64	326	408.0	2527±76	181.1	1.68±0.33	1.43±0.35	0.87	0.062
	SV2 05B	78.33	196	261.1	2336±72	183.0	2.62±0.14	1.60±0.10	1.70	0.134
	SV2 06B	48.45	140	167.9	2172±90	105.2	3.08±0.29	1.81±0.12	2.05	0.099
	SV2 07B	32.05	98	118.9	2625±136	84.1	1.88±0.19	2.32±0.18	0.56	0.018
	SV2 08B	34.48	49	73.5	3270±111	112.7	2.11±0.19	1.91±0.20	1.02	0.035
	SV2 09B	23.65	22	35.4	3613±138	85.4	2.25±0.16	2.26±0.19	0.96	0.023
	SV2 10B	19.30	11	16.4	3157±151	60.9	3.18±0.23	2.47±0.24	1.77	0.034
	SV2 11B	11.29	5	8.2	3201±177	36.1	11.05±0.18	2.95±0.09	9.37	0.106
	SV2 12B	93.25	0.68	3.1	2901±64	270.5	2.27±0.15	2.09±0.14	1.08	0.101
1918m	SV1+2#2	16.16	980	1200	3131±346	50.6	5.69±0.56	2.54±0.26	4.24	0.069
	SV+2#3	102.84	490	734.4	3407±62	350.4	1.04±0.11	1.87±0.20	-0.03	-0.003
	SV1+2#4	76.39	326	408.0	3532±74	269.8	1.60±0.07	1.49±0.07	0.75	0.057
	SV1+2#5	73.23	196	261.1	3758±75	275.2	1.25±0.14	1.85±0.30	0.20	0.015
	SV1+2#6	39.83	140	167.9	4202±110	167.4	1.25±0.22	1.47±0.13	0.41	0.016
	SV1+2#7	30.08	98	118.9	4227±104	127.2	3.26±0.38	2.01±0.28	2.11	0.064
	SV1+2#8	21.43	49	73.5	4569±148	97.9	4.04±0.42	1.90±0.28	2.96	0.063
	SV1+2#9	13.29	22	35.4	4254±201	56.5	2.87±0.55	1.30±0.14	2.13	0.028
	SV1+2#10	10.21	11	16.4	4349±234	44.4	7.95±0.39	2.88±0.23	6.31	0.064
	SV1+2#11	16.24	5	8.2	4435±190	72.0	3.11±0.32	2.77±0.33	1.53	0.025
	SV1+2#12	53.07	0.68	3.1	4432±100	235.2	0.49±0.12	0.71±0.09	0.09	0.005

* Bacon (1984)

Table 2.2. Summary of rate constants estimated by thorium isotopes.

References	Site	Adsorption (y^{-1})	Desorption(y^{-1})	Aggregation (y^{-1})	Disaggregation(y^{-1})
Lavelle et al. (1991)	Puget Sound	10-42	316	50±3 - 90±20	90±15 - 630±190
Nozaki et al.(1987) particulate data	Western Pacific	0.20±0.27 - 0.44±1.2	0.88±1.2– 1.89±5.1	2.36±5.9-12.3±213	148±370-788±1400
Nozaki et al. (1987) total data	Western Pacific			0.18	62
				0.14±0.01	50±5
Nozaki et al.(1987) total and particulate data	Western Pacific			0.11±0.03	16±9
Bacon et al. (1989)	Arctic Ocean	0.16 – 0.47	2.6 – 9.8		
Bacon and Anderson (1982)	Panama Basin	0.2 – 1.3	1.3 – 6.3		
Nozaki et al. (1981)	Pacific Ocean	1.5	6.3		
Clegg et al. (1991)	Equatorial Pacific	1-4	2.5±1.0	<0.1~50	<50->365
	North Pacific	3-70	2.5±1.0	<1-~40	~65
	North Pacific, range below100m	1-3	2.5±1.0	~0.7	~65
Clegg and Whitfield (1991)		0.2-2.6	1.8	3.7-640	15-6500
Munane et al. (1990)	North Pacific	0.5±1.0	1.0±0.1	0.2±0.01	0.8±0.2
Cochran et al (1993)	North Atlantic (²³⁴ Th)	-	-	1.1-33	126-407
	North Atlantic (²²⁸ Th)	-	-	-0.5-20	108-281
Cochran et al (2000)	Ross Sea, S. Ocean	-	-	0.04-0.2	2.4-13.8
This study	DYFAMED	0.09-1.04	0.04-52.03	0.09-2.11	1.16-2.42

Table 2.3. The source and sink terms for ^{234}Th (upper) and ^{230}Th (lower). A negative sign before a number indicates a sink; a positive number indicates a source. (Units: dpm/m³/y)

A). For ^{234}Th

	313m			524m			1918m		
	dissolved	Fast	Slow	dissolved	Fast	Slow	dissolved	Fast	Slow
decay*	1736	-27.7	-1043	2024	-94	-982	1586	-104	-866
adsorption	-1742	214	1528	-2204	453	1751	-3301	465	2845
desorption	5.08	-0.50	-4.58	179	-7.42	-171	1663	-53.9	-1609
reminerlization	1.23	-	-1.23	1.19	-	-1.19	61.61	-	-61.6
Sinking flux		-389	-275		-528	-413		-351	-243
aggregation		208	-208		112	-112		8.30	-8.30
disaggregation		-4.41	4.41		-2.39	2.39		-23.67	23.7
SUM	-0.03	-0.01	-0.03	-0.07	-66.51	69.55	-8.97	-59.32	80.03

* for the dissolved phase, “decay” means the difference of uranium radioactive decay production and thorium radioactive decay loss; for particulate thorium, “decay” means loss via radioactive decay.

B). For ^{230}Th

	313 m			524 m			1918 m		
	Dissolved	Fast	Slow	Dissolved	Fast	Slow	Dissolved	Fast	Slow
decay*	0.025	0.000	-0.000	0.025	0.000	0.000	0.025	0.000	0.000
adsorption	-0.090	0.011	0.079	-0.143	0.029	0.114	-0.223	0.031	0.192
desorption	0.003	-0.000	-0.003	0.077	-0.004	-0.073	0.193	-0.011	-0.182
reminerlization		-	-0.001		-	-0.001		-	-0.007
Sinking flux		-0.122	0.035		-0.073	0.007		-0.016	-0.007
aggregation		0.112	-0.112		0.048	-0.048		0.001	-0.001
disaggregation		-0.001	0.001		-0.001	0.001		-0.005	0.005
SUM	-0.062	0.000	-0.001	-0.041	-0.001	0.000	-0.005	0.000	0.000

* for the dissolved phase, “decay” means the difference of uranium radioactive decay production and thorium radioactive decay loss; for particulate thorium, “decay” means loss via radioactive decay.

Table 2.4. Particle compositions for fast- and slow-sinking classes (Reproduced from Lee et al., 2009).

Depth (m)		Organic matter (mg/g)	Lithogenic (mg/g)	Opal.H2O (mg/g)	CaCO ₃ (mg/g)
313	fast	93.71	202.28	188.24	159.86
	slow	108.24	179.89	249.65	141.35
524	fast	72.94	284.34	152.89	153.48
	slow	83.69	250.42	180.94	179.64
1918	fast	50.97	268.95	137.94	250.40
	slow	62.22	283.70	114.09	266.71

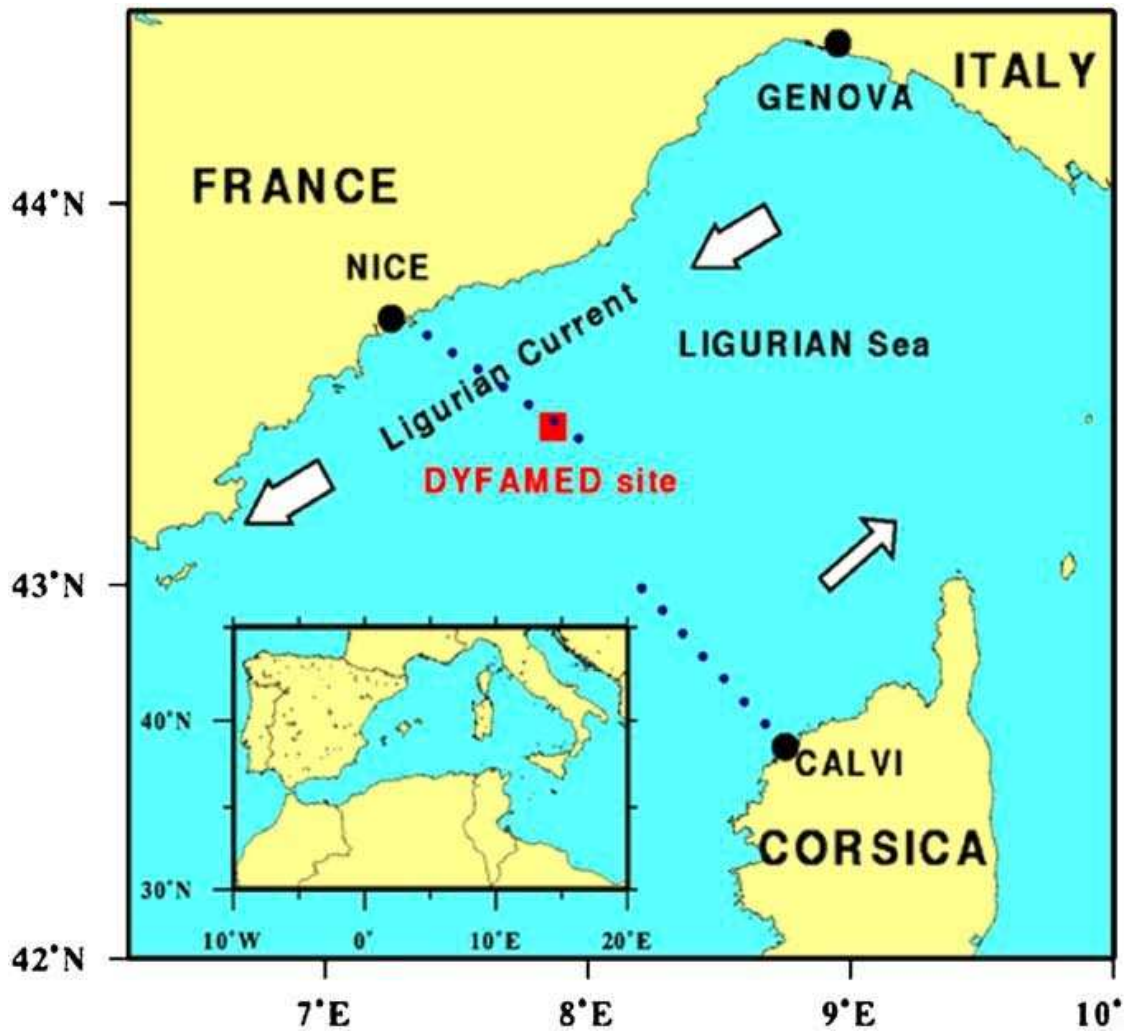


Figure 2.1. Location of the DYFAMED time-series site (Reproduced from Bourguet et al., 2009).

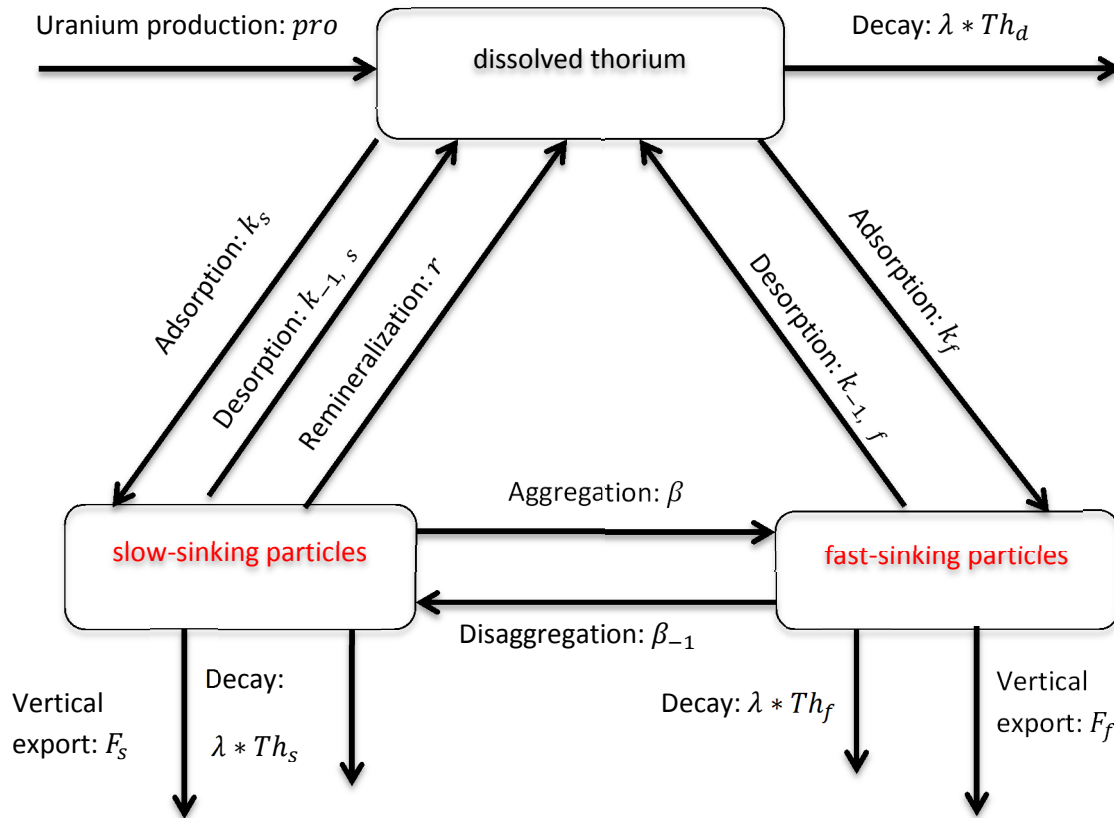


Figure 2.2. A box model describes thorium cycling. Dissolved thorium interacts with particulate thorium via adsorption, desorption, and remineralization of slow-sinking particles. In addition, dissolved thorium has a source from uranium radioactive decay and is lost via radioactive decay. Thorium on different sinking classes is exchanged via particle aggregation and disaggregation. Particulate thorium is lost through radioactive decay, vertical export, and desorption; and is gained from adsorption.

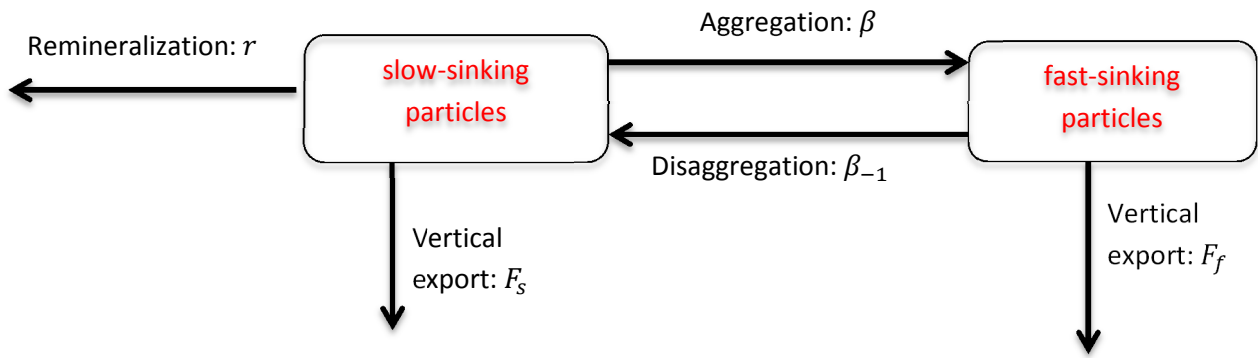


Figure 2.3. A box model describes particle cycling. Slow-sinking particles can turn into fast-sinking particles by aggregation; and fast-sinking particles can disaggregate to form slow-sinking particle. Slow-sinking particles are also lost by remineralization, which process is ignored for fast-sinking particles.

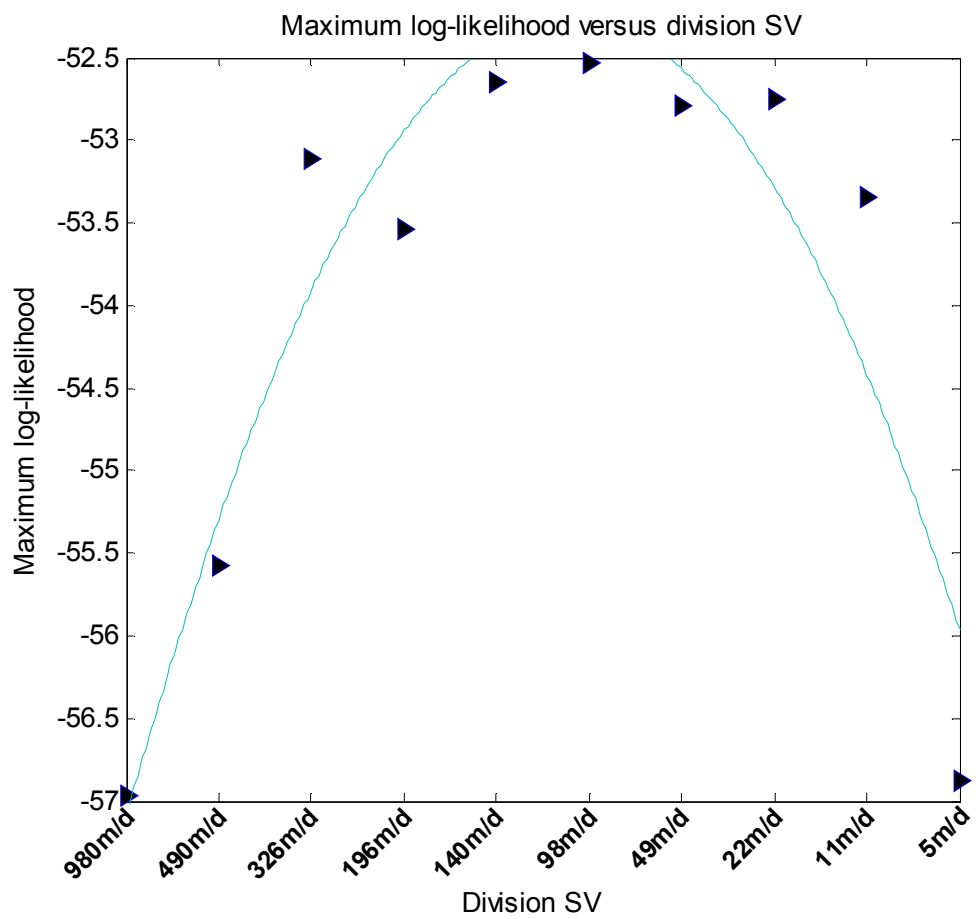


Figure 2.4. Maximum likelihood versus division settling velocity (SV), at which sinking particles were separated into fast- and slow-sinking classes as shown in the box model. The division SV means particles with sinking velocity equal to or greater than the division SV are grouped in the fast-sinking class; the rest are grouped into the slow-sinking class.

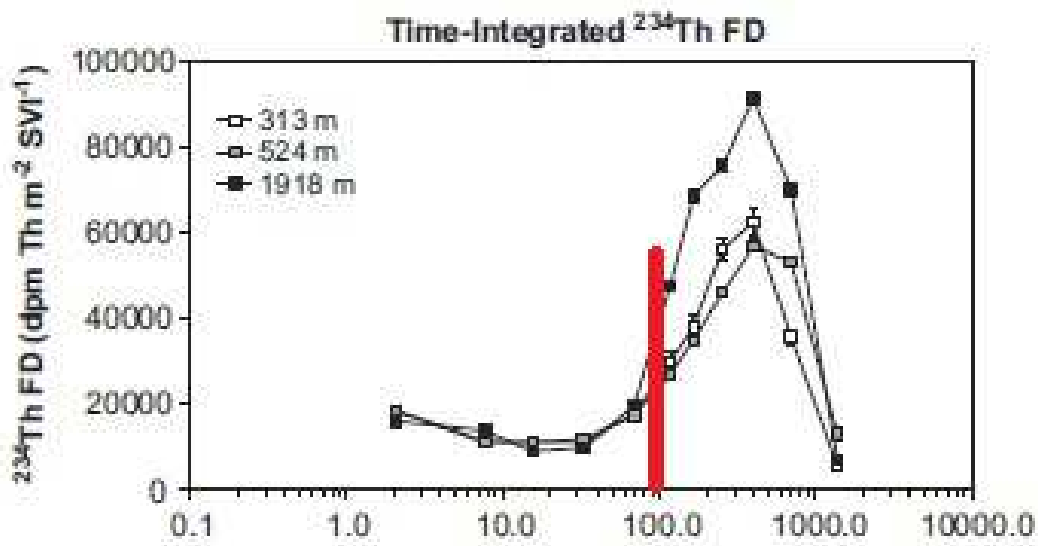


Figure 2.5. Time-integrated ^{234}Th flux density versus settling velocity with depth: SV2 at 313 m, average of SV1 and SV2 at 524 m and 1918 m. The red line separate different distribution patterns: on its left ^{234}Th flux densities were the same at different depths; on its right ^{234}Th flux density generally increased with depth. (Reproduced from Szlosek et al., 2009).

Chapter 3 : Systematic investigation of the sensitivity of the total inverse method to prior parameter values

Abstract

In this study, the total inverse method was examined with the MedFlux thorium sediment trap data (^{234}Th & ^{230}Th) obtained using Indented Rotating Sphere (IRS) Settling Velocity (SV) sediment traps in 2005 at the French Joint Global Ocean Flux Studies (DYFAMED) time-series site. By using different sets of prior estimates, prior estimates from the likelihood method and from a literature, it allows us to evaluate if and how posterior estimates change with changing prior information. The results indicate that adsorption, desorption, and remineralization rate constants are relatively well constrained by the method and the data, but that the posterior disaggregation rate constants differ widely when different priors are used. We then continued to examine likelihood sensitivities to changing priors by plotting their likelihood profiles, which indicate that likelihood is more sensitive to adsorption rate constants of both fast- and slow-sinking particles, aggregation rate constants, and remineralization rate constants than to desorption rate constants of slow-sinking particles, and is least sensitive to disaggregation rate constants and desorption rate constants of fast-sinking particles. When the whole set of parameters increased or decreased simultaneously by 2 times and the data were kept constant, the posterior parameters, including the one having the most sensitive likelihood profile, show different changing patterns, which indicates

posterior estimations depend on prior estimations, and it is unable to predict which estimations are less dependent on their prior information.

1. Introduction:

Part of our knowledge about particle cycling in the ocean comes from the study of thorium distributions due to the fact that thorium has high particle-affinity (Moore and Millward, 1988). Distributions of thorium isotopes are highly influenced by particle remineralization, aggregation, and disaggregation, and in turn thorium isotopes are excellent tracers of particle cycling. Previous researchers have taken advantage of this property and used thorium tracers to study particle cycling; for example, ^{230}Th bundled with ^{231}Pa have been used to study ocean circulation (e.g., Yu et al., 1996; Marchal, et al., 2000; Guihou et al., 2010); two or three (^{228}Th , ^{230}Th , and ^{234}Th) thorium isotopes have been used together to infer thorium adsorption and desorption rate constants (e.g., Bacon and Anderson, 1982; Nozaki et al., 1987), and particle aggregation, disaggregation, sinking rates (e.g., Murnane et al., 1990, 1994, 1996; Cochran et al., 1993, 2000; Murnane, 1994).

Particle-thorium interaction rate constants in the ocean are estimated using box models that separate particles into two classes (e.g., Tsunogai and Minagawa, 1978; Murnane et al., 1990, 1994; Murnane, 1994; Marchal and Lam, 2012): a large “sinking” class and a small “non-sinking” class. Thorium isotopes exchange between these two classes along with particle aggregation and disaggregation: large particles disaggregate into smaller particles and small particles aggregate to form larger particles. The box

model relates dissolved thorium (or other particle-reactive metals) to particulate thorium via adsorption, desorption, and remineralization.

The total inverse method, based on a least-square criterion, is widely used to infer parameters for the box model (e.g., Murnane et al., 1994, 1996; Marchal and Lam, 2012). This method was originally developed to deal with largely under-determined problems (i.e. data points are less than the number of parameters needed to be estimated; Tarantola and Valette, 1982a). Later developments made it capable to deal with either over- or under-determined problems (Tarantola and Valette, 1982a). In this theory, data and parameters are described with probability densities, and both data and parameters are optimized within ranges defined by their variances. Theoretical relationships that connect data and parameters are also described with probability densities for incorporation of theoretical errors that come from inappropriate assumptions or incomplete knowledge about their relationships.

To apply this method, a set of prior values must be assigned to data and parameters. Prior information for data comes from measurements; and prior information for parameters comes from literature values. Considering spatial and temporal variations, literature-reported parameters usually exhibit large variations; for example, according to the literature (Nozaki et al., 1981; Bacon and Anderson, 1982; Clegg et al., 1991; Murnane et al., 1994, 1996) adsorption rate constants range from $0.2 - 70 \text{ y}^{-1}$ and disaggregation rate constants range from $0.8 - 6500 \text{ y}^{-1}$. For a given unstudied area, it is difficult to choose a set of relatively accurate prior values from such a wide range, which poses a question if the total inverse method can be trusted to yield reliable parameter estimates.

In contrast to the total inverse method, the likelihood method treats data points as coming from a statistical distribution, and deals only with over-determined problems, which mean the number of parameters must be less than the number of data points, and determines a unique set of answers without altering original data. An advantage of the likelihood method is that it can deal with either linear or non-linear problems, whereas the total inverse method can be only applied to solve linear or weakly non-linear problems. Specifically in the thorium model, only with the likelihood method could one test whether better estimations can be obtained if second-order reaction kinetics rather than first-order reaction kinetics are used. In Chapter II, particle-thorium and particle-particle interaction rate constants have been estimated using the likelihood method.

In this paper, we use the results from the likelihood method (Chapter II) to divide the eleven sinking velocity categories, which were sorted by the SV traps based on particle settling velocities, into two sinking classes--fast- and slow-sinking classes. We then use prior values from both literature (Nozaki et al., 1987) and likelihood estimation (Chapter II) to calculate posterior particle-thorium interaction rate constants, and compare the posterior results obtained from these two different sets of priors to see how the posterior results depend on the choice of prior values. We then apply new estimates that use prior values that are half the likelihood results and twice the likelihood results, to test systematically the sensitivity of posterior results to changing prior estimates.

Parameter sensitivities have been studied by changing a specific data point, for example, by decreasing or increasing activity of dissolved ^{234}Th , (Murnane et al., 1990; Marchal and Lam, 2012) to check whether specific parameter(s) is (are) sensitive to the

changing data. For these tests, the same prior information for the parameters has been used. In the present paper, instead of changing one type of data, we test parameter sensitivity by plotting likelihood profiles. In practice, we systematically change the value of a parameter and keep others constant, and calculate a maximum likelihood for each change, then plot the parameter with likelihood. From likelihood profiles, we can assess how strongly likelihood is sensitive to a parameter, and so how well that parameter can be estimated.

2. Methods

2.1. Data acquisition and analysis

The data used in this study were sampled in 2005 at the French JGOFS DYFAMED time series site (water depth 2300m) (**Fig. 2.1**) at the Mediterranean Sea with Indented Rotating Sphere (IRS) sediment traps operating in Settling Velocity (SV) mode. A detailed description of the site is available at Lee et al. (2009), and of the operating mechanism of an IRS SV trap is available at Peterson et al. (1993; 2005, 2009). A schematic diagram of a SV trap is shown in **Fig.1.3**.

Traps were deployed at three depths on March 4 and recovered on May 1, 2005 for a total of deployment time of 55 days. The actual deployment depths measured by pressure sensors were 313 m, 524 m, and 1918 m. At each depth there were two SV traps and a Time Series (TS) trap. All sampling tubes were poisoned with mercuric

chloride. Sinking particles were collected and sorted into 11 settling velocity categories by SV traps, with minimum settling velocities of each category ranging from 0.68 to 980 m/d. After recovery, particles were split for different analyses, including radioisotopes and organic biomarkers. The data are available online at <http://www.bco-dmo.org/>.

The data used in the present paper are particle fluxes, ^{234}Th fluxes, and ^{230}Th fluxes. The two SV traps at 1918 m were combined to ensure measurement accuracy, since thorium activities were low in each SV trap. We combined the two SV traps at 313 m and 524 m in the same way as was done at 1918 m. The data we used are therefore particle mass fluxes, ^{234}Th fluxes, and ^{230}Th fluxes in 11 settling velocity categories at each of the three depths.

2.2. Box models

The box models used in this study are identical to the box models in Chapter II (**Fig. 2.2** and **Fig. 2.3**). We divided particles based on their sinking velocities into fast- and slow-sinking classes; in contrast to the box model in Murnane, (1994), Murnane et al. (1994, 1996), and Marchal and Lam, (2012), we allow thorium exchange between the dissolved phase and the fast-sinking class via adsorption and desorption, and ignore remineralization of fast-sinking particles due to their short residence time. For particle cycling, the box model we used is almost identical to that in Murnane (1994), Murnane et al. (1994, 1996), and Marchal and Lam (2012), except that we used settling velocity to divide particles into two classes, instead of dividing particles based on their size and assuming small particles are “non-sinking “ particles. All the interactions

between particles and between thorium and particles are assumed to follow first-order kinetics.

2.3. Total inverse method

2.3.1. Theory and algorithm

The basic argument of the total inverse method is that every measurement has error, and that therefore, instead of using a constant value, data are assumed to have normal distributions; and that if both prior and theoretical error probability density functions have normal form, the posterior probability density is also normally distributed (Tarantola and Valette, 1982a). The limit to where a parameter or a data point can vary in the inverse process is confined by its variance, which is decided based on the confidence assigned to the prior estimate: if one has high confidence, then one uses a relatively small variance, otherwise one uses a large variance.

Equations in Chapter II have been rewritten in accordance with the form $f(x) = 0$ used in the total inverse method (Tarantola and Valette, 1982a), where $f(x)$ is a combination of functions that depicts the system.

$$f(x) = \begin{Bmatrix} f^1(x^1 \dots x^m) \\ \vdots \\ f^r(x^1 \dots x^m) \end{Bmatrix} = 0 \quad (1)$$

Equations in Chapter II were modified by moving all interaction terms to the right side. On the left side we used “source minus sink (SMS)” terms, which are theoretically zero if steady states are assumed.

Equation for the dissolved thorium is

$$SMS(d) = \lambda \times ([U] - [Thd]) + ([Ths] \times k_{-1,s} + [Thf] \times k_{-1,f}) - [Thd] \times (k_f + k_s) \quad (2)$$

For slow-sinking particles, it is

$$SMS(slow) = [Thd] \times k_s + [Thf] \times \beta_{-1} - [Ths] \times (k_{-1,s} + \beta + r + \lambda) - Fs \quad (3)$$

For fast-sinking particles, it is

$$SMS(fast) = [Thd] \times k_f + [Ths] \times \beta - [Thf] \times (\beta_{-1} + k_{-1,f} + \lambda) - Ff \quad (4)$$

Equations for particles are modified in the same way.

For slow-sinking particles, it is

$$SMSp(slow) = [P_f] \times \beta_{-1} - [P_s] \times (r + \beta) - F_{p,s} \quad (5)$$

For fast-sinking particle, it is:

$$SMSp(fast) = [P_s] \times \beta - [P_f] \times \beta_{-1} - F_{p,f} \quad (6)$$

where $[Thd]$, $[Ths]$, and $[Thf]$ represent concentrations of dissolved thorium, slow-, and fast-sinking particulate thorium, respectively; $[P_s]$ and $[P_f]$ are slow- and fast-sinking particle concentrations, respectively; Fs and Ff represent vertical exports of slow- and fast-sinking particulate thorium, respectively; $F_{p,s}$ and $F_{p,f}$ represent vertical exports of slow- and fast-sinking particles, respectively; $[U]$ represents uranium concentration; k_s , $k_{-1,s}$ and r are adsorption rate constant, desorption rate constant, and remineralization rate constant of slow-sinking particles, respectively; $k_{-1,f}$ and k_f are desorption rate constant and adsorption rate constant of fast-sinking particles, respectively; β_{-1} and β are disaggregation and aggregation rate constants, respectively.

As mentioned above, measurement data are allowed to change in the inverse method, so data are also treated as “parameters”. Therefore, the vector x in Eq. 1

includes both rate constants (parameters) and measurement data, and the problem becomes non-linear because it contains products such as $[Thd] \times k_s$. The non-linear function $f(x) = 0$ defines a manifold of the system. The normally distributed prior probability density function (Eq. 7) contains on the manifold a probability density function that can be treated as posterior density function (Tarantola and Valette, 1982b):

$$\rho(x) = const. \times \exp \left\{ -\frac{1}{2} (x - x_0)^T \times C_0^{-1} \times (x - x_0) \right\} \quad (7)$$

where x_0 is prior information of the vector x ; T means transpose; C_0 denotes a covariance matrix. The way to build C_0 is discussed below. We are trying to find a vector \hat{x} that makes the posterior probability as high as possible, which is equivalent to making the exponential $s(x) = \frac{1}{2} (x - x_0)^T \times C_0^{-1} \times (x - x_0)$ as small as possible, while satisfying the condition: $f(\hat{x}) = 0$. The solution is found using a fixed-point method by iterating the following equation (Tarantola and Valette, 1982b):

$$\hat{x}_{k+1} = x_0 + C_0 \cdot F_0^T \cdot (F_k \cdot C_0 \cdot F_k^T)^{-1} \cdot \{F_k \cdot (\hat{x}_k - x_0) - f(\hat{x}_k)\} \quad (8)$$

where F is a matrix formed by partial derivatives, which are taken at the current point \hat{x}_k .

$$F^{ik} = \frac{\partial f^i}{\partial x^k} \quad (9)$$

The iteration is stopped when all the elements differ by less than 1% from those of the previous iteration.

However, when a normal distribution is assumed for a parameter, it can go negative in the inverse process if its value is small and its corresponding variance is relatively large. Negative values are not acceptable for thorium activities and rate

constants. To keep them positive, lognormal distributions instead of normal distributions were assumed as prescribed in Murnane (1994) because lognormal and normal distributions are approximately equivalent when the standard deviation is small.

Lognormal transformation was done according to the equation:

$$y' = \log(y) \quad (10)$$

where y are the variables that must be kept positive. Vertical export terms do not need lognormal transformation, because negative values are acceptable to these terms.

Equations are transformed accordingly to cope with lognormal transformed data and parameters, for example the dissolved ^{234}Th balance equation becomes:

$$\begin{aligned} SMS(dTH) = & \lambda \times (e^{\log([U])} - e^{\log([Thd])}) - (e^{\log(k_s)} + e^{\log(k_f)}) \times e^{\log([Thd])} \\ & + (e^{\log([Ths])} \times e^{\log(k_{-1,s})} + e^{\log([Thf])} \times e^{\log([k_{-1,f}]])} \end{aligned} \quad (11)$$

2.3.2. Prior information and covariance matrix determinations

Prior estimations used in the total inverse method were assigned as follows: for particulate thorium activities we used the sediment trap measurements; for thorium fluxes, uranium concentrations, and dissolved thorium concentrations, we used the values or calculations as described in Chapter II. For the adsorption, desorption, aggregation, and disaggregation rate constants, prior estimations were either from the likelihood estimations (Chapter II) or from a literature (Nozaki et al., 1987) (as shown in **Table 3.1**). The same prior values were initially assigned to the slow- and fast-sinking classes.

A uniform value of 0.05 was assigned as the relative errors for particulate ^{234}Th , which falls in the range of Szlosek et al. (2009). For ^{230}Th , the relative error used was 0.2 that was the same value used in Marchal & Lam (2012). For adsorption, desorption, aggregation, and disaggregation rate constants, the relative errors used were 1.0. For dissolved uranium, the relative error was 0.01; and for dissolved thorium, the relative error was 0.1. Because lognormal distribution has been assumed for thorium and uranium concentrations, and parameters, the relative errors have to be changed accordingly to variances as described in Marchal and Lam (2012):

$$\text{variance}_i = \log(1 + \varepsilon_i^2) \quad (12)$$

where ε is relative error. For vertical export terms, no lognormal transformation is needed, their variances were set to equal to the absolute values of the flux terms. The large variances given to the flux terms are used to counter for the potential theoretical errors. The covariance matrix (C_0) is a diagonal matrix: the elements on the diagonal are the variance of the prior estimation; the off-diagonal values are set equal to zero if we assume the covariance are zero.

2.4. Posterior results and covariance

The calculation of the error covariance is actually an approximation by using an equation prescribed in Tarantola and Valette (1982b) for linear systems:

$$C = C_0 - C_0 \cdot F^T \cdot (F \cdot C_0 \cdot F^T)^{-1} \cdot F \cdot C_0 \quad (13)$$

where C is posterior error covariance matrix; C_0 is prior error covariance matrix. One should remember that this error covariance is for lognormal transformed values. To convert to regular covariance, the formula in Aitchison and Brown (1957) (p.8, Eq. 2.8) (Marchal and Lam, 2012) was used:

$$\sigma_{a_1}^2 = \exp\left(\sigma_{\widehat{\ln a_1}}^2 + 2\widehat{\ln a_1}\right)\left(\exp\left(\sigma_{\widehat{\ln a_1}}^2\right) - 1\right) \quad (14)$$

where a_1 is a specific parameter or data point that has been lognormal transferred; $\widehat{\ln a_1}$ is the posterior estimation; $\sigma_{a_1}^2$ and $\sigma_{\widehat{\ln a_1}}^2$ are regular and posterior estimation of error variance for parameter a_1 , respectively. Posterior variances are obtained from the posterior covariance matrix. One needs to pay attention to the fact that the anti-log of a posterior estimate gives an estimation of median instead of mean (Marchal and Lam, 2012). A posterior mean value for a parameter is calculated via the following equation (Aitchison and Brown, 1957):

$$Mean_{a_1} = \exp\left(\widehat{\ln a_1} + \frac{\sigma_{\widehat{\ln a_1}}^2}{2}\right) \quad (15)$$

Both median and mean estimations for parameters are presented in **Table 3.1**.

2.5. Sensitivity tests

Sensitivity tests have been done in three ways. First, the measurement data were kept constant (including prior values and their variances); the prior parameter values from the likelihood method prediction and from literature (Nozaki et al., 1987) were used to test if different prior estimates would produce the same posterior

predictions. The comparison is shown in **Table 3.1**. Second, likelihood profiles (**Fig. 3.1**) were drawn by systematically varying a specific parameter while keeping data and other parameters constant. A likelihood profile can tell us how sensitive likelihood is to a specific parameter, in other words, the ability of the data to estimate the parameter. Third, the prior parameters from the likelihood estimation were simultaneously reduced or increased by factors of 2 to check if posterior estimates are influenced by the prior values of other parameters. Posterior estimate ratios, posterior estimates based on prior values that were from increased or decreased estimates versus posterior estimates based on likelihood results, were plotted in **Figs. 3.2**. In these tests, we supplied sufficient variances (relative error equal or greater than one) for the parameters to exclude the possibility that discrepancy of posterior results was caused by narrow ranges (defined by parameter variances) in which parameters were allowed to vary in the inverse process.

3. Results

3.1. Total inverse method parameter estimations

Posterior results (both mean and median) based on different sets of prior values (the likelihood results of Chapter II and results of Nozaki et al. 1987) are presented in **Table 3.1**. As can be seen, in both cases the posterior results are “successfully” constrained by the prior values and corresponding covariance. For most cases, the

posterior standard deviations are smaller than the prior ones (**Table 3.1**), which is a sign that our knowledge about the parameters is “improving” (Tarantola and Valette, 1982b).

The terms of “successful” and “improving” come from the function of the total inverse method that is used to improve our knowledge about a system. According to Tarantola and Valette (1982a, 1982b), for an unstudied system, one can describe it with information coming from other similar studies (prior information). This information, however, has large uncertainties (large variances). After applying the total inverse method, if a parameter has been confined in a narrower range compared with prior information, one can say our knowledge about this system is improved. The term “successful”, therefore, means “consistency” with previous studies; whereas, decreased standard deviations mean “improving”.

According to **Table 3.1**, the posterior results of remineralization, adsorption, and desorption rate constants of both slow- and fast-sinking particles agreed relatively well with each other although different sets of prior values have been used. However, the posterior disaggregation rate constants have large discrepancies, even though these parameters were allowed to change in wide ranges.

3.2. Parameter sensitivities to varied priors

Fig. 3.1 shows likelihood profiles, which indicate likelihood is most sensitive to the adsorption rate constants (both slow- and fast- sinking particles), aggregation, and remineralization rate constants: small changes of these parameter values can cause

huge likelihood changes. Likelihood is less sensitive to desorption rate constant of slow-sinking particles compared to adsorption, aggregation, and remineralization rate constants, and is least sensitive to desorption rate constants of fast-sinking particles and disaggregation rate constants. The change of disaggregation rate constant from 0 to 70 y^{-1} causes a change of log-likelihood of only ~ 6 , which is equivalent to a difference of $\sim \exp(6)$ between model prediction and measurement. To induce such a change, adsorption rate constants of slow-sinking particles only need to change from 0.8 to 1.1 y^{-1} ; adsorption by slow-sinking particles from 3 to 8 y^{-1} .

Fig. 3.2 shows posterior estimation ratios at different depths. In general, at depths of 313 m and 524 m, posterior estimates show almost similar patterns: adsorption rate constants (of both slow- and fast-sinking classes) and desorption rate constants of slow-sinking class do not show significant changes when their prior values change; remineralization rate constants, desorption rate constants of fast-sinking particle, and aggregation rate constants change in the same ratio as the prior estimates; disaggregation rate constants show more variations than others. At 1918 m, except for remineralization rate constants of slow-sinking particles, all the other parameters show large variances with changing prior parameters with different degrees.

3.3. Posterior estimates of data

One feature of the total inverse method is that it adjusts not only parameters, but also measurement data. The posterior data along with posterior parameters at three

trap depths are presented in **Tables 3.2** (A, B, C). The posterior estimates fall in ranges defined by the prior information as can be seen in **Tables 3.2** (A, B, C). The most severe deviation from prior estimates occurred at particle vertical exports (both slow- and fast-sinking classes) at 313 m and 524 m probably due to the high variances (variance equal the absolute value of prior values) used, which were assigned to vertical transport items to account for potential model errors or non-steady state conditions.

4. Discussion

4.1. Uniqueness of posterior estimates

One drawback of the total inverse method is that result uniqueness is not guaranteed. One reason as described in Tarantola and Valette (1982b) is “sparsely” distributed data. In this study, the total inverse method predicted posterior values with up to 2-orders of magnitude differences for some parameters (e.g., disaggregation rate constant) when it was seeded by different prior information (**Table 3.1**). Therefore, it is important to first consider the data. The sediment trap data have two isotopes (^{234}Th and ^{230}Th) and particle mass information available at three depths. Compared with the number of parameters (7 parameters at each depth makes a total of 21 parameters at three depths) needed to be estimated, the data are relatively sparse. In addition, the total inverse method treats the measurement data as unknown; and allows them to alter, which increase the possibility that different answers may exist. What we care

about is whether these different answers are all acceptable in the current oceanographic settings.

Due to geographic, seasonal, diurnal, and depth variations, there exist vast variations for a parameter. For example, according to the literature (Murnane et al., 1990; Clegg and Whitfield, 1991) disaggregation rate constants can range from 0.8 to 6500 y^{-1} as shown in **Table 2.2**. Both ends of the 2-orders of magnitude difference in our predictions are covered by the reported range, which gives us false confidence that both predictions are correct. However, it is not acceptable that the same data predict such different answers, which motivates us to determine which process is responsible for this difference, the data? The method? or both?

4.2. Sensitivity tests

In spite of posterior similarity of adsorption rate constants and discrepancy of disaggregation rate constants found in the current study, we also noticed that adsorption, desorption, and aggregation rate constants in the literature have relatively narrow ranges, whereas disaggregation rate constants have a relatively broad range as shown in **Table 2.2**. The reported adsorption rate constants range from 0.2 to 70 y^{-1} ; and the disaggregation rate constants range from 0.8 to 6500 y^{-1} (Nozaki et al., 1987; Bacon et al., 1989; Murnane et al., 1990; Clegg and Whitfield, 1991; Clegg et al., 1991; Cochran et al., 1993, 2000).

We may be able to explain the variation in ranges of the disaggregation, adsorption, and desorption rate constants. If we go back to the data and balance functions, taking Eq. (4) as an example, concentration of dissolved ^{234}Th in the studied location is around 2500 dpm/m^3 , whereas particulate ^{234}Th concentrations on fast- or slow-sinking particles (large “sinking” or small “non-sinking” particles in Murnane (1994)) are two to three orders of magnitude lower than the dissolved ^{234}Th . By assuming first-order reaction kinetics for adsorption and disaggregation, adsorption contribution is the product of adsorption rate constant and concentration of the dissolved ^{234}Th ; and disaggregation contribution is the product of disaggregation rate constant and concentration of fast-sinking particulate ^{234}Th . Due to the huge activity difference between the dissolved and fast-sinking particulate ^{234}Th , if we assume other parameters and data are constant, a small change of adsorption rate constant would cause a great change in disaggregation rate constant. For example, in the current study, if the contributions of vertical export and slow-sinking ^{234}Th are kept constant, a 10% decrease of adsorption rate constant (from 0.4 y^{-1} to 0.36 y^{-1}) will cause a ~5000% increase of disaggregation rate constant (from 8 y^{-1} to 400 y^{-1}).

To continue to test the total inverse method, sensitivity tests have been done by plotting likelihood profiles. In the tests, we calculated a series of maximum likelihoods by systematically changing a parameter while fixing other parameters and data at constant values. Then likelihood was plotted against the changing parameter. The results are presented in **Fig. 3.1**, which shows parameters have different impacts on likelihood. For example, the change of disaggregation rate constants from 0 to 16 y^{-1} induced a change of log-likelihood of only ~0.5 (a difference of $\exp(0.5)$ between model

prediction and measurement). However, the change of adsorption rate constant from 0.1 to 0.8 y^{-1} caused a log-likelihood change of 14 (a difference of $\exp(14)$ between model prediction and measurement). The sensitivity tests indicate that the combination of thorium isotopes is good at estimating adsorption rate constants, but not at disaggregation rate constants. The reason why there is a huge range for disaggregation rate constant reported in the literature could partially be attributed to the inverse method and the inappropriate prior estimates used.

Since likelihood profiles revealed how well a parameter can be estimated by data, it is still unclear about the extent to which a posterior parameter estimate can be influenced by prior values of other parameters. Another set of sensitivity tests, therefore, were conducted by simultaneously decreasing or increasing the whole set of likelihood estimates while keeping the data constant. The results are presented in **Fig. 3.2**, which indicates at 313 m and 524 m the posterior adsorption (of both slow- and fast-sinking classes) and desorption (of slow-sinking particles) rate constants are not influenced by the changing prior values; the other parameters show almost the same changing pattern with their prior values; at 1918 m only posterior remineralization rate constants do not change with prior information. The results, on one hand, prove the statement that the total inverse method does not guarantee a unique set of results, on the other hand they indicate that although likelihood values are highly sensitive to some parameters, they can also be influenced by the choice of prior values of other parameters.

4.3. Posterior estimates of data and model error

It has been noticed that the predicted particle vertical exports at 313 m and 524 m deviate from their prior values severely, whereas, at 1918 m, the prediction agreed very well with the prior value. As mentioned above large variances have been assigned to the export terms to counteract theoretical relationship errors. The severe posterior export deviations at the first two shallow depths probably indicate that the models at those depths had large errors. As pointed out in Marchal and Lam (2012), the box model is only a crude description of particle dynamics in the ocean. Instead of specifying a specific model error term as had been done in Marchal and Lam (2012), we assigned large variances to the vertical export flux terms for two reasons: first, nobody knows how large the model errors are, arbitrary assignments might have impacts on parameter predictions; second, vertical transport terms in our models are separated with parameters; assigning large variances has the same function as specifying separated model errors, which has been done in Marchal and Lam (2012).

Conclusions

The total inverse method is not a reliable method to make consistent predictions on particle-thorium interaction rate constants, at least with the current data: posterior estimations have large discrepancies when different sets of prior information were used. Posterior estimations are not only dependent on their prior information, but also influenced by the choice of prior estimates for other parameters.

Reference:

- Aitchison J. and Brown J. A. C., 1957. The Lognormal Distribution (With Special Reference to Its Uses in Economics). Cambridge University Press, New York, 176pp.
- Bacon, M.P., and Anderson, R.F., 1982. Distribution of thorium isotopes between dissolved and particulate forms in the deep sea. *Journal of Geophysical Research*, 87, 2045-2056.
- Bacon, M.P., Huh, C.A., Moore, R.M., 1989. Vertical profiles of some natural radionuclides over the Alpha Ridge, Arctic Ocean. *Earth Planet. Sci. Lett.*, 95, 15-22.
- Clegg, S.L., and Whitfield, M., 1991. A generalized model for the scavenging of trace metals in the open ocean, II, thorium scavenging, *Deep Sea Research, Part A*, 38, 91-120.
- Clegg, S.L., Bacon, M.P., Whitfield, M., 1991. Application of a generalized scavenging model to thorium isotope and particle data at Equatorial and high-latitude sites in the Pacific Ocean, *J. Geophys. Res*, 96, 20655-20670.
- Cochran, J.K., Buesseler, K.O., Bacon, M.P., Livingston, H., 1993. Thorium isotopes as indicators of particle dynamics in the upper ocean: results from the JGOFS North Atlantic Bloom Experiment. *Deep-Sea Research I* 40, 1569-1595.
- Cochran, J.K., Buesseler, K.O., Bacon, M.P., Wang, H.W., Hirschberg, D.J., Ball, L., Andrews, J., Crossin, G., Fleer, A., 2000. Short-lived thorium isotopes (^{234}Th , ^{228}Th) as indicators of POC export and particle cycling in the Ross Sea, Southern Ocean. *Deep-Sea Research II*, 47, 3451-3490.
- Fleisher, M. and Anderson, R., 2003. Assessing the collection efficiency of Ross Sea sediment traps using ^{230}Th and ^{231}Pa . *Deep-Sea Research II*, 50, 693-712.
- Guihou, A., Pichat, S., Nave, S., Govin, A., Labeyrie, L., Michel, E., Waelbroeck, C., 2010. Late slowdown of the Atlantic Meridional Overturning circulation during the last glacial inception: new constraints from sedimentary ($^{231}\text{Pa}/^{230}\text{Th}$). *Earth and Planetary Science Letters*, 289, 520-529.
- Lee, C., Armstrong, R.A., Cochran, J.K., Engel, A., Fowler, S.W., Goutx, M., Masque, P., Miquel, J.C., Peterson, M., Tamburini, C., Wakeham, S., 2009. MedFlux: Investigations of particle flux in the Twilight Zone. *Deep-Sea Research II*, 56, 1363-1368.

- Marchal, O., Francois, R., Stoker, T. F., Joos, F., 2000. Ocean thermohaline circulation and sedimentary $^{231}\text{Pa}/^{230}\text{Th}$ ratio. *Paleoceanography*, Vol. 15 (6), 625-641.
- Marchal, O. and Lam, P., 2012. What can paired measurements of Th isotope activity and particle concentration tell us about particle cycling in the ocean? *Geochimica et Cosmochimica Acta* 90, 126-148.
- Moore, R. M. and G. E. Millward, 1988. The kinetics of reversible Th reactions with marine particles, *Geochim. Cosmochim. Acta*, 52, 113-118.
- Murnane, R.J., Sarmiento, J.L., Bacon M.P., 1990. Thorium isotopes, particle cycling models, and inverse calculations of model rate constants. *Journal of Geophysical Research*, 95(C9), 16195-16206.
- Murnane, R. J., 1994. Determination of thorium and particle matter cycling parameters at station P: A reanalysis and comparison of least squares techniques. *Journal of Geophysical Research*, 99 (C2), 3393-3405.
- Murnane, R.J., Cochran, J.K., sarmiento, J.L., 1994. Estimates of particle- and thorium-rates in the northwest Atlantic Ocean. *Journal of Geophysical Research*, 99 (C2), 3373-3392.
- Murnane, R., Cochran, J., Buesseler, K., Bacon, M., 1996. Least-squares estimates of thorium, particle, and nutrient cycling rate constants from the JGOFS North Atlantic Bloom Experiment. *Deep-Sea Research I*, 43(2), 239-258.
- Nozaki, Y., Horibe, Y., Tsubota, H., 1981. The water column distribution of thorium isotopes in the western North Pacific, *Earth Planet Science Letter*, 54, 203-216.
- Nozaki, Y., Yang, J.S., Yamada, M., 1987. Scavenging of thorium in the ocean, *J. Geophys. Res.*, 92, 772-778.
- Peterson, M.L., Wakeham, S.G., Lee, C., Askea, M., Miquel, J.C., 2005. Novel techniques for collection of sinking particles in the ocean and determining their settling rates. *Limnology and Oceanography methods*, 3, 520-532.
- Peterson, M.L., Fabres, J., Wakeham, S.G., Lee, C., Alonso, I.J., Miquel, J.C., 2009. Sampling the Vertical Particle flux in the upper water column using a large diameter free-drifting NetTrap adapted to an Indented Rotating Sphere Sediment trap. *Deep Sea Research II*, 56, 1547-1557.
- Press, W.H., Flannery, B.P., Teukolsky, S.A., Vetterling, W.T., 1986. *Numerical Recipes*. Cambridge University Press, Cambridge, England.
- Szlosek, J., Cochran, J.K., Miquel, J.C., Masque, P., Armstrong, R.A., Fowler, S.W., Gasser, B., Hirschberg, D.J., 2009. Particulate organic carbon- ^{234}Th relationships in particles separated by settling velocity in the northwest Mediterranean Sea. *Deep Sea Research II*, 56, 1519-1532.

- Tarantola, A., and Valette, B., 1982a. Inverse problem=Quest for information. *Journal of Geophysics*. 50, 159-170.
- Tarantola, A., and Valette, B., 1982b. Generalized nonlinear inverse problems solved using the least square criterion. *Reviews of Geophysics and Space Physics* 20(2), 219-232.
- Tsunogai, S., and Minagawa, M., 1978. Settling model for the removal of insoluble chemical elements in seawater. *Geochemical Journal*, 12, 47-56.
- Yu, E.-F., Francois, R., Bacon, M., 1996. Similar rates of moder and last-glacial ocean thermohaline circulation inferred from radiochemical data. *Nature*, 379(22), 689-694.

Table 3.1. Posterior result comparisons at the depth of 313 m. Two sets of prior information were used in the total inverse method: one set was from the likelihood results; the other was from Nozaki et al. (1987), the results of which was frequently cited as prior information in similar studies. All units are y^{-1} .

	Likelihood Prior	Posterior mean	Posterior median	Nozaki, (87) Prior	Posterior mean	Posterior Median
Adsorption(s)	0.61±0.61	0.42±0.004	0.42	0.20±0.20	0.43±0.01	0.43
Desorption(s)	0.04±0.04	0.44±0.054	0.44	0.88±0.88	0.74±0.08	0.74
Remineralization(s)	0.01±0.01	0.01±0.009	0.01	0.10±0.10	0.05±0.04	0.04
Desorption(f)	0.30±0.30	0.39±0.300	0.31	0.88±0.88	1.13±0.88	0.89
Adsorption(f)	0.09±0.09	0.06±0.001	0.06	0.20±0.20	0.09±0.02	0.09
Aggregation	2.11±2.11	0.36±0.100	0.35	12.25±12.25	13.91±3.98	13.33
Disaggregation	2.42±2.42	9.71±5.060	8.61	785.00±785.00	522.19±148.22	500.55

Table 3.2. Result of the total inverse method at three trap depths with prior parameter information from the likelihood method. The units of adsorption, desorption, remineralization, aggregation, and disaggregation rate constants are y^{-1} . Thorium activities, both ^{234}Th and ^{230}Th , have the same unit of dpm/m^3 with uranium (^{238}U and ^{234}U); particle concentration has mg/m^3 ; thorium vertical export has $\text{dpm}/\text{m}^3/\text{y}$; and particle vertical export has a unit of $\text{mg}/\text{m}^3/\text{y}$.

A).

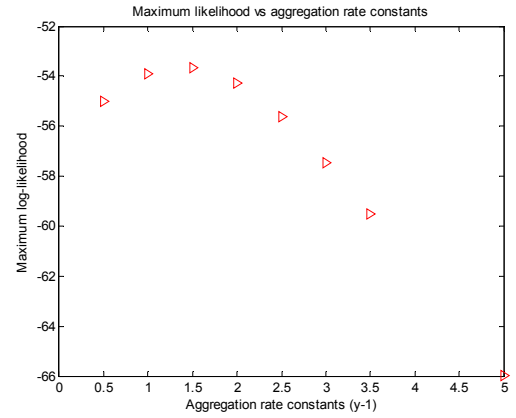
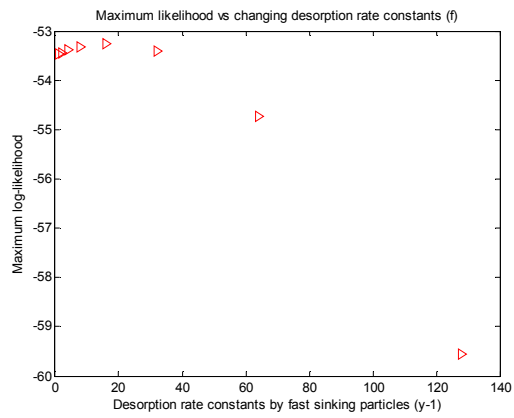
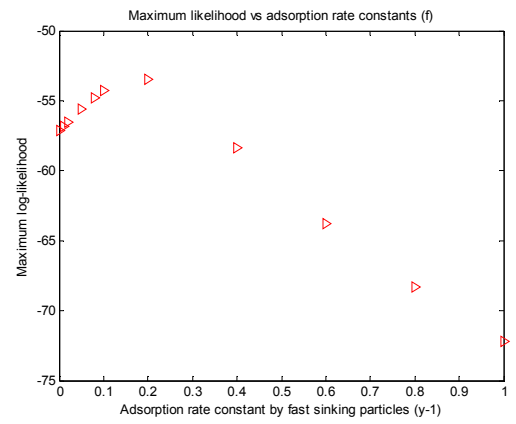
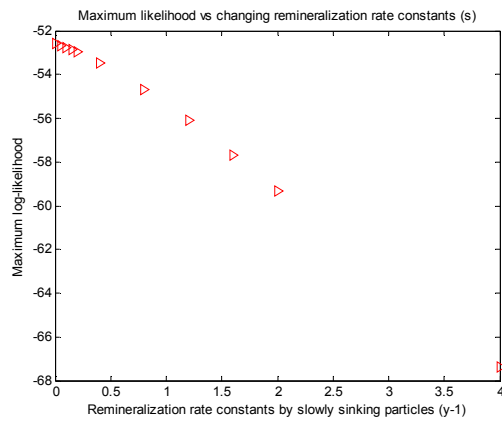
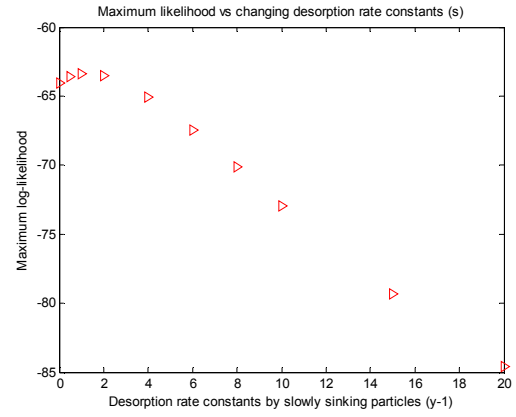
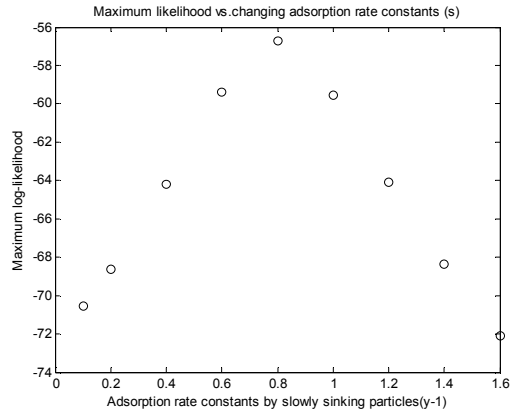
Prior information from likelihood results							
		313 m		524 m		1918 m	
parameters	Prior	Estimate	Prior	Estimate	prior	Estimate	
Adsorption(s)	0.61	0.42	0.71	0.48	1.04	0.80	
Desorption(s)	0.04	0.44	1.73	1.36	15.43	10.32	
Remineralization	0.01	0.01	0.02	0.01	0.54	0.93	
Desorption(f)	0.30	0.31	1.61	1.64	52.03	44.43	
Adsorption(f)	0.09	0.06	0.18	0.06	0.25	0.14	
Aggregation	2.11	0.35	1.13	0.22	0.09	0.06	
Disaggregation	2.42	8.61	1.39	7.19	1.16	2.55	
^{234}Th (s)	99.42	97.84	100.39	100.67	90.14	91.22	
^{230}Th (s)	0.05	0.06	0.04	0.04	0.01	0.01	
^{234}Th (f)	2.64	2.64	2.62	2.63	4.30	4.31	
^{230}Th (f)	0.00	0.00	0.00	0.00	0.00	0.00	
Conc. Particle (s)	32.68	32.44	33.66	33.44	20.36	20.37	
Conc. Particle (f)	0.91	0.92	1.07	1.07	1.11	1.11	
^{234}Th flux (s)	35.87	35.66	12.42	12.43	-11.03	-11.00	
^{234}Th flux(f)	147.95	147.41	127.30	128.64	106.65	107.17	
^{230}Th flux(s)	0.11	0.01	0.03	0.02	-0.05	0.04	
^{230}Th flux(f)	0.27	0.02	0.11	0.01	-0.05	-0.01	
Particle flux(s)	17.58	-3.60	0.53	-0.15	-16.52	-15.88	
Particle flux(f)	150.26	3.31	74.57	-0.25	-1.12	-0.73	
^{238}U	2700	2766	2700	2619	2700	2580	
^{234}U	3078	3207	3078	3071	3078	3051	
Dissolved ^{230}Th	0.130	0.120	0.160	0.161	0.170	0.179	
Dissolved ^{234}Th	2525	2648	2500	2502	2520	2475	

B).

Prior information is 2* likelihood results						
parameters	313 m		524 m		1918 m	
	Prior	Estimate	Prior	Estimate	Prior	Estimate
Adsorption(s)	1.21	0.43	1.42	0.50	2.08	1.45
Desorption(s)	0.07	0.51	3.47	1.50	30.86	26.54
Remineralization	0.02	0.02	0.03	0.02	1.08	0.88
Desorption(f)	0.60	0.62	3.22	3.28	104.05	80.85
Adsorption(f)	0.17	0.07	0.36	0.06	0.51	0.21
Aggregation	4.22	0.74	2.25	0.43	0.17	0.13
Disaggregation	4.85	25.39	2.77	14.13	2.33	3.30
²³⁴ Th (s)	99.42	98.42	100.39	101.22	90.14	92.21
²³⁰ Th (s)	0.05	0.06	0.04	0.04	0.01	0.01
²³⁴ Th (f)	2.64	2.64	2.62	2.63	4.30	4.32
²³⁰ Th (f)	0.00	0.00	0.00	0.00	0.00	0.00
Conc. Particle (s)	32.68	32.47	33.66	33.45	20.36	20.32
Conc. Particle (f)	0.91	0.92	1.07	1.07	1.11	1.11
²³⁴ Th flux (s)	35.87	35.75	12.42	12.46	-11.03	-11.00
²³⁴ Th flux(f)	147.95	148.44	127.30	129.56	106.65	107.22
²³⁰ Th flux(s)	0.11	0.00	0.03	0.02	-0.05	0.06
²³⁰ Th flux(f)	0.27	0.03	0.11	0.01	-0.05	-0.03
Particle flux(s)	17.58	-1.37	0.53	-0.07	-16.52	-16.79
Particle flux(f)	150.26	0.86	74.57	-0.60	-1.12	-1.00
²³⁸ U	2700	2712	2700	2571	2700	2515
²³⁴ U	3078	3166	3078	3054	3078	3050
Dissolved ²³⁰ Th	0.130	0.123	0.160	0.164	0.170	0.187
Dissolved ²³⁴ Th	2525	2593	2500	2453	2520	2409

C).

Prior information is 0.5* likelihood results						
	313 m		524 m		1918 m	
parameters	Prior	Estimate	Prior	Estimate	Prior	Estimate
Adsorption(s)	0.30	0.41	0.36	0.47	0.5	0.63
Desorption(s)	0.02	0.38	0.87	1.22	7.71	6.57
Remineralization	0.01	0.00	0.01	0.01	0.27	0.75
Desorption(f)	0.15	0.15	0.80	0.81	26.01	26.47
Adsorption(f)	0.04	0.06	0.09	0.06	0.13	0.10
Aggregation	1.06	0.21	0.56	0.11	0.04	0.03
Disaggregation	1.21	1.77	0.69	3.35	0.58	0.89
²³⁴ Th (s)	99.42	97.1	100.4	100.1	90.2	99.4
²³⁰ Th (s)	0.05	0.06	0.04	0.04	0.01	0.05
²³⁴ Th (f)	2.64	2.64	2.62	2.62	4.30	2.64
²³⁰ Th (f)	0.00	0.00	0.00	0.00	0.00	0.00
Conc. Particle (s)	32.68	32.47	33.66	33.44	20.41	32.68
Conc. Particle (f)	0.91	0.91	1.07	1.07	1.11	0.91
²³⁴ Th flux (s)	35.87	35.55	12.42	12.41	-11.03	-11.02
²³⁴ Th flux(f)	147.9	146.3	127.3	127.7	106.7	106.8
²³⁰ Th flux(s)	0.11	0.01	0.03	0.02	-0.05	0.03
²³⁰ Th flux(f)	0.27	0.02	0.11	0.01	-0.05	-0.01
Particle flux(s)	17.58	-5.43	0.53	-0.33	-16.52	-14.90
Particle flux(f)	150	5.27	74.57	0.11	-1.12	-0.33
²³⁸ U	2700	2826	2700	2666	2700	2652
²³⁴ U	3078	3262	3078	3088	3078	3072
Dissolved ²³⁰ Th	0.130	0.117	0.160	0.158	0.170	0.171
Dissolved ²³⁴ Th	2525	2709	2500	2550	2520	2547



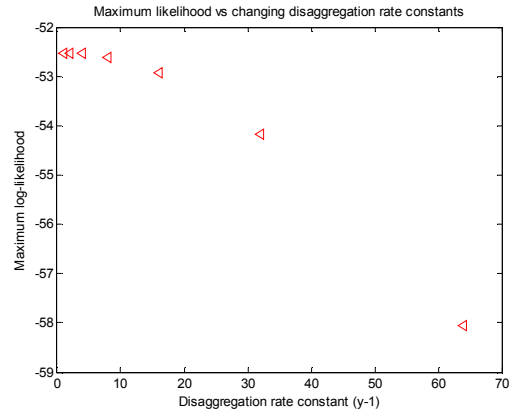


Figure 3.1. Likelihood sensitivity tests. These tests were done by systematically changing a parameter at the same time fixing data and other parameters. A maximum likelihood was calculated for each change, and then was plotted with the changing parameter.

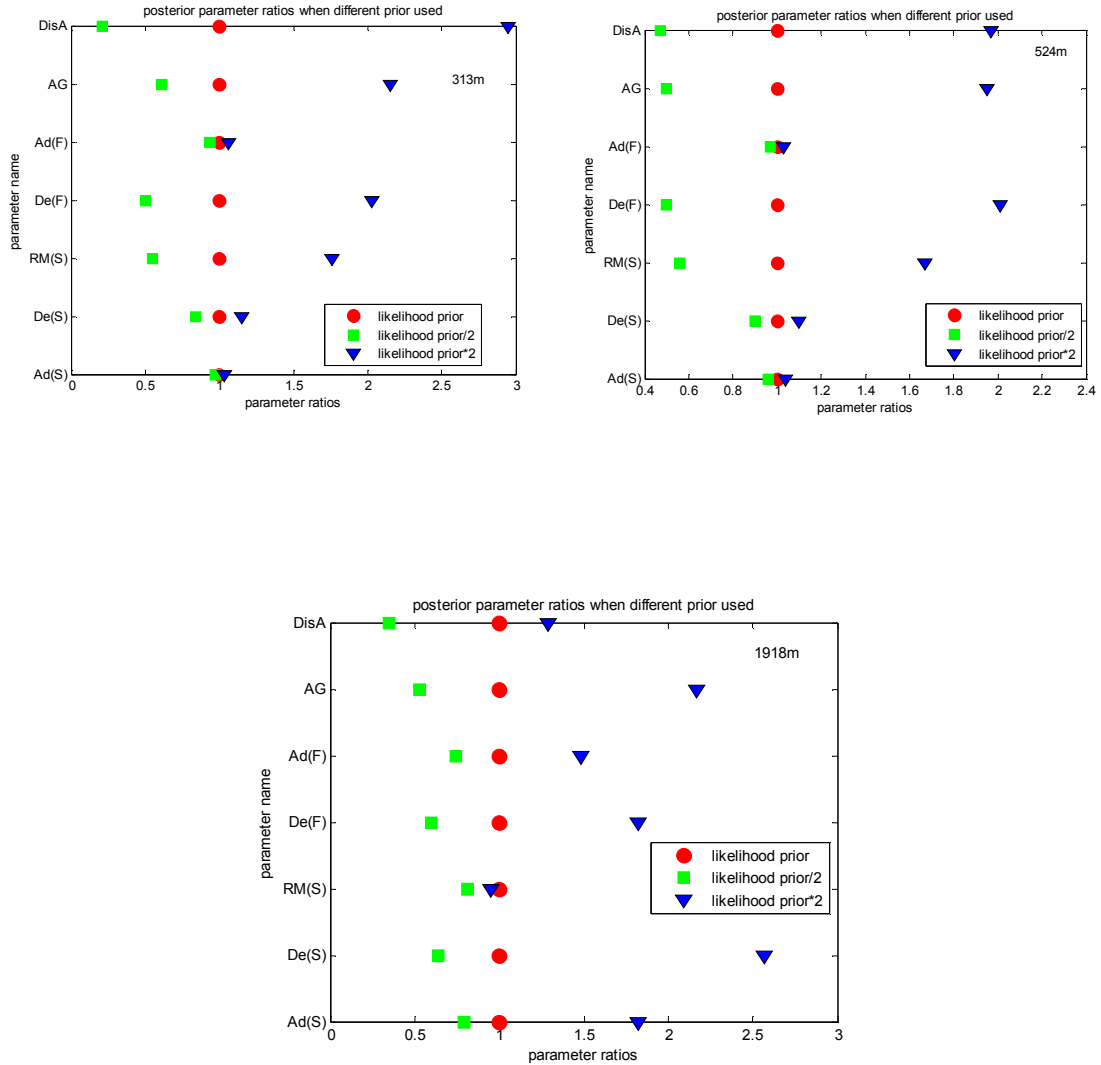


Figure 3.2. Posterior parameter ratios at 313 m, 524 m, and 1918 m. The red dots are the ratios of posterior parameter results calculated based likelihood results versus themselves. The green square represent the ratios of posterior parameter values based on half the likelihood results as versus corresponding posterior parameter values based on likelihood results. The blue triangles represent the ratios of posterior parameter values based on twice the likelihood results versus corresponding posterior parameter values based on likelihood results.

Chapter 4 : Using maximum likelihood method and MedFlux pigment data to constrain particle exchange and organic matter remineralization rate constants

Abstract

Here we constructed a box model to describe chloropigment and organic matter (OM) cycling. The box model was fit to chloropigment data sampled in the 2005 MedFlux project using Indented Rotating Sphere (IRS) sediment traps operating in Settling Velocity (SV) mode. Maximum likelihood was used to estimate particle aggregation, disaggregation, and organic matter remineralization rate constants. The 11 settling velocity categories collected by SV sediment traps were grouped into two sinking velocity classes (fast-sinking and slow-sinking classes) to decrease the number of parameters that needed to be estimated. The cutoff SV of 5 m/d for chloropigments is much less than that (98 m/d) obtained when thorium activities from the same samples were compared. Organic matter degradation rate constants were estimated to be 1.16, 1.55, and 1.11 y^{-1} , which are equivalent to degradation half-lives of 0.60, 0.45, and 0.62 years, at 313 m, 524 m, and 1918 m, respectively. Rate constants of chlorophyll *a* degradation to pheopigments (pheophorbide, pheophytin, and pyropheophorbide) were estimated to be 0.88, 0.93, and 1.17 y^{-1} , at 313 m, 524 m, and 1918 m, respectively. Aggregation rate constants are almost constant through depth with the highest value of

0.07 y^{-1} at 524 m. Disaggregation rate constants are highest at 524 m and lowest at 1918 m, with values of 13.82 y^{-1} and 9.60 y^{-1} , respectively.

1. Introduction

Sinking particles play a pivotal role in the oceanic “biological pump” that transfers photosynthesized products and energy from the euphotic zone into the deep ocean (McCave, 1975; Honjo, 1980). However, the transfer efficiency is low: only a small portion of organic matter survives transit through the water column (Hedges, 1992). Particle sinking velocity, a factor that controls particle residence time, plays an important role in regulating transfer efficiency. Where Stokes’ Law holds, larger particles sink faster, and aggregation of small particles into large particles increases transfer efficiency.

The extent to which particles aggregate and disaggregate has been estimated with radiochemical tracers (e.g., Nozaki et al., 1987; Murnane et al., 1990, 1994; Clegg et al., 1991; Cochran et al., 1993; 2000). However, parameters estimated using radionuclides sometimes have wide ranges. For example, the range of disaggregation rate constants estimated by Clegg and Whitfield (1991) were 15 - 6500 y^{-1} ; and Murnane et al. (1990; and Chapter II) estimated disaggregation rate constants of 0.8 y^{-1} and $\sim 2 y^{-1}$, respectively. In spite of geographical, seasonal, and depth influences, as pointed out in Chapter III the widely varied disaggregation rate constants were caused partially by the use of radionuclide tracers. Instead of using radionuclide data, we

applied the likelihood method to chloropigment tracers to seek better results. In contrast to radionuclides, pigment tracers are themselves an integral part of particles, and therefore should more accurately record gross particle cycling.

Chlorophyll *a* (Chl *a*), an important light absorber found in all phytoplankton, undergoes degradation during particle transit from surface water into the deep sea. The degradation can be caused either by photolysis to colorless compounds, or by zooplankton degradation to pheopigments (pheophorbide, pheophytin, and pyropheophorbide; Szymczak-Zyla et al., 2008), which have ring structures similar to that of Chl *a* (Sun et al., 1993a). Chl *a* is used as a proxy to represent biomass of algae, which are small in size and sink slowly, whereas pheopigments are the products of herbivore grazing, and are therefore inside zooplankton fecal pellets, which are assumed to sink fast in the water column (Welschmeyer and Lorenzen, 1985). During their transit through the water column, particles are thought to continuously exchange their compositions through aggregation and disaggregation (Hill, 1998). Thus, Chl *a* and pheopigments can be used as proxies to record particle exchanges, because they have very distinct sources.

The purpose of this paper is to estimate particle aggregation and disaggregation rate constants, and organic carbon degradation rate constants, using pigment data obtained at the French JGOFS DYFAMED time-series (TS) site (**Fig. 2.1**) in 2005 during the MedFlux Program. The present modeling study was motivated by the findings of Abramson et al. (2010), in which pigment compositions were compared between particles sampled by *in-situ* large volume pumps, which are assumed to sample both “sinking” and “non-sinking” particles indiscriminately, and particles sampled by Time

Series (TS) sediment traps that sampled passively “sinking” particles. Abramson et al. (2010) showed that there were distinct differences in pigment composition between particles sampled by pumps and by sediment traps during the high-productivity spring bloom period, and that pigment composition differences became less apparent during the low-productivity summer period. These observations suggested that during the spring bloom, particle exchanges were limited, while during the low-productive summer period particle exchanges were extensive.

However, Abramson et al. (2010) were not able to estimate quantitatively the rate at which rate particles exchange. In this paper, we study particle exchange from a quantitative view by estimating particle exchange rate constants. Rather than using TS sediment trap and pump data, the present paper uses settling velocity (SV) sediment trap data, which include pigment and organic matter fluxes in 11 settling velocity categories.

2. Methods

2.1. Sampling location and sampling methods

Sinking particles were collected using Indented Rotating Sphere (IRS) SV sediment traps, which were deployed at the French JGOFS DYFAMED site (43° 20'N, 7° 40'E) (**Fig. 2.1**) in 2005 (Lee et al., 2009a). The sampling site, though only ~53 km off the coast of Nice in the Ligurian Sea, has many open-ocean characteristics because the terrestrial influence is largely cut off by the cross-coastal Ligurian current (Marty, 2002).

As a site located in the northern hemisphere mid-latitude, it experiences a phytoplankton spring bloom from March to April followed by stratification and a period of low primary production in summer. The decrease of stratification in autumn promotes another, smaller phytoplankton bloom, which is terminated by decreased temperature and intensified mixing in winter.

The IRS sediment trap was originally invented to exclude swimmers (Peterson et al., 1993); this innovation was later exploited to allow it to sort sinking particles based on particle settling velocity (Peterson et al., 1993, 2005, 2009). The operating mechanism has been detailed in Peterson et al. (1993, 2005, 2009). Generally, as shown in **Fig. 1.3**, sinking particles are first caught by a cylindrical particle interceptor; they then deposit on an indented sphere that is programmed to rotate. The rotation of the ball dumps the particles deposited on its surface into a skewed funnel that leads to a 12-chamber sampling carousel, on which there are 11 sampling tubes, filled with filtered sea water sampled at trap depths, and poisoned with HgCl_2 . The first sampling chamber is an open drain to prevent loss of sample in an open tube during trap deployment and recovery. Different rotation schedules of the rotating sphere and of the sampling carousel can separate particles based on either collection date (time-series [TS] mode) or particle settling velocity (SV mode).

Total particulate organic carbon (TPC) and particulate organic carbon (POC) analyses were performed as described in Hedges and Stern (1984), and were summarized in Lee et al. (2009b) and Abramson et al. (2010). TPC was determined using a Carlo Erba EA-1100 CHN analyzer. POC was determined after removing inorganic carbon by fuming POC samples in HCl vapor for 2 hours. Analytical error was

~2%. Chloropigments were extracted in acetone, and quantified with high performance chromatography as described by Wakeham et al. (2009).

2.2. The box model

In building a box model that describes chloropigment cycling, we made the following assumptions over the time scale of sinking particles. (1), primary production at our study depths, which were below the euphotic zone (313 m -1918 m), was ignored; (2), steady state was assumed; (3), particle aggregation, disaggregation, Chl *a* degradation, and organic matter degradation were all assumed to have first-order reaction kinetics in agreement with Murnane et al. (1994, 1996) and Stephens et al. (1997); (4), Chl *a* was assumed to degrade into pheopigments only in slow-sinking particles; and the amount of Chl *a* lost by degradation was assumed to equal to the amount of pheopigments gained (Shuman and Lorenzen, 1975); (5), pheopigments were assumed to have the same degradation rate constants as total organic matter; (6), Chl *a* and organic matter degradation in fast-sinking particles were neglected due to their short residence time in the water column.

The box model is shown in **Fig. 4.1** that describes the exchanges between fast- and slow-sinking classes through aggregation and disaggregation: slow-sinking particles can contribute to the mass of fast-sinking particles by aggregation; and fast-sinking particles can disaggregate to form slow-sinking particles. Pigments are exchanged between the two classes along with particle aggregation and disaggregation.

Chl *a* in slow-sinking particles degrades into pheopigments. Organic carbon and pheopigments in slow-sinking particles remineralize into inorganic carbon.

2.3. Mathematical description of the box model

With the assumptions stated above, we can assign mathematical functions to the various terms in the box model. Net vertical export ($\text{g m}^{-3}\text{y}^{-1}$), as shown in **Fig. 4.1**, is obtained by dividing flux ($\text{g m}^{-2}\text{y}^{-1}$) differences into depth differences.

$$F_{i,z_s-z_d} = \frac{f_{z_d,i} - f_{z_s,i}}{z_d - z_s} \quad (1)$$

where F_{i,z_s-z_d} means vertical export ($\text{g m}^{-3}\text{y}^{-1}$) of sinking velocity category *i* from depth z_s to depth z_d ; $f_{z_d,i}$ and $f_{z_s,i}$ mean particle sinking fluxes ($\text{g m}^{-2}\text{y}^{-1}$) measured by the sediment traps (presented in **Table 4.1**) at depth z_d and z_s , respectively.

Pigment (and organic matter) concentration in a SV category is calculated via an equation that is similar to Eq. (12) in Armstrong et al. (2009). For example, concentration of Chl *a* is calculated as follow:

$$[Chl. a]_i (\mu\text{g} \cdot \text{m}^{-3}) = \frac{f_i (\mu\text{g} \cdot \text{m}^{-2} \cdot \text{d}^{-1})}{SV_i (\text{m} \cdot \text{d}^{-1})} \quad (2)$$

where f_i and SV_i represent Chl-*a* flux and particle settling velocity of SV category *i*, respectively. Instead of using minimum sinking velocities as measured by SV traps, we use mid-SVs, which are calculated by averaging two adjacent minimum SVs. Flux and

SV data are summarized in **Table 4.1**. As stated in Armstrong et al. (2009), concentration calculated in this way represents concentration outside a sediment trap.

The 11 SV categories were combined into two classes to decrease the number of parameters to be estimated. If there are u SV categories that have been group into slow- or fast-sinking class, its total Chl-*a* concentration ($[Chl\ a]_u$) is a summation of Chl-*a* concentration in each SV category:

$$[Chl\ a]_u = \sum_{i=1}^u [Chl\ a]_i \quad (3)$$

Total vertical export are calculated similarly:

$$[F_{z_s-z_d}]_u = \sum_{i=1}^u [F_{z_s-z_d}]_i \quad (4)$$

In practice, vertical export at 313 m was the average of vertical exports $F_{(313-524)}$ and $F_{(313-1918)}$; at 524 m was the average of $F_{(313-524)}$ and $F_{(524-1918)}$; and at 1918 m was the average of $F_{(313-1918)}$ and $F_{(524-1918)}$.

The mathematical equation for Chl *a* in slow-sinking particles is

$$F_s^{chl.a} = [Chl\ a]_f \times k_{-1} - [Chl\ a]_s \times k_1 - [Chl\ a]_s \times d_1 \quad (5)$$

For pheopigments ([pheo]) in slow-sinking particles, the equation we used is

$$F_s^{pheo} = [Chl\ a]_s \times d_1 + [pheo]_f \times k_{-1} - [pheo]_s \times d_2 - [pheo]_s \times k_1 \quad (6)$$

For Chl *a* in fast-sinking particles, the equation we used is

$$F_f^{chl.a} = [Chl\ a]_s \times k_1 - [Chl\ a]_f \times k_{-1} \quad (7)$$

For pheopigments ([pheo]) in fast-sinking particles, the equation we used is

$$F_f^{pheo} = [pheo]_s \times k_1 - [pheo]_f \times k_{-1} \quad (8)$$

For organic matter ([OM]) in slow-sinking particles, the equation we used is

$$F_s^{org} = [OM]_f \times k_{-1} - [OM]_s \times k_1 - [OM]_s \times d_2 \quad (9)$$

For organic matter ([OM]) in fast-sinking particles, the equation we used is

$$F_f^{org} = [OM]_s \times k_1 - [OM]_f \times k_{-1} \quad (10)$$

where items in square parenthesis represent item concentrations ($\mu\text{g}/\text{m}^3$ for pigments and mg/m^3 for OM); k_1 , k_{-1} , and d_2 represent aggregation, disaggregation, and OM degradation rate constants, respectively; d_1 represents the rate constant, at which Chl *a* degrades into pheopigments.

Particle interaction rate constants were found by maximizing a likelihood statistic with Gaussian error (Edwards, 1992; Hilborn and Mangel, 1997; Armstrong, et al., 2002; 2009). The estimator equation used is as follow:

$$\log \mathcal{L} = -\frac{n}{2} \times \log\left(\frac{\sum_{i=1}^n (\hat{F}(i) - F(i))^2}{n}\right) \quad (11)$$

where \mathcal{L} is the likelihood that we try to maximize; n is the number of data points; $\hat{F}(i)$ represents model predicted vertical export flux; and $F(i)$ is vertical flux calculated from sediment trap measurements.

3. Results

3.1. Division SV

Fig. 4.2 shows maximum likelihood versus different division SVs, A division SV is defined as a settling velocity at which the 11 settling velocity categories are separated into “slow-“ and “fast-sinking” classes: settling velocities equal to or greater than the division SV are grouped into fast-sinking class, the rest are grouped into slow-sinking class. Maximum likelihood shows a generally decreasing trend with increasing division SV. Maximum likelihood is highest at division SV of 5 m/d, which indicates particles with SV equal to or greater than 5 m/d should be grouped in the fast-sinking class in the box model.

3.2. Rate constants.

Estimated rate constants are reported in **Table 4.2**. Aggregation rate constants are almost constant with depth. Disaggregation rate constants peak at 524 m, and are approximately the same at 313 m and 1918 m. Chl-a degradation rate constants, which are defined as a rate constant of Chl-a degradation into pheopigments (pheophorbide, pheophytin, and pyropheophorbide), increase slightly with depth from 0.88 y^{-1} at 313 m to 1.18 y^{-1} at 1918 m. Organic-matter degradation rate constants, the rate constant of OM remineralizing into inorganic carbon, are highest at 524 m with a value of 1.55 y^{-1} ; they are 1.16 y^{-1} and 1.11 y^{-1} at 313 m and 1918 m, respectively.

Parameter sensitivity tests are shown in **Fig. 4.3**. When compared with similar tests that were performed with thorium data (Chapter III), tests in this paper indicate that changes in maximum likelihood versus parameter values are more sensitive with pigment data than tests with thorium data.

4. Discussion

When compared with the thorium tracers ^{234}Th and ^{230}Th that have been used in Chapter II, the pigment tracers used in this paper have the following characteristics. Chl *a* and its degraded products are an integral part of the particles; they therefore can more accurately record particle exchange than thorium tracers can. In contrast, thorium isotopes are particle-reactive tracers (Moore and Millward, 1988), which are constantly adsorbed onto particles and desorb off particles. Adsorption and desorption processes can dominate particle-thorium interactions, which may result in less accurate estimations of aggregation and disaggregation rate constants. This is because when first-order reaction kinetics were assumed, the contributions of adsorption and desorption are much higher than those of aggregation and disaggregation, which makes the weights of aggregation and disaggregation in the balance equation small. Additionally, compared to the box model describing thorium cycling, the box model of pigment cycling is simpler, which means that fewer parameters must be estimated, allowing more data per parameter for more accurate estimation.

4.1. Division SV

In the 2005 MedFlux program, IRS SV sediment traps separated particles into 11 settling velocity categories with minimum particle settling velocities of 980 m/d, 490 m/d, 326 m/d, 196 m/d, 140 m/d, 98 m/d, 49 m/d, 22 m/d, 11 m/d, 5 m/d, and 0.68 m/d, respectively. Compared to the division SV separating the thorium data (98 m/d, Chapter II), the division SV dividing the pigment data in the present paper is lower at 5 m/d. The different division SVs might be due to the different characters of thorium and pigments as discussed above. It could also be caused by the different model structures, because the pigment model excludes adsorption and desorption; only particulate pigment and organic matter concentration could influence the results. **Fig. 4.4** shows Chl-*a* concentration at different settling velocity categories, from which it is apparent that concentration of Chl *a* in the slowest sinking velocity category (>0.68 m/d) (slow-sinking class in the box model) is much higher than in any other SV categories. This concentration distribution further supports the appropriateness of the 5 m/d division SV determined by the likelihood method.

4.2. Aggregation and disaggregation rate constants

In Chapter II, aggregation and disaggregation rate constants were estimated using the maximum likelihood method and thorium data sampled in the 2005 MedFlux program. For comparison, aggregation rate constants calculated with pigment data are lower at all three depths than those estimated with thorium data, whereas

disaggregation rate constants are higher in the current study than in Chapter II. One possible reason could be the different division SVs. This is because there are fewer sources that contribute to aggregation, but more sources that contribute to disaggregation, when “slow” and “fast” particles are divided at 5 m/d SV instead of at 98 m/d.

To check the above explanation, the division SV prediction in this paper (5 m/d) was applied to the 2005 Medflux ^{234}Th and ^{230}Th data. Particle mass information was used in the thorium model, because other particle components rather than OM were thought also to be responsible for thorium adsorption (Geibert and Usbeck 2004). To allow a fair comparison, the particle mass data used in the thorium model (Chapter II) were substituted with OM data used in this chapter. The results along with results cited from Chapter II are shown in **Table 4.3**. As can be seen, aggregation decreased and disaggregation increased when division SV 5 m/d were used, which is consistent with the above explanation. Comparisons between **Table 4.2** and **Table 4.3** show that when the same division SV was used, aggregation, disaggregation, and OM degradation rate constants predicted by thorium and pigment tracers are in relatively good agreement.

Comparisons with other studies (Nozaki et al., 1987; Clegg et al., 1991; Cochran et al., 1993, 2000; Murnane, 1994; Munane et al., 1990) indicate that the aggregation rate constants estimated in this study are at the lower end of the reference ranges. Possible reasons could be due to (1) different tracers: in the above references thorium tracers were used; (2) geographical or seasonal variation: the area of this study was in the Mediterranean Sea and the areas studied in the references were in the Pacific or western Atlantic. According to Murnane (1994), aggregation rate constants estimated at

different locations could differ by 2 orders of magnitude. According to Abramson et al. (2010), the extent of particle exchange could be distinctly different if sampling seasons are different.

4.3. Chl *a* and OM degradation rate constants

Sun et al. (1993b) studied Chl-*a* degradation by applying a “Multi-G” model, in which organic matter are assumed to have different pools with different lability and different decomposition rate constants (Whelan and Farrington, 2013). Sun et al. (1993b) concluded that first-order degradation rate constants of labile Chl *a*, which was quantitatively about 75% of total Chl *a*, were 0.25 d^{-1} (90 y^{-1}), and of refractory Chl *a* were about $0.03 - 0.09 \text{ d}^{-1}$ ($10 - 30 \text{ y}^{-1}$) for oxic sediments. Stephens et al. (1997) also reported first-order reaction rate constants that ranged from 1 to 75 y^{-1} in sediment sampled at four abyssal sites in the equatorial Pacific. The rate constants found in this study are at the lower end of the reported range. Considering the different studied environments: water column in this study versus sediment environment in cited references, it is reasonable for us to get lower degradation rate constants, since there are less organisms in the water column than in sediments. Additionally, Chl-*a* degradation defined in this study was degraded into pheopigments. Pigments can also be degraded into colorless products and thus our degradation rate constant should be smaller than when degradation is defined as total degradation.

Westrich and Berner (1984) reported that degradation rate constants of labile organic carbon were $24 \pm 4 \text{ y}^{-1}$, while those of less reactive POC or TOC were 1.4 ± 0.7

y^{-1} . Our estimation that POC degradation rate constants range from 1.11-1.55 y^{-1} is in good agreement with previous results, since at the depth of 313 m, most labile POC is supposed to have degraded; our estimated rate constant should be for less reactive POC.

4.4. Parameter value sensitivity tests

Sensitivity tests (**Fig. 4.3**) show that likelihood in this paper is more sensitive to the parameter values compared with the thorium sensitivities found in Chapter III. For example, in Chapter III the change of disaggregation rate constants from 0 - 70 y^{-1} caused a log-likelihood change of only ~ 6 , which means a difference of $\sim \exp(6)$ between model prediction and measurement, whereas by using the chloropigment data the change of disaggregation rate constant from 0 - 10 y^{-1} induced a log-likelihood change of ~ 40 ($\sim \exp(40)$) difference between model prediction and measurement). The other parameters all show sensitivity improvements at different degrees. The comparisons indicate that aggregation and disaggregation rate constants estimated using pigment data may more accurate than those estimated using thorium data.

An interesting feature about **Fig. 4.3** is that maximum log-likelihood in the aggregation and OM degradation sensitivity tests peaks at around -15, which is different from the maximum log-likelihood (around -7) at which all parameters are at their optimum values. The reason for the difference is due to the method with which we did the sensitivity tests. For example, if we were testing sensitivity of disaggregation rate

constants, we kept data constant and parameters other than disaggregation rate constants at their optimized values, while at the same time, we varied the disaggregation rate constant, which was the same at all the three depths. A maximum likelihood was calculated for every changed disaggregation rate constant. Because optimized disaggregation rate constants were depth dependent, by using the same value at all three depths in the test, we did not allow the system to reach optimum maximum log-likelihood. The deviation of highest maximum likelihood from the optimum maximum likelihood when depth specific disaggregation rate constants were used indicates that disaggregation rate constant and OM degradation rate constant were sensitive to depth.

The sensitivity tests of rate constants of Chl-*a* degradation into pheopigments and aggregation tell different stories. Maximum log-likelihood peaked at around -7 at 0.9 y^{-1} in the sensitivity test of the Chl-*a* degradation rate constant, at about 0.05 y^{-1} of the test of the aggregation rate constant. The results indicate that if we applied 0.9 y^{-1} as the Chl-*a* degradation rate constant and 0.05 y^{-1} as the aggregation rate constant at all three depths, the highest maximum likelihood was almost the same as the optimum maximum likelihood when all the parameter values were at optimum values. This is easy to understand for the Chl-*a* degradation rate constant, because the average value of the three depths is almost 0.9 y^{-1} . For the aggregation rate constant, maximum likelihood shows a plateau at values between 0 and 0.1 y^{-1} , and then decreases sharply as the value increases, which means aggregation rate constant should be constrained in the range of 0- 0.1 y^{-1} , and not be depth-sensitive.

4.5. Process contributions

To compare our results to those of Abramson et al. (2010), we first made an assumption that particles in the slow-sinking class (0.68 m/d) of our box model were equivalent to the particles sampled by large volume *in-situ* pumps in Abramson et al. (2010); particles in the fast-sinking class (>5.44 m/d) were equivalent to the particles sampled by TS sediment traps. We then calculated process contributions by multiplying rate constants with corresponding concentrations. The results are shown in **Table 4.4**. As can be seen, although aggregation rate constants are as low as 0.02 y^{-1} as shown in **Table 4.2**, particles did exchange their components by aggregation and disaggregation, which is in good agreement with the results in Abramson et al. (2010) (Fig. 6). However, we cannot conclude how aggregation and disaggregation change seasonally as was done by Abramson et al. (2010), because SV sediment traps integrated particles during the entire deployment period.

As can be seen in **Table 4.4**, all sinking particle contributions are positive, which means, by definition, sinking serves as a source. The “source” here does not mean tracers were supplied by upwelling or advection; instead it means the amount of tracers coming into the box from the upper layer is greater than the amount of tracers leaving the box at the lower layer as shown in **Fig. 4.5**. This explanation is in agreement with Eq. 5.

5. Conclusions

This study confirms that pigments may have characteristics that differ from those of thorium, as reflected by the optimum division SVs. By using pigment tracers, we can obtain more accurate estimations than by using thorium tracers, as reflected by the sensitivity tests: likelihoods are more sensitive to parameters when the pigment data are used than when the thorium data are used. Multiple tracers should be used to get a comprehensive picture about particle exchange dynamics.

References

- Abramson, L., Lee, C., Liu, Z., Wakeham, S.G., Szlosek, J., 2010. Exchange between suspended and sinking particles in the northwest Mediterranean as inferred from the organic composition of in situ pump and sediment trap samples. *Limnol. Oceanogr.*, 55 (2), 725-739.
- Armstrong, R.A., Lee, C., Hedges, J.I., Honjo, S., Wakeham, S., 2002. A new, mechanistic model for organic carbon fluxes in the ocean based on the quantitative association of POC with ballast material. *Deep-Sea Res. II* 49, 219–236.
- Armstrong, R.A., Peterson, M.L., Lee, C., Wakeham, S.G., 2009. Settling velocity spectra and the ballast ratio hypothesis. *Deep Sea Research II*, 56, 1470-1478.
- Clegg, S.L., and Whitfield, M., 1991. A generalized model for the scavenging of trace metals in the open ocean, II, thorium scavenging, *Deep Sea Research, Part A*, 38, 91-120.
- Clegg, S.L., Bacon, M.P., Whitfield, M., 1991. Application of a generalized scavenging model to thorium isotope and particle data at Equatorial and high-latitude sites in the Pacific Ocean, *J. Geophys. Res.*, 96, 20655-20670.
- Cochran, J.K., Buesseler, K.O., Bacon, M.P., Livingston, H., 1993. Thorium isotopes as indicators of particle dynamics in the upper ocean: results from the JGOFS North Atlantic Bloom Experiment. *Deep-Sea Research I* 40, 1569-1595.
- Cochran, J.K., Buesseler, K.O., Bacon, M.P., Wang, H.W., Hirschberg, D.J., Ball, L., Andrews, J., Crossin, G., Fleer, A., 2000. Short-lived thorium isotopes (^{234}Th , ^{228}Th) as indicators of POC export and particle cycling in the Ross Sea, Southern Ocean. *Deep-Sea Research II*, 47, 3451-3490.

- Edwards, A.W.F., 1992. Likelihood. Johns Hopkins University Press, Baltimore, MD.
- Geibert, W. and Usbeck, R., 2004. Adsorption of thorium and protactinium onto different particle types: Experimental findings. *Geochimica et Cosmochimica Acta*, 68(7): 1489-1501.
- Hedges, J.I., 1992. Global biogeochemical cycles: progress and problems. *Marine Chemistry*, 39, 67-93.
- Hedges, J.I. and Stern, J.H., 1984. Carbon and nitrogen determinations of carbonate marine sediment. *Organic Geochemistry*, 27, 319-361.
- Hill, P.S., 1998. Controls on floc size in the sea. *Oceanography* 11: 13-18.
- Hilborn, R. and Mangel, M., 1997. *The ecological detective: confronting models with data*. Princeton University Press, Princeton, New Jersey, pp.133.
- Honjo, S., 1980. Material fluxes and modes of sedimentation in the mesopelagic and bathypelagic zones. *Journal of Marine Research*, 38, 53-97.
- Lee, C., Armstrong, R.A., Cochran, J.K., Engel, A., Fowler, S.W., Goutx, M., Masque, P., Miquel, J.C., Peterson, M., Tamburini, C., Wakeham, S., 2009a. MedFlux: Investigations of particle flux in the Twilight Zone. *Deep-Sea Research II*, 56, 1363-1368.
- Lee, C., Peterson, M.L., Wakeham, S.G., Armstrong, R.A., Cochran, J.K., Miquel, J.C., Fowler, S.W., Hirschberg, D., Beck, A., Xue, J., 2009b. Particulate organic matter and ballast fluxes measured using time-series and settling velocity sediment traps in the northwestern Mediterranean Sea. *Deep-Sea Research II*, 56, 1420-1436.
- Marchal, O. and Lam, P., 2012. What can paired measurements of Th isotope activity and particle concentration tell us about particle cycling in the ocean? *Geochimica et Cosmochimica Acta* 90, 126-148.
- Marty, J.C., 2002. The DYFAMED time-series program (French JGOFS). *Deep-Sea Research II*, 49, 1963-1964.
- McCave, I.N., 1975. Vertical flux of particles in the ocean. *Deep Sea Research*, 22, 491-520.
- Moore, R. M., and G. E. Millward, 1988. The kinetics of reversible Th reactions with marine particles, *Geochim. Cosmochim. Acta*, 52, 113-118.
- Murnane, R. J., 1994. Determination of thorium and particle matter cycling parameters at station P: A reanalysis and comparison of least squares techniques. *Journal of Geophysical Research*, 99 (C2), 3393-3405.

- Murnane, R.J., Sarmiento, J.L., Bacon M.P., 1990. Thorium isotopes, particle cycling models, and inverse calculations of model rate constants. *Journal of Geophysical Research*, 95(C9), 16195-16206.
- Murnane, R.J., Cochran, J.K., sarmiento, J.L., 1994. Estimates of particle- and thorium-rates in the northwest Atlantic Ocean. *Journal of Geophysical Research*, 99 (C2), 3373-3392.
- Nozaki, Y., Yang, J.S., Yamada, M., 1987. Scavenging of thorium in the ocean, *J. Geophys. Res.*, 92, 772-778.
- Peterson, M.L., Hernes, P.J., Thoreson, D.S., Hedges, J.I., Lee, C., Wakeham, S.G., 1993. Field evaluation of a valved sediment trap. *Limnol. Oceanogr.* 38, 1741-1761.
- Peterson, M.L., Wakeham, S.G., Lee, C., Askea, M., Miquel, J.C., 2005. Novel techniques for collection of sinking particles in the ocean and determining their settling rates. *Limnology and Oceanography methods*, 3, 520-532.
- Peterson, M.L., Fabres, J., Wakeham, S.G., Lee, C., Alonso, I.J., Miquel, J.C., 2009. Sampling the Vertical Particle flux in the upper water column using a large diameter free-drifting NetTrap adapted to an Indented Rotating Sphere Sediment trap. *Deep Sea Research II*, 56, 1547-1557.
- Shuman, F.R. and Lorenzen, C.J., 1975. Quantitative degradation of chlorophyll a by a marine herbivore. *Limnol. Oceanogr.* 20: 580-568.
- Stephens, M.P., Kadko, D.C., Smith, C.R., Latasa, M., 1997. Chlorophyll-a and pheopigments as tracers of labile organic carbon at the central equatorial Pacific seafloor. *Geochimica et Cosmochimica Acta*, 61(21), 4605-4619.
- Sun, M.-Y., Lee, C., Aller, R.C., 1993a. Laboratory studies of oxic and anoxic degradation of chlorophyll-a in Long Island Sound sediments. *Geochim. Cosmochim. Acta.* 57, 147-157.
- Sun, M.-Y., Lee, C., Aller, R.C., 1993b. Anoxic and oxic degradation of ¹⁴C-labeled chloropigments and a ¹⁴C-labeled diatom in Long Island Sound sediments. *Limnol. Ocean.* 38. 1438-1451.
- Szymczak-Zyla, M., Kowalewska, G., Louda, J.W., 2008. The influence of microorganisms on chlorophyll a degradation in the marine environment. *Limnol. Oceanogr.*, 53(2), 85-862.
- Wakeham, S.G., Lee, C., Peterson, M.L., Liu, Z., Szlosek, J., Putnam, I., Xue, J., 2009. Organic compound composition and fluxes in the Twilight Zone—time series and settling velocity sediment traps during MEDFLUX. *Deep-Sea Research II*, 56, 1437-1453.

- Welschmeyer, N.A. and Lorenzen, C.J., 1985. Chlorophyll budgets: zooplankton grazing and phytoplankton growth in a temperate fjord and the Central Pacific Gyres. *Limnol. Oceanogr.*, 30(1), 1-21.
- Westrich, J.T. and Berner, R.A., 1984. The role of sedimentary organic matter in bacterial sulfate reduction: The G model tested. *Limnol. Ocean.* 29, 236-249.
- Whelan, J.K., and Farrington, J.W., 2013. Organic matter: productivity , accumulation, and preservation in recent and ancient sediments. Columbia University Press. pp. 185-186.

Table 4.1. Settling velocity fluxes (ug/m²/d) for 2005 of composite pigments and organic matter. In 2005 deployment, there were two SV traps at each depth. Data in two SV traps are combined via the following equation: $f_{\text{composite}} = \text{SV1}_{\text{mass}} / (\text{SV1}_{\text{mass}} + \text{SV2}_{\text{mass}}) * \text{SV1}(f) + \text{SV2}_{\text{mass}} / (\text{SV1}_{\text{mass}} + \text{SV2}_{\text{mass}}) * \text{SV2}(f)$.

mid-SV (m/d)	composite Chl a (ug/m ² /d)	composite ppb* (ug/m ² /d)	composite pyro* (ug/m ² / d)	composite pptn* (ug/m ² /d)	composite OM (mg/m ² / d)
Depth: 313 m					
1200	0.174	0.322	0.707	0.444	1.968
734.4	1.041	2.113	5.328	1.038	6.654
408.0	1.773	2.775	9.696	1.589	4.593
261.1	2.290	3.548	16.018	2.010	5.535
167.9	1.026	1.765	5.827	0.852	3.059
118.9	1.384	1.837	6.503	0.917	2.573
73.4	1.229	2.122	9.121	1.094	3.603
35.4	0.997	1.616	5.205	0.807	2.405
16.3	0.682	1.442	4.153	0.732	3.271
8.16	0.763	1.326	5.096	0.617	2.535
3.11	2.851	4.889	16.436	2.716	8.092
Depth: 524 m					
1200	2.469	1.653	5.377	0.491	2.971
734.4	1.728	2.941	6.550	3.992	8.053
408.0	1.334	1.801	5.889	0.710	3.798
261.1	1.447	2.883	7.974	1.351	3.560
167.9	0.561	1.006	3.902	0.596	1.755
118.9	0.749	1.059	2.527	0.650	1.506
73.4	0.631	1.032	2.235	0.449	1.496
35.4	0.568	0.966	2.259	0.482	1.624
16.3	0.447	0.784	2.455	0.394	1.641
8.16	0.666	1.224	4.436	0.618	2.763
3.11	2.123	4.400	8.878	2.342	6.533
Depth: 1918 m					
1200	0.154	0.177	0.934	0.389	0.844
734.4	1.616	2.593	6.729	2.046	4.262
408.0	0.874	1.623	2.717	1.002	3.120
261.1	1.121	2.161	4.561	1.536	3.052
167.9	0.547	1.000	2.614	0.572	1.642
118.9	0.519	0.892	2.840	0.444	0.988
73.4	0.463	0.872	2.883	0.777	1.603
35.4	0.283	0.546	1.656	0.499	0.990
16.3	0.218	0.343	1.352	0.434	0.812
8.16	0.313	0.397	1.217	0.214	1.158
3.11	0.874	1.489	5.175	1.102	3.103

* ppb is an abbreviation for *pheophorbide*; pyro is an abbreviation for *pyropheophorbide*; pptn is an abbreviation for *pheophytin*.

Table 4.2. Parameters estimated by the pigment data and the maximum likelihood method at a division settling velocity of 5 m/d. (unit: y^{-1})

Parameters	313 m	524 m	1918 m
Aggregation (k_1)	0.02	0.07	0.02
Disaggregation (k_{-1})	10.47	13.82	9.60
<i>Chl a</i> degradation (d_1)	0.88	0.93	1.17
OC degradation (d_2)	1.16	1.55	1.11

Table 4.3. Rate constants (y^{-1}) calculated with thorium data at division SVs of 5 m/d and 98 m/d. Values at division SV of 98 m/d are those cited from Chapter II, in which total particle mass rather than organic matter was used (see text for further explanations).

Parameters	Division SV=5 m/d			Division SV=98m/d		
	313m	524m	1918m	313m	524m	1918m
Aggregation	0.01	0.02	0.02	2.11	1.13	0.09
Disaggregation	7.69	6.05	7.86	2.42	1.39	1.16
OC degradation	0.83	0.70	0.34	0.01*	0.02*	0.54*

* total particle remineralization rate constants.

Table 4.4. Contribution of each process. Negative values indicate sinks. Positive values are sources (units: mg/m³/y for OM, µg/m³/y for chloropigments).

Process	313 m		524 m		1918 m	
	Fast-sinking	Slow-sinking	Fast-sinking	Slow-sinking	Fast-sinking	Slow-sinking
Aggregation (Chl a)	1.68	-1.68	1.25	-1.25	0.51	-0.51
Disaggregation (Chl a)	-3.31	3.31	-3.27	3.27	-1.16	1.16
Chl-a degradation	-	-3.70	-	-2.89	-	-1.51
Sinking (Chl a)	1.63	2.06	2.02	0.87	0.65	0.86
Aggregation (pheo-)	14.14	-14.14	9.19	-9.19	4.57	-4.57
Disaggregation (pheo-)	-29.51	29.51	-27.43	27.43	-8.69	8.69
Degradation (pheo-)	-	-41.11	-	-35.63	-	-12.61
Chl-a degradation	-	3.70	-	2.89	-	1.51
Sinking (pheo-)	15.36	22.05	18.24	14.50	4.12	11.61
Aggregation (OM)	4.76	-4.76	3.84	-3.84	1.83	-1.83
Disaggregation (OM)	-11.12	11.12	-11.87	11.87	-4.06	4.06
Degradation (OM)	-	-13.84	-	-14.90	-	-5.04
Sinking (OM)	6.36	7.48	8.03	6.87	2.23	2.81

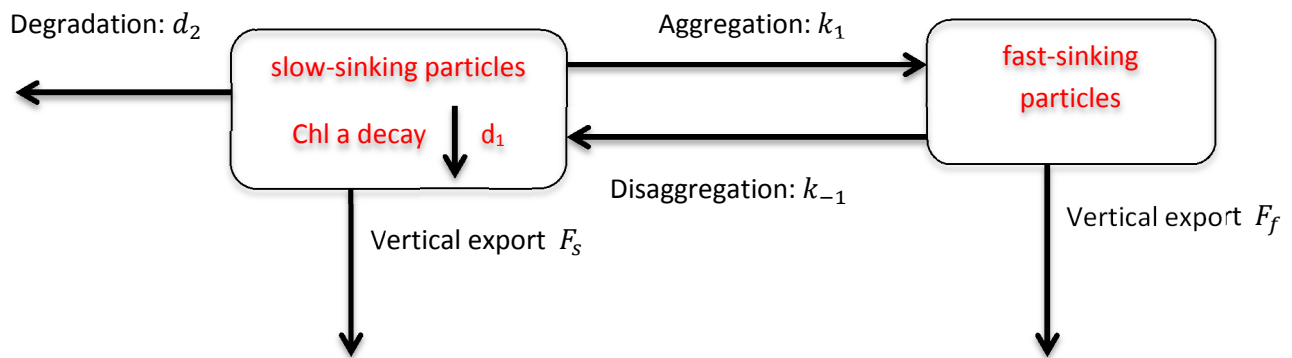


Figure 4.1. A conceptual model describing particulate pigment cycling. Slow- and fast-sinking particle sinking rates were measured using IRS Settling Velocity (SV) sediment traps. Since the shallowest trap depth was 313 m, primary production is neglected. Aggregation and disaggregation describe particle exchange between the two groups: slow-sinking particles aggregate to form faster sinking particles, and fast-sinking particles disaggregate into slower sinking particles. Chl-*a* degradation products (pheophorbide, pheophytin, and pyropheophorbide) in slow-sinking particles have two sources: *in-situ* degradation of Chl *a* and disaggregation of fast-sinking particles containing the pheopigments. Chl *a* in fast-sinking particles can increase due to aggregation of slow-sinking particles, and can be lost by disaggregation (degradation is neglected since much of the pheopigment production occurs during grazing process in the euphotic zone). d_1 is defined as the rate constant of Chl-*a* degradation into pheophorbide, pheophytin, and pyropheophorbide, and we assume this is the only way that Chl *a* is lost. To account for Chl *a* lost in other reactions, we make the assumption that the rate of loss is similar to that of total organic matter; this gives us a minimum loss rate, as we might expect pigment loss to be somewhat faster than total OM. Therefore, d_2 is defined as the degradation rate constant of organic matter including all the chloropigments. Degradation loss of both Chl *a* and organic matter in fast-sinking particles is assumed to be slow enough to be neglected. Chl *a* and organic matter degradation, aggregation, and disaggregation are assumed to have first-order reaction kinetics.

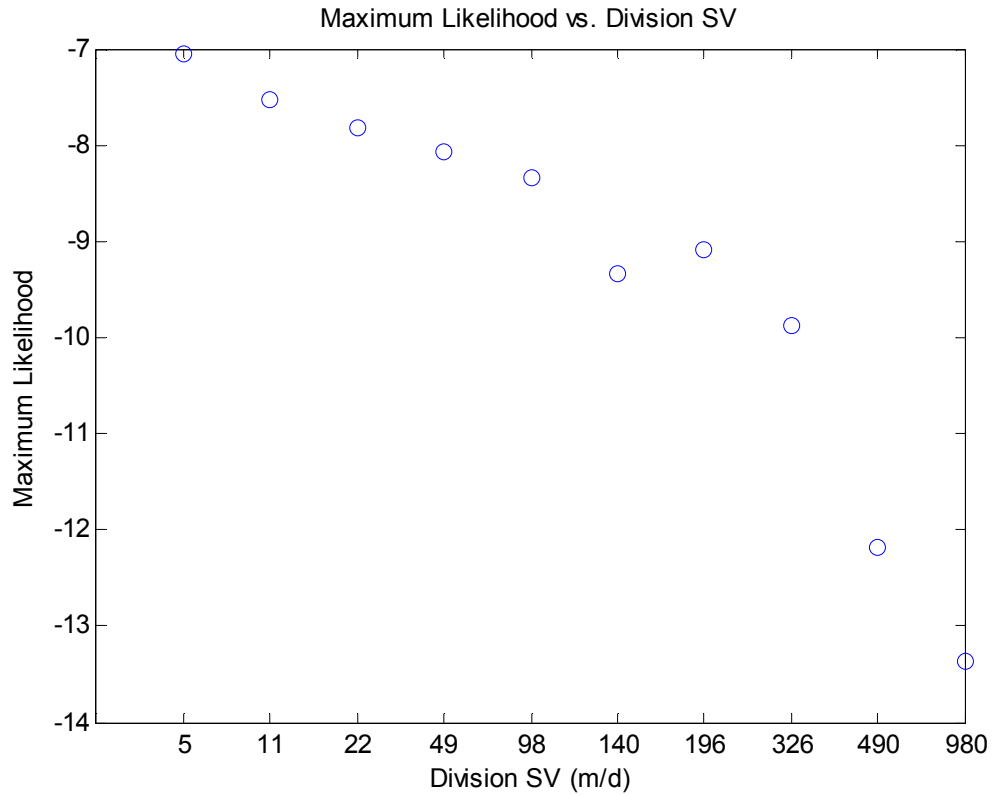
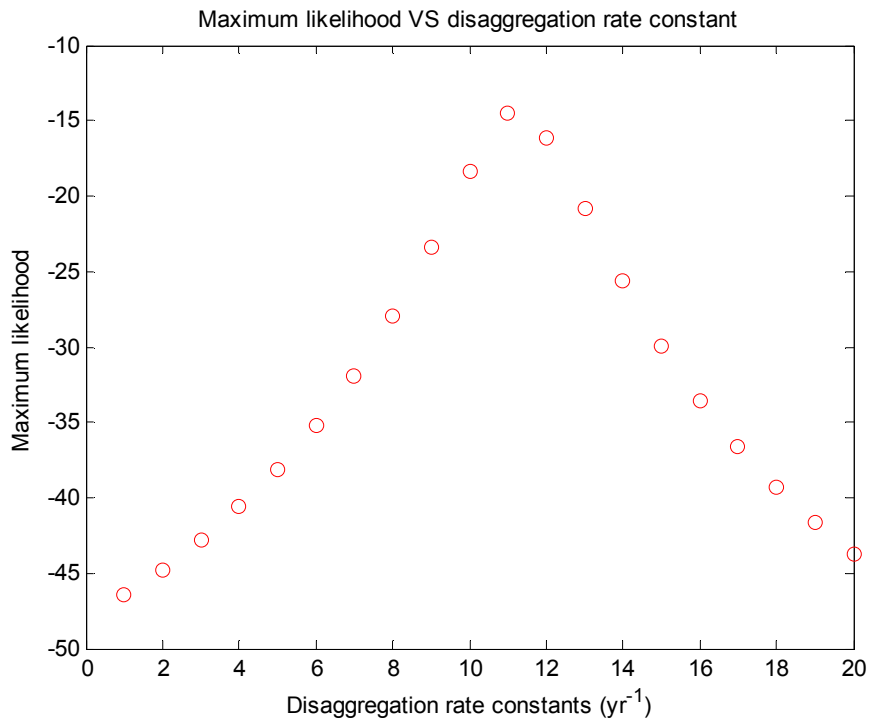
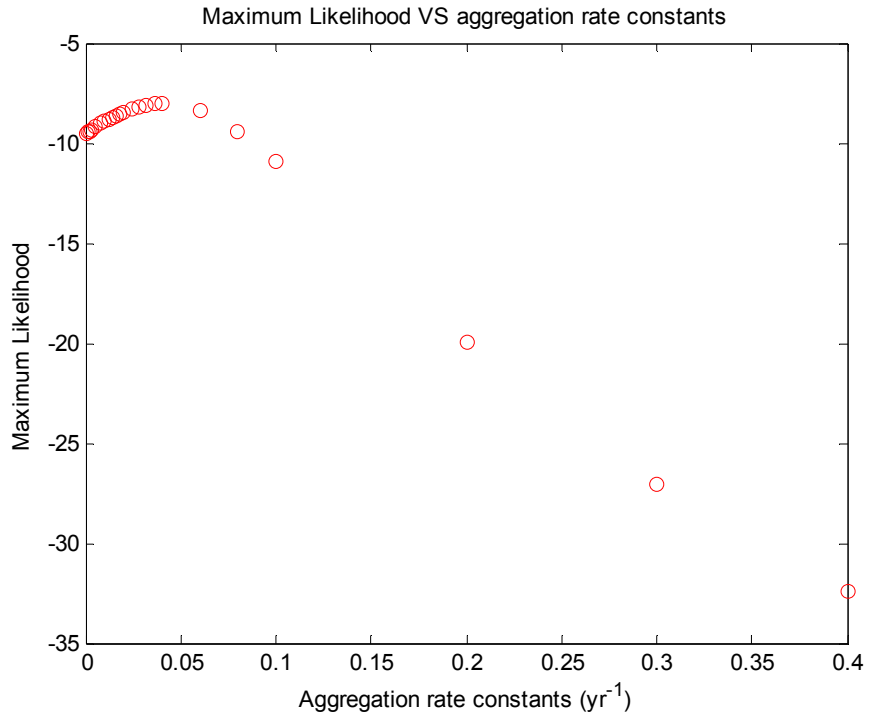


Figure 4.2. Maximum likelihood versus division SV. The division SV means that particles with SVs equal to or greater than the division SV will be grouped into the fast-sinking class, and particles with lower SV than the division SV will be grouped into slow-sinking class in the box model. We tentatively divided the 11 SV categories separated by the IRS SV traps into two classes at every possible SV, and maximum likelihoods were calculated at each division SV, then were plotted versus division SV.



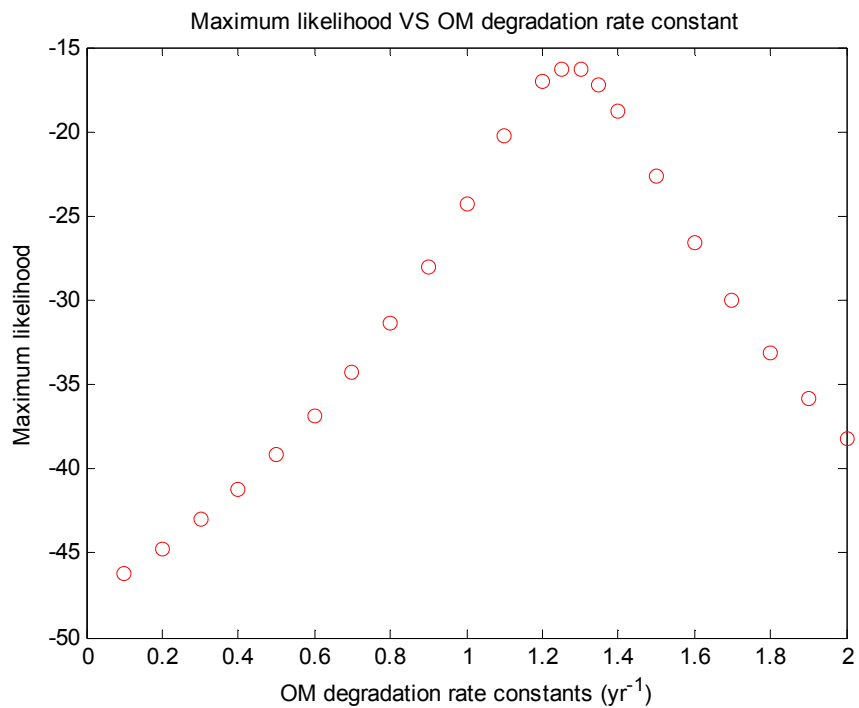
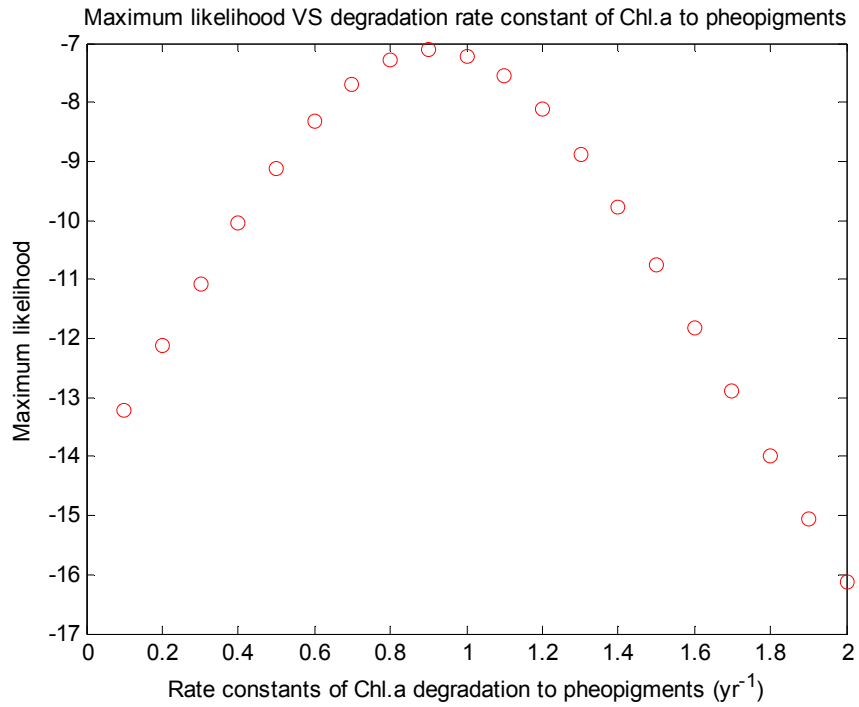


Figure 4.3. Parameter sensitivity tests. The sensitivity tests were done by progressively changing the tested parameter, which were set the same for all the three depths, while keeping other parameters at their optimized values and data constant.

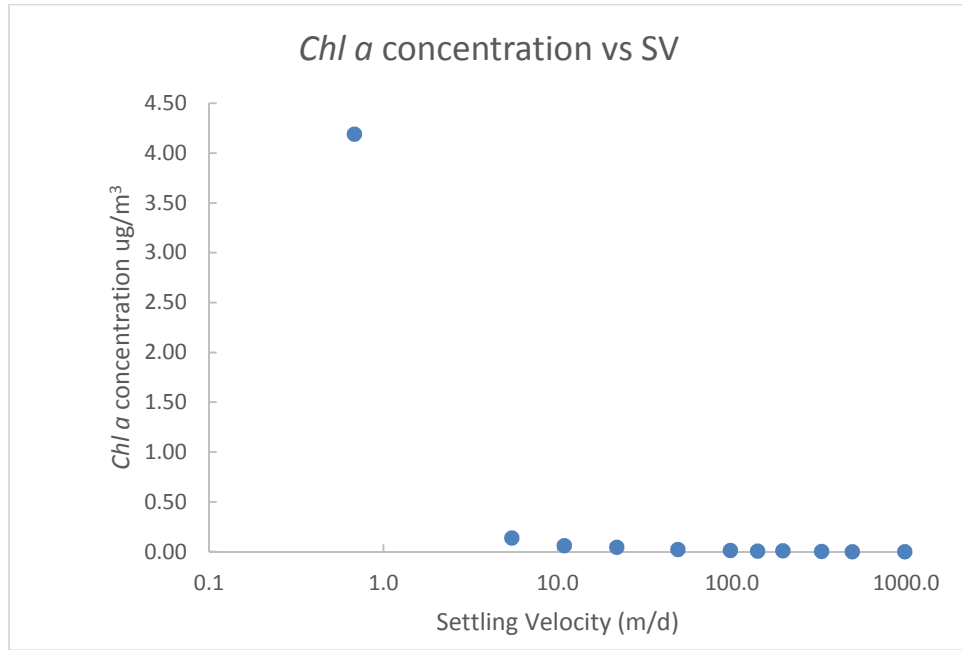


Figure 4.4. Chl-a concentration ($\mu\text{g}/\text{m}^3$) plotted versus particle sinking velocity (m/d). Chl-a concentrations were calculated by applying Eq. 2. The calculated concentrations actually represent the concentrations outside the sediment trap (Armstrong et al., 2009).

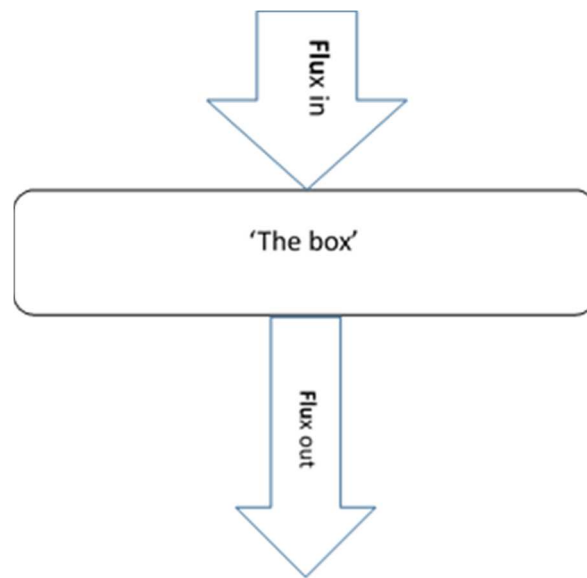


Figure 4.5. Cartoon explanation of sinking flux. According to Eq. 1, sinking flux is the difference between flux-in and flux-out. If flux-in is greater than flux-out, the sinking flux is positive and server as a source, and vice versa.

Chapter 5 : Conclusions

Conclusions:

Particle aggregation and disaggregation have an important influence on the efficiency of the “biological pump”, which is responsible for transporting photosynthesized organic matter into the deep ocean and fueling the benthic organisms. Particle remineralization is another important oceanographic factor, which has an influence on carbon and nutrient cycling, and is also important to marine pollutions. In this thesis, I used both thorium and pigment tracers sampled using IRS SV sediment traps at the French JGOFS DYFAMED site in the Mediterranean Sea to estimate particle aggregation, disaggregation, and particle remineralization rate constants. The mathematical method used was the likelihood method. The total inverse method was evaluated by seeding it with different sets of prior estimates. All the data used were sampled using IRS SV sediment traps in the 2005 MedFlux project.

I constructed a new conceptual model describing particle-thorium interactions in the ocean. Compared with previous models (Murnane, 1994; Murnane, et al., 1990, 1994; Marchel and Lam, 2010), the new model had the following features: (1), this model for the first time allowed the direct interactions between fast-sinking particles and the dissolved thorium; (2), this model permitted slow-sinking particles to have a finite sinking velocity, which was measured using SV sediment traps; (3), particles were separated based on particle sinking velocity instead of particle size, which avoided the

assumption that small particles sank slower than big particles, which, based on McDonnell and Buesseler,(2010) might be wrong.

The 11 settling velocity categories sorted by SV sediment traps were separated into two sinking classes to decrease the number of parameters needed to be estimated, and to fit the conceptual model. Particle-thorium adsorption and desorption rate constants, particle-particle aggregation and disaggregation rate constants, and particle remineralization rate constants were estimated by the likelihood method. Generally, fast-sinking particles had higher desorption rate constants, and lower adsorption rate constants than slow-sinking particles, which was probably caused by their different chemical compositions. This is because slow-sinking particles had higher organic contents than fast-sinking particles. According to Chuang et al. (2014) organic matter could enhance thorium adsorption.

Multiplication of a calculated rate constant with the corresponding concentration gives an estimation about a process contribution, with which the ^{234}Th depth distribution (reported in Szlosek et al., 2009) was explained; for slow-sinking particles, radioactive decay loss of ^{234}Th was compensated mainly by adsorption, thus flux densities at deep traps were quantitatively similar to that in shallower traps; for fast-sinking particles adsorption and aggregation added ^{234}Th onto sinking particles and radioactive decay loss was negligible, which explained why deep traps had higher ^{234}Th flux densities than shallower traps.

The total inverse method was evaluated by using different sets of prior estimates, prior information from the likelihood method results and from a previous study (Nozaki

et al., 1987). Comparisons of the posterior estimates indicated the adsorption, remineralization, and aggregation rate constants agreed relatively well; and disaggregation rate constants had large variations when different prior estimates were used.

I continued to test the total inverse method by plotting likelihood profiles, which indicated that likelihood was extremely sensitive to the adsorption rate constants (both slow- and fast-sinking particles) and slow-sinking particle remineralization rate constants, less sensitive to the slow-sinking particle desorption rate constants and aggregation rate constants, and least sensitive to the disaggregation rate constants. The sensitive tests illustrated that disaggregation rate constants predicted using thorium data and the total inverse method might be inaccurate, which also explained why literature reported disaggregation rate constants had a wide range.

The test was continued by comparing posterior estimates based on prior information obtained by simultaneously increasing or decreasing all likelihood estimations by 2 times. The results showed that at 313 m and 524 m adsorption rate constants (of both the slow- and fast-sinking classes) and desorption rate constants (of the slow-sinking class) did not change apparently when prior estimates increased or decreased, whereas at 1918 m only remineralization rate constants kept constant; and other posterior parameters decreased or increased in the same direction as prior estimates. This test indicated that posterior parameters were not only influenced by the data, but also impacted by the choice of prior values for other parameters.

In Abramson et al. (2010), chloropigment were used to study particles aggregation and disaggregation by comparing pigment compositions between particles sampled by *in-situ* large volume pumps and TS sediment traps. However, Abramson et al. (2010) were not able to reach qualitative conclusions.

I constructed a conceptual box model to describe chloropigment cycles in the ocean and fit the model with chloropigment data sampled using SV sediment traps. The likelihood method was used to estimate particle aggregation and disaggregation rate constants, and organic matter and Chl-a degradation rate constants. Results showed that the division SV that was used to divide the 11 settling velocity categories into two sinking classes was lower than that when thorium data were considered. The division SV was consistent with pigment concentration distributions, because particles with settling velocities below and above the division SV had distinctly different concentrations (Chapter IV). Aggregation rate constants estimated using chloropigment data were lower, and disaggregation rate constants were higher, than those using thorium data. The differences were probably caused by either the different division SVs or by different tracers.

Process contributions indicated that there were particle aggregation and disaggregation happened in the sampling period, which was in agreement with Abramson et al. (2010). Likelihood sensitivity tests showed that likelihood was much more sensitive to parameter values when pigment data rather than thorium data were used.

References

- Abramson, L., Lee, C., Liu, Z., Wakeham, S.G., Szlosek, J., 2010. Exchange between 485 suspended and sinking particles in the northwest Mediterranean as inferred from the 486 organic composition of in situ pump and sediment trap samples. *Limnol. Oceanogr.*, 55 487 (2), 725-739.
- Chuang, C.Y., Santschi, P.H., Wen L.S., Guo, L., Xu, C., Zhang, S., Jiang, Y., Ho, Y.F., Schwehr, K.A., Quigg, A., Hung, C.C., 2014. Binding of Th, Pa, Pb, Po, and Be radionuclides to marine colloidal macromolecular organic matter. *Marine Chemistry*. doi: 10.1016/j.marchem.2014.10.014
- Marchal, O. and Lam, P., 2012. What can paired measurements of Th isotope activity and particle concentration tell us about particle cycling in the ocean? *Geochimica et Cosmochimica Acta* 90, 126-148.
- McDonnell, A.M.P. and Buesseler, K.O., 2010. Variability in the average sinking velocity of marine particles. *Limnol. Oceanogr.*, 55(5), 2085-2096.
- Murnane, R.J., Sarmiento, J.L., Bacon M.P., 1990. Thorium isotopes, particle cycling models, and inverse calculations of model rate constants. *Journal of Geophysical Research*, 95(C9), 16195-16206.
- Murnane, R. J., 1994. Determination of thorium and particle matter cycling parameters at station P: A reanalysis and comparison of least squares techniques. *Journal of Geophysical Research*, 99 (C2), 3393-3405.
- Murnane, R.J., Cochran, J.K., sarmiento, J.L., 1994. Estimates of particle- and thorium-rates in 522 the northwest Atlantic Ocean. *Journal of Geophysical Research*, 99 (C2), 3373-3392.
- Nozaki, Y., Yang, J.S., Yamada, M., 1987. Scavenging of thorium in the ocean, *J. Geophys. Res.*, 92, 772-778.
- Szlosek, J., Cochran, J.K., Miquel, J.C., Masque, P., Armstrong, R.A., Fowler, S.W., Gasser, B., Hirschberg, D.J., 2009. Particulate organic carbon-²³⁴Th relationships in particles separated by settling velocity in the northwest Mediterranean Sea. *Deep Sea Research II*, 56, 1519-1532.

Bibliography

- Abramson, L., Lee, C., Liu, Z., Wakeham, S.G., Szlosek, J., 2010. Exchange between suspended and sinking particles in the northwest Mediterranean as inferred from the organic composition of in situ pump and sediment trap samples. *Limnol. Oceanogr.*, 55(2), 725-739.
- Aitchison J. and Brown J. A. C., 1957. *The Lognormal Distribution (With Special Reference to Its Uses in Economics)*. Cambridge University Press, New York, 176pp.
- Alonso-Gonzalez, I.J., Aristegui, J., Lee, C., Sanchez-Vidal, A., Calafat, A., Fabres, J., Sangra, P., Pere, M., Hernandez-Guerra, A., & Beritez-Barrios, V., 2010. Role of slowly settling particles in the ocean carbon cycle. *Geophysical Research Letters*, L13608, doi:10.1029/2010GL043827.
- Armstrong, R.A., Lee, C., Hedges, J.I., Honjo, S., Wakeham, S., 2002. A new, mechanistic model for organic carbon fluxes in the ocean based on the quantitative association of POC with ballast material. *Deep-Sea Res. II* 49, 219–236.
- Armstrong, R.A., Peterson, M.L., Lee, C., Wakeham, S.G., 2009. Settling velocity spectra and the ballast ratio hypothesis. *Deep Sea Research II*, 56, 1470-1478.
- Bacon, M.P., and Anderson, R.F., 1982. Distribution of thorium isotopes between dissolved and particulate forms in the deep sea. *Journal of Geophysical Research*, 87, 2045-2056.
- Barnett, T.P., Adam, J.C., Lettenmaier, D.P., 2005. Potential impacts of a warming climate on water availability in snow-dominated regions. *Nature*, 438, 303-309.
- Bourguet, N., Goutx, M., Ghiglione, J.F., Mireille, P.P., Mevel, G., Momzikoff, A., Mousseau, L., Guigue, C., Garcia, N., Raimbault, P., Pete, R., Oriol, L., Lefevre, D., 2009. Lipid biomarkers and bacterial lipase activities as indicators of organic matter and bacterial dynamics in contrasted regimes at the DYFAMED site, NW Mediterranean. *Deep Sea Research II*, 56, 1454-1469.
- Bourne, M. D., Thomas, A. L., Niocaill, C. M., & Henderson, G. M., 2012. Improved determination of marine sedimentation rates using ²³⁰Thxs. *Geochemistry Geophysics Geosystems*, 13(1). doi:10.1029/2012GC004295.

- Buat-Menard, P., J. Davis, E. Remoudaki, J.C. Miquel, G. Bergametti, G. Lambert, C.E. Ezat, C. Quétel J., La Rosa and S.W. Fowler., 1989. Non-steady-state biological removal of atmospheric particles from Mediterranean surface waters. *Nature*, 340: 131-134.
- Buesseler, K., 1998. The decoupling of production and particulate export in the surface ocean. *Global Biogeochemical Cycles*, 12(2), 297-310.
- Buesseler, K.O., Lamborg, C.H., Boyd, P.W., Lam, P.J., Trull, T.W., Bidigare, R.R., Bishop, J.K.B., Casciotti, K.L., Dehairs, F., Elskens, M., Honda, M., Karl, D.K., Siegel, D.A., Silver, M.W., Steinberg, D.K., Valdes, J., Mooy, B. V., Wilson, S., 2007. Revisiting carbon flux through the ocean's twilight zone. *Science*, 316, 567-570.
- Chase, Z., Anderson, R.F., Fleisher, M.Q., Kubik, P.W., 2002. The influence of particle composition and particle flux on scavenging of Th, Pa and Be in the ocean. *Earth and Planetary Science Letters*, 204(1-2), 215-229.
- Chuang, C.Y., Santschi, P.H., Wen L.S., Guo, L., Xu, C., Zhang, S., Jiang, Y., Ho, Y.F., Schwehr, K.A., Quigg, A., Hung, C.C., 2014. Binding of Th, Pa, Pb, Po, and Be radionuclides to marine colloidal macromolecular organic matter. *Marine Chemistry*. doi: 10.1016/j.marchem.2014.10.014.
- Clegg, S. L. and M. Whitfield, 1990. A generalized model for the scavenging of trace metals in the open ocean, I, Particle cycling, *Deep Sea Res.*, 37, 809-832.
- Clegg, S.L., Bacon, M.P., Whitfield, M., 1991. Application of a generalized scavenging model to thorium isotope and particle data at equatorial and high-latitude sites in the Pacific Ocean. *Journal of Geophysical Research*, 96(C11), 20655-20670.
- Clegg, S.L. and Whitfield, M., 1991. A generalized model for the scavenging of trace metals in the open ocean, II, thorium scavenging, *Deep Sea Research, Part A*, 38, 91-120.
- Cochran, J.K., Buesseler, K.O., Bacon, M.P., Livingston, H., 1993. Thorium isotopes as indicators of particle dynamics in the upper ocean: results from the JGOFS North Atlantic Bloom Experiment. *Deep-Sea Research I* 40, 1569-1595.
- Cochran, J.K., Buesseler, K.O., Bacon, M.P., Wang, H.W., Hirschberg, D.J., Ball, L., Andrews, J., Crossin, G., Fleer, A., 2000. Short-lived thorium isotopes (^{234}Th , ^{228}Th) as indicators of POC export and particle cycling in the Ross Sea, Southern Ocean. *Deep-Sea Research II*, 47, 3451-3490.
- Cochran, J.K., Miquel, J.C., Armstrong, R.A., Fowler, S.W., Masque, P., Gasser, B., Hirschberg, D., Szlosek, J., Rodriguez y Baena, A.M., Verdeny, E., Stewart,

- G.M., 2009. Time-series measurement of ^{234}Th in water column and sediment trap samples from the Northwest Mediterranean Sea. *Deep Sea Research II*, 56(18), 1487-1501.
- Coale, K. and Bruland, K., 1985. ^{234}Th and ^{238}U disequilibria within the California Current. *Limnology and Oceanography*, 32(2), 189-200.
- Doney, S.C. and Schimel, D.S., 2007. Carbon and climate system coupling on timescales from the precambrian to the anthropocene. *Annual Review of Environment and Resources*, 32, 31-66.
- Doney, S.C., Fabry, V.J., Feely, R.A., Kleypas, J.A., 2009. Ocean Acidification: the other CO₂ problem. *Annual Review of Marine Sciences*, 1, 169-192.
- Ducklow, H.W., Steinberg, D.K., Buesseler, K.O., 2011. Upper Ocean Carbon Export and the Biological Pump. *Oceanography*, 14(4), 50-58.
- Edwards, A.W.F., 1992. *Likelihood*. Johns Hopkins University Press, Baltimore, MD.
- Eppley, R. W. and Peterson, B. J., 1979. Particulate organic matter flux and planktonic new production in the deep ocean. *Nature* 282, 677-680.
- Feely, R., Sabine, C., Takahashi, T., & Wanninkhof, R., 2001. Uptake and storage of carbon dioxide in the oceans: the global CO₂ survey. *Oceanography*, 14(4), 18–32.
- Fleisher, M. and Anderson, R., 2003. Assessing the collection efficiency of Ross Sea sediment traps using ^{230}Th and ^{231}Pa . *Deep-Sea Research II*, 50, 693-712.
- Geibert, W. and Usbeck, R., 2004. Adsorption of thorium and protactinium onto different particle types: Experimental findings. *Geochimica et Cosmochimica Acta*, 68(7): 1489-1501.
- Guihou, A., Pichat, S., Nave, S., Govin, A., Labeyrie, L., Michel, E., Waelbroeck, C., 2000. Late slowdown of the Atlantic Meridional Overturning circulation during the last glacial inception: new constraints from sedimentary ($^{231}\text{Pa}/^{230}\text{Th}$). *Earth and Planetary Science Letters*, 289, 520-529.
- Hedges, J.I. and Stern, J.H., 1984. Carbon and nitrogen determinations of carbonate marine sediment. *Organic Geochemistry*, 27, 319-361.
- Hedges, J.I., Baldock, J.A., Gélinas, Y., Lee, C., Peterson, M., Wakeham, S.G., 2001. Evidence for non-selective preservation of organic matter in sinking marine particles. *Nature*, 409, 801-804.

- Hilborn, R. and Mangel, M., 1997. The ecological detective: confronting models with data. Princeton University Press, Princeton, New Jersey, pp.133.
- Hill, P.S., 1998. Controls on floc size in the sea. *Oceanography* 11: 13-18.
- Honeyman, B. and Santschi, P., 1989. A Brownian-pumping model for oceanic trace metal scavenging: Evidence from Th isotopes. *Journal of Marine Research*, 47, 951-992.
- Honjo, S., 1980. Material fluxes and modes of sedimentation in the mesopelagic and bathypelagic zones. *Journal of Marine Research*, 38, 53-97.
- Jackson, G.A. and Burd A.B., 1998. Aggregation in the marine environment. *Environ Sea Technol* 32:2805–2814.
- Karakas, G., Nowald, N., Schäfer-Neth, C., Iversen, M.,H., Barkmann, W; Fischer, G. Marchesiello, P, Schlitzer, R., 2009. Particle camera and settling chamber measurements at site PC (GeoB11834-3) and SC (GeoB12914-4) off Cape Blanc/Mauritania. doi:10.1594/PANGAEA.755951
- Kriest, I. and Evans, G., 2000. A vertically resolved model for phytoplankton aggregation, *Proc. Indian Acad. Sci. (Earth Planet. Sci.)*, 109, 453–469.
- Lavelle, J. W., Cokelet, E.D., Cannon, G.A., 1991: A model study of density intrusions into and circulation within a deep, silled estuary: Puget Sound. *J. Geophys. Res.*, 96, 16 779-16 800.
- Lee, C., Wakeham, S.G., Hedges, J.I., 2000. Composition and flux of particulate amino acids and chloropigments in equatorial Pacific seawater and sediments. *Deep-Sea Res. I* 47: 1535-1568.
- Lee, C., Armstrong, R.A., Cochran, J.K., Engel, A., Fowler, S.W., Goutx, M., Masque, P., Miquel, J.C., Peterson, M., Tamburini, C., Wakeham, S., 2009a. MedFlux: Investigations of particle flux in the Twilight Zone. *Deep-Sea Research II*, 56, 1363-1368.
- Lee, C., Peterson, M.L., Wakeham, S.G., Armstrong, R.A., Cochran, J.K., Miquel, J.C., Fowler, S.W., Hirschberg, D., Beck, A., Xue, J., 2009b. Particulate organic matter and ballast fluxes measured using time-series and settling velocity sediment traps in the northwestern Mediterranean Sea. *Deep-Sea Research II*, 56, 1420-1436.
- Mann, K.H. and Lazier, J.R.N., 1991. Dynamics of marine ecosystems : biologicalphysical interactions in the oceans. Blackwell Scientific Publications, Boston.

- Marchal, O., Francois, R., Stoker, T.F., Joos, F., 2000. Ocean thermohaline circulation and sedimentary $^{231}\text{Pa}/^{230}\text{Th}$ ratio. *Paleoceanography*, Vol. 15 (6), 625-641.
- Marchal, O. and Lam, P., 2012. What can paired measurements of Th isotope activity and particle concentration tell us about particle cycling in the ocean? *Geochimica et Cosmochimica Acta* 90, 126-148.
- Marty, J.C., 2002. The DYFAMED time-series program (French JGOFS). *Deep-Sea Research II*, 49, 1963-1964.
- McCave, I.N., 1975. Vertical flux of particles in the ocean. *Deep Sea Research*, 22, 491-520.
- McDonnell, A.M.P. and Buesseler, K.O., 2010. Variability in the average sinking velocity of marine particles. *Limnol. Oceanogr.*, 55(5), 2085-2096.
- Metropolis, N., Rosenbluth, A.W., Rosenbluth, M.N., Teller, A.H., Teller, E., 1953. Equation of state calculations by fast computing machines. *Journal of Chemical Physics* 21, 1087–1092.
- Migon, C., 1993. Riverine and atmospheric inputs of heavy metals in the Ligurian Sea. *Science of the Total Environment*, 138, 289-299.
- Moore, R. M. and G. E. Millward, 1988. The kinetics of reversible Th reactions with marine particles, *Geochim. Cosmochim. Acta*, 52, 113-118.
- Murnane, R.J., Sarmiento, J.L., Bacon M.P., 1990. Thorium isotopes, particle cycling models, and inverse calculations of model rate constants. *Journal of Geophysical Research*, 95(C9), 16195-16206.
- Murnane, R. J., 1994. Determination of thorium and particle matter cycling parameters at station P: A reanalysis and comparison of least squares techniques. *Journal of Geophysical Research*, 99 (C2), 3393-3405.
- Murnane, R.J., Cochran, J.K., sarmiento, J.L., 1994. Estimates of particle- and thorium-rates in the northwest Atlantic Ocean. *Journal of Geophysical Research*, 99 (C2), 3373-3392.
- Murnane, R.J., Cochran, J.K., Buesseler, K.O., Bacon, M.P., 1996. Least-squares estimates of thorium, particle, and nutrient cycling rate constants from the JGOFS North Atlantic Bloom Experiment. *Deep-Sea Research I*, 43(2), 239-258.
- Nozaki, Y., Horibe, Y., Tsubota, H., 1981. The water column distribution of thorium isotopes in the western North Pacific, *Earth Planet Science Letter*, 54, 203-216.

- Nozaki, Y., Yang, J.S., Yamada, M., 1987. Scavenging of thorium in the ocean, *J. Geophys. Res.*, 92, 772-778.
- Owens, S.A., Buesseler, K.O., Sims, K.W.W., 2011. Re-evaluating the ^{238}U -salinity relationship in seawater: Implications for the ^{238}U - ^{234}Th disequilibrium method. *Marine Chemistry*, 127(1-4), 31-39.
- Peterson, M.L., Hernes, P.J., Thoreson, D.S., Hedges, J.I., Lee, C., Wakeham, S.G., 1993. Field evaluation of a valved sediment trap. *Limnol. Oceanogr.* 38, 1741-1761.
- Peterson, M.L., Wakeham, S.G., Lee, C., Askea, M., Miquel, J.C., 2005. Novel techniques for collection of sinking particles in the ocean and determining their settling rates. *Limnology and Oceanography methods*, 3, 520-532.
- Peterson, M.L., Fabres, J., Wakeham, S.G., Lee, C., Alonso, I.J., Miquel, J.C., 2009. Sampling the Vertical Particle flux in the upper water column using a large diameter free-drifting NetTrap adapted to an Indented Rotating Sphere Sediment trap. *Deep Sea Research II*, 56, 1547-1557.
- Press, W.H., Flannery, B.P., Teukolsky, S.A., Vetterling, W.T., 1986. *Numerical Recipes*. Cambridge University Press, Cambridge, England.
- Roy-Barman, M., Coppola, L., Souhaut, M., 2002. Thorium isotopes in the western Mediterranean Sea: an insight into the marine particle dynamics. *Earth and Planetary Science Letters*, 196, 191-174.
- Roy-Barman, M., Lemaitre, C., Ayrault, S., Jeandel, C., Souhaut, M., Miquel, J.C., 2009. The influence of particle composition on Thorium scavenging in the Mediterranean Sea. *Earth and Planetary Science Letters*, 286, 526-534.
- Sabine, C.L. and Feely, R.A., 2007. The oceanic sink for carbon dioxide. In *Greenhouse Gas Sinks*, ed. D. Reay, N. Hewitt, J. Grace, K. Smith, pp. 31-49. Oxfordshire: CABI Publishing.
- Santschi, P., Li, Y., Bell, J., 1979. Natural radionuclides in the water of Narragansett Bay. *Earth and Planetary Sciences Letters*, 45, 201-213.
- Shuman, F.R. and Lorenzen, C.J., 1975. Quantitative degradation of chlorophyll a by a marine herbivore. *Limnol. Oceanogr.* 20: 580-568.
- Siegenthaler, U. and Sarmiento, J., 1993. Atmospheric carbon dioxide and the ocean. *Nature*, 365, 119-125.
- Solomon, S., D. Qin, M. Manning, R.B. Alley, T. Berntsen, N.L. Bindoff, Z. Chen, A. Chidthaisong, J.M. Gregory, G.C. Hegerl, M. Heimann, B. Hewitson, B.J.

- Hoskins, F. Joos, J. Jouzel, V. Kattsov, U. Lohmann, T. Matsuno, M. Molina, N. Nicholls, J. Overpeck, G. Raga, V. Ramaswamy, J. Ren, M. Rusticucci, R. Somerville, T.F. Stocker, P. Whetton, R.A. Wood and D. Wratt, 2007: Technical Summary. In: *Climate Change 2007: The Physical Science Basis. Contribution of Working Group I to the Fourth Assessment Report of the Intergovernmental Panel on Climate Change* [Solomon, S., D. Qin, M. Manning, Z. Chen, M. Marquis, K.B. Averyt, M. Tignor and H.L. Miller (eds.)]. Cambridge University Press, Cambridge, United Kingdom and New York, NY, USA.
- Stephens, M.P., Kadko, D.C., Smith, C.R., Latasa, M., 1997. Chlorophyll-a and pheopigments as tracers of labile organic carbon at the central equatorial Pacific seafloor. *Geochimica et Cosmochimica Acta*, 61(21), 4605-4619.
- Sun, M.-Y., Lee, C., Aller, R.C., 1993a. Laboratory studies of oxic and anoxic degradation of chlorophyll-a in Long Island Sound sediments. *Geochim. Cosmochim. Acta*. 57, 147-157.
- Sun, M.-Y., Lee, C., Aller, R.C., 1993b. Anoxic and oxic degradation of ¹⁴C-labeled chloropigments and a ¹⁴C-labeled diatom in Long Island Sound sediments. *Limnol. Ocean.* 38. 1438-1451.
- Szlosek, J., Cochran, J.K., Miquel, J.C., Masque, P., Armstrong, R.A., Fowler, S.W., Gasser, B., Hirschberg, D.J., 2009. Particulate organic carbon-²³⁴Th relationships in particles separated by settling velocity in the northwest Mediterranean Sea. *Deep Sea Research II*, 56, 1519-1532.
- Szymczak-Zyla, M., Kowalewska, G., Louda, J.W., 2008. The influence of microorganisms on chlorophyll a degradation in the marine environment. *Limnol. Oceanogr.*, 53(2), 85-862.
- Tarantola, A. and Valette, B., 1982a. Inverse problem=Quest for information. *Journal of Geophysics*. 50, 159-170.
- Tarantola, A. and Valette, B., 1982b. Generalized nonlinear inverse problems solved using the least square criterion. *Reviews of Geophysics and Space Physics* 20(2), 219-232.
- Trull, T.W., Bray, S.G., Buesseler, K.O., Lamborg, C.H., Manganini, S., Moy, C., Valdes, J., 2008. In situ measurements of mesopelagic particle sinking rates and the control of carbon transfer to the ocean interior during the Vertical Flux in the Global Ocean (VERTIGO) voyages in the North Pacific. *Deep-Sea Res. II* 55: 1684–1695.

- Tsunogai, S. and Minagawa, M., 1978. Settling model for the removal of insoluble chemical elements in seawater. *Geochemical Journal*, 12, 47-56.
- Waite, A., Fisher, A., Thompson, P. A., Harrison, P. J., 1997. Sinking rate versus cell volume relationships illuminate sinking rate control mechanisms in marine diatoms. *Marine Ecology-Progress Series* 157, 97-108.
- Wakeham, S. G. and Lee, C., 1993. Production, transport, and alteration of particulate organic matter in the marine water column. In: M.H. Engel and S. A. Macko (eds) *Organic Geochemistry*, pp. 145-169. Plenum Press.
- Wakeham, S.G., Lee, C., Peterson, M.L., Liu, Z., Szlosek, J., Putnam, I., Xue, J., 2009. Organic compound composition and fluxes in the Twilight Zone—time series and settling velocity sediment traps during MEDFLUX. *Deep-Sea Research II*, 56, 1437-1453.
- Welschmeyer, N.A. and Lorenzen, C.J., 1985. Chlorophyll budgets: zooplankton grazing and phytoplankton growth in a temperate fjord and the Central Pacific Gyres. *Limnol. Oceanogr.*, 30(1), 1-21.
- Westrich, J.T. and Berner, R.A., 1984. The role of sedimentary organic matter in bacterial sulfate reduction: The G model tested. *Limnol. Ocean.* 29, 236-249.
- Whelan, J.K., and Farrington, J.W., 2013. *Organic matter: productivity, accumulation, and preservation in recent and ancient sediments*. Columbia University Press. pp. 185-186.
- Xue, J., and Armstrong, R.A., 2009. An improved “benchmark” method for estimating particle settling velocities from time-series sediment trap fluxes. *Deep Sea Research II*, 56(18), 1479-1486.
- Yu, E.-F., Francois, R., Bacon, M., 1996. Similar rates of modern and last-glacial ocean thermohaline circulation inferred from radiochemical data. *Nature*, 379(22), 689-694.